

Continuous Direct Air Capture: understanding mass transfer in reactive absorption of carbon dioxide

Experimenting and modelling a novel DAC absorption process

Andrea De Matteis

Continuous Direct Air Capture: understanding mass transfer in reactive absorption of carbon dioxide

Experimenting and modelling a novel DAC absorption process

by

Andrea De Matteis

to obtain the degree of Master of Science
at the Delft University of Technology,
to be defended publicly on Friday December 18, 2020 at 10:00 AM.

Student number:	4728378	
Company Supervisors:	Ir. M. Sinha,	ZEF B.V.
	Ir. J. van Kranendonk,	ZEF B.V.
Thesis committee:	Prof. dr. ir. E. Goetheer,	TU Delft, (chair of committee)
	Dr. R. Delfos,	TU Delft
	Dr. ir. M. J. Tummers,	TU Delft

This thesis is confidential and cannot be made public until December 18, 2022.

An electronic version of this thesis is available at <http://repository.tudelft.nl/>.

Abstract

Increase in global energy demand has brought to a massive rise in greenhouse gases emissions. In particular, the continuously increasing atmospheric concentration of carbon dioxide is a major concern among the scientific community. This paved the way for an intense research of CO_2 emissions mitigating technologies. Those ones including carbon capture, storage and utilisation are seen as part of the solution for this global problem. In this framework, Zero Emission Fuels (ZEF), a startup company located in Delft (The Netherlands) set the ambitious goal of developing a micro process plant producing methanol from ambient air and sunlight only.

Part of the process involves direct capture of CO_2 from the atmosphere (direct air capture) with the use of a pure tetraethylenepentamine (TEPA) absorbent. ZEF sets itself aside from the rest of the industry developing an absorber which collects CO_2 with no support structure by continuously flowing TEPA inside open channels. Previous research shows how this approach brings limitations connected to slowly diffusing CO_2 molecules in the absorbent liquid film in proximity of the gas-liquid interface.

In this framework, circulation of TEPA particles from the gas-liquid interface into the bulk of the flowing absorbent is seen as a viable solution to improve the process. This thesis focuses on investigating this hypothesis by inducing mixing on the liquid side. That is done by building two experimental setups investigating both passive and active mixing. Experimental results show that active mixing can be used to improve the rate of CO_2 absorption, while passive mixing does not bring significant advantages.

Results from the passive mixing experiments are further investigated by modelling the fluid dynamics of the process through a Direct Numerical Simulation of the particular Stokes' flow in the engineered absorption channel.

The process is characterized with the definition of a theoretical framework describing mass transfer in the liquid side. Following an analogy with ice formation on top of a frozen lake, this theory, also known as the "Ice-Sheet" theory, shines some light on the way this diffusion limitations are happening at a molecular level. In particular, a highly viscous, heavily loaded layer of sorbent on the gas-liquid interface is believed to be the cause for observed CO_2 diffusion limitations.

This theory is backed-up by defining its mathematical equivalent in the form of a mass transfer model. Comparing the results of the model with experimental results, a very good agreement is observed. That is believed to add credibility to the proposed theory. Moreover, that is also found to be in line with the latest knowledge available in literature about CO_2 absorption in TEPA films.

Finally, the experimental results and the developed models are used to engineer a new iteration of ZEF's absorber on a cost reduction basis.

Acknowledgments

This report is the result of a research project which lasted for the last nine months. The project would not have been the same without the contribution of some people I would like to thank.

Firstly, I would like to thank my TU supervisors: Professor Earl Goetheer and Dr. René Delfos. Every one of the biweekly meetings we have had in the last nine months was an extremely useful source of inspiration and constructive feedback. Insights coming from your expertise were fundamental to reach the set goals. I really appreciated your honesty and the feeling that we were always working as a team, having the common goal of making this project better and better with time.

Thanks a lot to the whole team of ZEF for accepting to develop this project and making me feel part of the team from day 1. Thanks to engineer Jan van Kranendonk for always being available to help. You always pushed me to achieve more and your critical thinking was always a very powerful tool which definitely improved the quality of this work.

A special thanks goes to engineer Mrigank Sinha. You were, hands down, the one who spent the most time in helping me. Our daily talks have been an extremely useful source of knowledge and ideas. I really want to thank you for all the effort you put in this project while still being extremely busy following other students. It was awesome to work together as both friends and colleagues. I am sure you and ZEF have a bright future ahead of you and I really hope you will be successful in making this world a bit more sustainable. Thanks a lot.

In a world dealing with a pandemic crisis, it would have been way more difficult to go through this last months without the help of my friends and family.

Thanks to my friends turned first into housemates and then into a family: Camilla and Daniele. Thanks to Camilla for all the time we spent together during those last years. From parties, to the quarantine, to the workouts, you have always been a source of positiveness and laughter. We developed a very special friendship that I am sure will last in the future as well. Thanks to Daniele for, well, being Daniele. From the Bachelor studies, through Forze to this last period you have always been a very loyal and important reference for me. I think it is not a case that we decided to go through this adventure together from day 1. Thanks to our Foulky Friday housemate Joost. We had so much fun in this last period and I am pretty sure that is a Friday tradition that will continue forever. Thanks also to Amina and Filippo, I am really grateful for the relationship we developed and I hope the future will bring us all together once again.

Thanks to my sweet Isabelle, out of the blue we developed a wonderful relationship that makes me happy every day. You helped me to overcome the stress of this period. I'm immensely grateful to have met you and I think it is extremely special and meaningful that all of that happened in such a delicate time.

Thanks to Luca, Riccardo, Simone, Lorenzo e Matteo for always being there to laugh together. I can't wait to see what the future holds for us and to spend some time with you at home once again.

Finally and most importantly, thanks to my family for making all of this possible. You were always fundamental in helping me following my road. I still remember you pushing me to pursue all the adventures I have had in the last three years. Your wisdom and advice is a true inspiration to me. I hope to make you proud with everything I do. Vi voglio bene e mi mancate un sacco. A Claudio, ho iniziato questi studi ispirandomi a te, continuerai a vivere per sempre in quello che faccio, grazie,

*Andrea De Matteis
Delft, December 2020*

Contents

List of Figures	ix
List of Tables	xiii
Abbreviations & nomenclature	xv
1 Introduction	1
1.1 Rise in global energy demand and CO_2 emissions	1
1.2 CO_2 emissions: mitigating technologies	2
1.2.1 Energy efficient technologies	2
1.2.2 Carbon capture, storage and utilisation technologies	3
1.3 The case of ZEF (Zero Emission Fuels)	4
1.4 Research goals and objectives	5
1.5 Thesis overview & report outline	6
2 Literature review	9
2.1 CO_2 capture in industry	9
2.1.1 Absorption technologies - Theory & Industrial Application	10
2.1.2 Adsorption technologies - Industrial Application	15
2.2 Direct Air Capture (DAC)	15
2.2.1 DAC in industry	15
2.2.2 DAC at ZEF	17
2.3 TEPA as the working fluid	22
2.4 Mixing at very low Reynolds number	25
2.4.1 Stokes flow theory	25
2.4.2 Micromixing: high Peclet number, slow diffusive mixing	26
2.5 Lessons learned	29
3 Experimental investigation	31
3.1 Previous work	31
3.2 Passive Mixing Experiments	33
3.2.1 Requirements	33
3.2.2 Setup Description	33
3.2.3 Methodology	36
3.2.4 Experimental plan	37
3.2.5 Assumptions	39
3.3 Active Mixing Experiments	39
3.3.1 Requirements	39
3.3.2 Setup Description	40
3.3.3 Methodology	42
3.3.4 Experimental plan	43
3.3.5 Assumptions	43
4 Modelling	45
4.1 Stokes Flow DNS Solver	45
4.1.1 Model description	46
4.1.2 DNS solver	49
4.1.3 Model assumptions	52
4.2 Mass transfer model	52
4.2.1 Model description	53
4.2.2 Model Assumptions	56

5	Results	59
5.1	Mixing Experiments	61
5.1.1	Passive Mixing Experiments	61
5.1.2	Active mixing experiments	66
5.1.3	Selection of the mixing strategy	69
5.2	Modelling	69
5.2.1	DNS Model	69
5.2.2	UMD mass transfer model	71
5.3	Process' physical interpretation: the "Ice-Sheet" equivalence	73
6	Absorption column engineering	77
6.1	Sorbent side design	77
6.1.1	Sensitivity analysis on sorbent side design	79
6.2	Air side design	81
6.3	Cost analysis	83
6.4	Absorber overview	86
7	Conclusions & Recommendations	89
7.1	Conclusions	89
7.2	Recommendations	92
7.2.1	Recommendations for future research	92
7.2.2	Recommendations for improving this research project	93
A	Detailed experimental methodology	95
A.1	Passive mixing experiments	95
A.2	Active mixing experiments	96
B	Autodesk CFD model	99
B.1	General overview of the simulation	99
B.2	Results of the simulation	101
B.2.1	OR results	101
B.2.2	SC results	102
B.2.3	OC results	102
B.2.4	KM results	103
C	DNS model validation	105
D	Detailed absorber design	107
D.1	Detailed sensitivity analysis	107
D.2	Cumulative vs. absolute STY	107
D.2.1	Cumulative vs. absolute STY: influence of rich loading	108
D.3	Air side design: governing equations for H_2O mass balance	108
D.4	Extra images for the conceptual absorber design	108
E	Extra plots	109
E.1	Active Mixing: absolute Space-Time Yield	109
E.2	Active Mixing: other plots	109
E.3	Passive Mixing: absolute Space-Time Yield	110
	Bibliography	111

List of Figures

1.1	Global energy consumption in million tonnes of oil equivalent [1]	1
1.2	Increase in global average temperature range with respect to pre-industrial levels according to NASA's Goddard Institute for Space Studies [2]	2
1.3	CO_2 emissions abatement scenario [3]	3
1.4	Overview of TRL for multiple technologies involved in CO_2 mitigation [4]	3
1.5	ZEF microplant concept [5]	4
1.6	Thesis flow chart	6
2.1	Overview of carbon capture technologies within power plants	9
2.2	Mass transfer models: a) film model; b) surface renewal model [6]	11
2.3	Two film theory with a) ideal and b) more realistic concentration gradients [6]	12
2.4	Very soluble gases [7]	13
2.5	Low solubility gases [7]	13
2.6	IGCC equipped for CO_2 physical absorption. The components added to the cycle are in black [8]	14
2.7	Example of a DAC system using a KOH solution [9]	16
2.8	Example of a process using amine adsorbents [10]	17
2.9	The Climeworks DAC unit	17
2.10	ZEF's DAC prototype 1 [11]	18
2.11	ZEF's DAC prototype 2 [12]	18
2.12	Test setup for the novel absorption process [13]	19
2.13	Inhomogeneous sorbent flow (acrylic test) [13]	19
2.14	Schematic of test setup for single-channel absorption experiments [14]	20
2.15	Test setup for single-channel absorption experiments [14]	20
2.16	CO_2 over sorbent mass ratio with and without induced mixing [14]	20
2.17	CO_2 loading at different sorbent flow rates [14]	21
2.18	loading at different air flow rates [14]	21
2.19	Design specification of ZEF's DAC prototype 3 [14]	22
2.20	Structure of a molecule of TEPA [15]	22
2.21	TEPA viscosity as a function of shear rate [16]	23
2.22	Results from the dry loading experiments [17]	24
2.23	Results from the wet loading experiments [17]	24
2.24	Example of two inlet channel segment [18]	27
2.25	Ultrasonic micromixer [19]	27
2.26	Channel with Obliquely Oriented ridges. A) Schematic diagram of the channel B) Optical micrograph showing mixing for a red and green stream C) Fluorescent confocal micrograph of different channel's cross sections [20]	27
2.27	Channel with ridges shaped as Staggered Herringbones. First one-and-a-half cycles A) Schematic diagram of the channel B) Confocal micrograph of different cross sections of the channel [20]	27
2.28	Micromixers with sinusoidally shaped side walls at different phase shifts (CFD and experiments) [21]	28
2.29	Kenics mixer geometry [22]	28
3.1	The fan used to provide the air flow rate	32
3.2	The syringe pump used to provide the sorbent flow rate	32
3.3	Cary 630 FTIR Spectrometer [23]	32
3.4	Empty Channel, front view	34
3.5	Detail of channel dimensions	34

3.6	Empty Channel, top view	34
3.7	Clamps dimensions	34
3.8	A Ultimaker 2+ 3D printer	35
3.9	Analog sling psychrometer	35
3.10	Final assembly of the experimental setup for passive mixing experiments	36
3.11	Staggered Herringbone Mixer, top view	37
3.12	Staggered Herringbone Mixer, perspective view	37
3.13	Bridges, top view	38
3.14	Bridges, cross sectional view	38
3.15	Schematic of the active mixing experimental setup	40
3.16	Surflo KGP-001 gear pump	41
3.17	Absorption plate CAD model and dimensions (front and bottom view)	41
3.18	Distributors, plates and collector assembly	41
3.19	Working active mixing experimental setup	42
4.1	Staggered Herringbone Mixer, CAD model view with axis	46
4.2	"Black box" view of the DNS solver	47
4.3	Open channel flow problem illustration	48
4.4	Lid-driven cavity flow problem illustration	49
4.5	Staggered grid	50
4.6	DNS solver algorithm	50
4.7	Unimolecular Diffusion (UMD) model	53
4.8	Unimolecular Diffusion (UMD) model: code algorithm	55
5.1	Overview of the main results presented in chapter 5	60
5.2	CO_2 per amine loading at different distances in the channel, for different volumetric flow rates	61
5.3	H_2O per amine loading at different distances in the channel, for different volumetric flow rates	61
5.4	CO_2 STY at different distances in the channel, for different volumetric flow rates	62
5.5	H_2O STY at different distances in the channel, for different volumetric flow rates	62
5.6	CO_2 per amine loading as function of the measured residence time and sorbent flow rate	62
5.7	H_2O per amine loading as function of the measured residence time and sorbent flow rate	62
5.8	CO_2 per amine loading at different distances in the channel, for different channel geometries, at 3 mL/hr flow rate	63
5.9	H_2O per amine loading at different distances in the channel, for different channel geometries, at 3 mL/hr flow rate	63
5.10	CO_2 per amine loading at different distances in the channel, for different channel geometries, at 1.5 mL/hr flow rate	63
5.11	H_2O per amine loading at different distances in the channel, for different channel geometries, at 1.5 mL/hr flow rate	63
5.12	CO_2 STY at different distances in the channel, for different channel geometries, at 3 mL/hr flow rate	64
5.13	H_2O STY at different distances in the channel, for different channel geometries, at 3 mL/hr flow rate	64
5.14	CO_2 STY at different distances in the channel, for different channel geometries, at 1.5 mL/hr flow rate	64
5.15	H_2O STY at different distances in the channel, for different channel geometries, at 1.5 mL/hr flow rate	64
5.16	Detail of a BR geometry during an experiment	65
5.17	CO_2 per amine loading when mixing is induced using bridges at different distances on the channel, per [14]	65
5.18	STY in function of CO_2 per amine loading, reference active mixing experiment	66
5.19	STY in function of H_2O per amine loading, reference active mixing experiment	66
5.20	STY in function of CO_2 per amine loading, comparison between the reference active mixing experiment and single channel experiments	67

5.21	STY in function of H_2O per amine loading, comparison between the reference active mixing experiment and single channel experiments	67
5.22	STY in function of CO_2 per amine loading, comparison between the reference and lower air flow rate active mixing experiment	67
5.23	STY in function of H_2O per amine loading, comparison between the reference and lower air flow rate active mixing experiment	67
5.24	STY in function of CO_2 per amine loading, comparison between the reference and higher sorbent flow rate active mixing experiment	68
5.25	STY in function of H_2O per amine loading, comparison between the reference and higher sorbent flow rate active mixing experiment	68
5.26	Velocity profile for the open channel flow in the Y direction with validation	70
5.27	Velocity vectors and streamlines for the lid-driven cavity flow	70
5.28	Connection between physical interpretation, mass transfer model and experimental results	71
5.29	UMD mass transfer model validation: active mixing experiment #1	72
5.30	UMD mass transfer model validation: active mixing experiment #3	72
5.31	UMD mass transfer model validation: passive mixing experiment #1	72
5.32	UMD mass transfer model validation: passive mixing experiment #2	72
5.33	UMD mass transfer model validation: passive mixing experiment #7	73
5.34	UMD mass transfer model validation: passive mixing experiment #4	73
5.35	Absorption of CO_2 in a polyamine sorbent, step #1	74
5.36	Absorption of CO_2 in a polyamine sorbent, step #2	74
5.37	Absorption of CO_2 in a polyamine sorbent, step #3	75
5.38	Concentration profile according to the "IS" theory	75
6.1	Main algorithm in the design of the sorbent side of the absorption column	78
6.2	Absorber area in function of the operational rich loading and sorbent residence time on the plate for a certain CO_2 capture rate	79
6.3	Absorber area in function of the required CO_2 capture and sorbent residence time on the plate for a rich loading of 5 moles of CO_2 per kilogram of TEPA	80
6.4	Main algorithm in the air side design of the absorption column	81
6.5	Mass balance for the air side: control volume	81
6.6	Required air flow rate in function of designed CO_2 outlet concentration	82
6.7	CO_2 concentration in air over the column length	82
6.8	Area and pump energy cost in function of sorbent plate residence time and pipe's internal diameter	84
6.9	Total cost of the absorber	85
6.10	Summary of the main features of the absorption column	86
6.11	Exploded view of the absorber	87
7.1	Example of plate design for combining active and passive mixing	93
B.1	Staggered Herringbone Mixer	100
B.2	Oblique Ridges	100
B.3	Sinusoidal Channel	100
B.4	Obstructed Channel	100
B.5	Kenics Mixer	100
B.6	SHM, traces	101
B.7	SHM, vorticity	101
B.8	OR, traces	102
B.9	OR, vorticity	102
B.10	SC, velocity vector	102
B.11	SC, vorticity	102
B.12	OC, traces	102
B.13	OC, vorticity	102
B.14	KM, traces	103
B.15	KM, vorticity	103

C.1	Open channel flow problem illustration	105
C.2	Residuals for the open channel flow	106
D.1	Absolute STY in function of the operational loading and the sorbent's plate residence time	108
D.2	Cumulative STY in function of the operational loading and the sorbent's plate residence time	108
D.3	Absorber design: circuit for the pump	108
D.4	Absorber design: top view	108
D.5	Absorber design: channel view	108
E.1	Active Mixing: absolute STY in function of CO_2 per amine loading	109
E.2	Active Mixing: absolute STY in function of H_2O per amine loading	109
E.3	Active Mixing: CO_2 per amine loading vs. time	109
E.4	Active Mixing: H_2O per amine loading vs. time	109
E.5	Active Mixing: CO_2 capture rate vs. time	110
E.6	Active Mixing: H_2O capture rate vs. time	110
E.7	Passive Mixing, 1.5 mL/hr: CO_2 absolute STY in function of space	110
E.8	Passive Mixing, 1.5 mL/hr: H_2O absolute STY in function of space	110
E.9	Passive Mixing, 3 mL/hr: CO_2 absolute STY in function of space	110
E.10	Passive Mixing, 3 mL/hr: H_2O absolute STY in function of space	110
E.11	Passive Mixing, sensitivity analysis: CO_2 absolute STY in function of space	110
E.12	Passive Mixing, sensitivity analysis: H_2O absolute STY in function of space	110

List of Tables

1	Abbreviations	xv
2	Nomenclature	xvi
1.1	Absorption column requirements	6
2.1	TEPA viscosity at different gas concentrations and different temperatures [14]	23
3.1	Experimental parameters: passive mixing	37
3.2	SHM geometrical parameters, refer to figure 2.27	38
3.3	Passive mixing, experimental plan.	39
3.4	Experimental parameters: active mixing	42
3.5	Active mixing, experimental plan.	43
5.1	Input conditions CFD model	69
5.2	Coefficient of determination and mean absolute error for the UMD mass transfer model	72
6.1	Inputs to the cost analysis	83
7.1	Active mixing, additional experiments	93
B.1	CFD simulation general info	101

Abbreviations & nomenclature

Abbreviation	Description
BP	British Petroleum
IPCC	Intergovernmental Panel on Climate Change
CCS	Carbon Capture and Storage
CCU	Carbon Capture and Utilization
UNIDO	United Nations Industrial Development Organization
EPRI	Electric Power Research Institute
TRL	Technology Readiness Level
ZEF	Zero Emission Fuels
DAC	Direct Air Capture
TEPA	Tetraethylenepentamine
DNS	Direct Numerical Simulation
CFD	Computational Fluid Dynamics
MEA	Monoethanolamine
MDEA	Diethanolamine
IL	Ionic Liquids
TSIL	Task-Specific Ionic Liquids
TSA	Temperature Swing Adsorption
VSA	Vacuum Swing Adsorption
STY	Space-Time Yield
PEI	Polyethylenimine
SHM	Staggered Herringbone Mixer
OR	Obliquely oriented Ridges
PMMA	Polymethyl Methacrylate
FTIR	Fourier Transform Infra-Red
EC	Empty Channel geometry
BR	Bridges geometry
NS	Navier Stokes
IS	Ice-Sheet
UMD	Unimolecular Diffusion
EMD	Equimolar counterdiffusion
MSD	Mean Square Displacement

Table 1: Abbreviations

Symbol	Name
CO_2	Carbon dioxide
H_2O	Water
H_2	Hydrogen
O_2	Oxygen
CH_3OH	Methanol
RNH_2	Primary amine
R_2NH	Secondary amine
R_2NCOOH	Zwitterion
R_2NCOO^-	Carbamate
R_3N	Tertiary amine
$R_3NH^+HCO_3^-$	Bicarbonate
NO_x	Nitrogen oxides
SO_x	Sulfur oxides
$NaOH$	Sodium hydroxide
KOH	Potassium hydroxide
$Ca(OH)_2$	Calcium hydroxide
K_2CO_3	Potassium carbonate
$CaCO_3$	Calcium carbonate
CaO	Calcium oxide
Re	Reynolds number
Pe	Peclet number

Table 2: Nomenclature

Introduction

The global warming emergency, related to a substantial increase in worldwide CO_2 emissions, is unanimously referred to be the biggest challenge that mankind will have to face in the 21st century. In the following chapter, this problem is briefly outlined, together with the different technologies that are currently used as a mitigation strategy. In this framework, the specific case of Zero Emission Fuels is defined and, finally, objectives for the following thesis project are outlined.

1.1. Rise in global energy demand and CO_2 emissions

As reported by the BP statistical review of world energy, the global energy consumption has increased by 2.9% in 2018 [1]. This growth is the strongest since 2010 and, as shown by figure 1.1, fossil fuels accounts for more than 83% of the overall energy production. Carbon dioxide, together with methane and nitrous oxide, are among the main emissions resulting from the burning of these fuels. Therefore, it comes with no surprise that global CO_2 emissions are increasing in correlation with the always increasing energy demand [24].

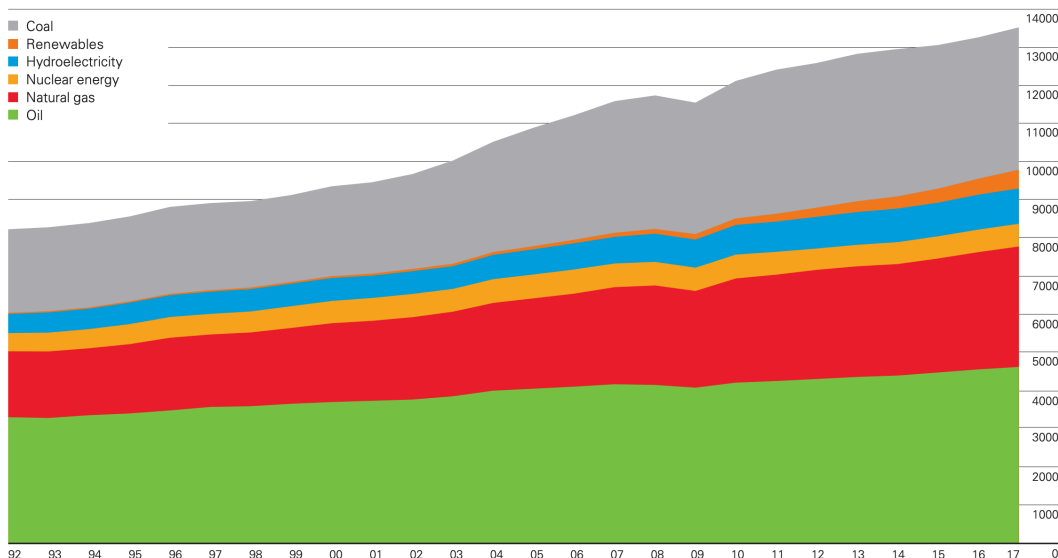


Figure 1.1: Global energy consumption in million tonnes of oil equivalent [1]

As stated by the Intergovernmental Panel on Climate Change (IPCC) [25], observations shows that the massive release in the atmosphere of these type of gases, also known as greenhouse gases, is the only reason that can explain the rise in the average temperatures of the Earth's climate system. Figure 1.2 shows how the average global surface temperature has risen with respect to pre-industrial levels in the last 50 years. This effect, better known as global warming, constitutes a very serious

threat to the equilibrium of the Earth's ecosystem. It is reported how the global average will reach and possibly overshoot, the 1.5 °C by 2050 [26]. Extreme weather conditions such as heavy precipitation, drought of coastal regions and frequent heat waves in most land regions are predicted to have impact on human systems and well-being in the foreseeable future [27]. In this framework, reduction of CO_2 emissions via a more sustainable industrial and social development has top priority in ongoing research. Various types of CO_2 mitigating technologies are being developed, some of which will be discussed in the following paragraph.

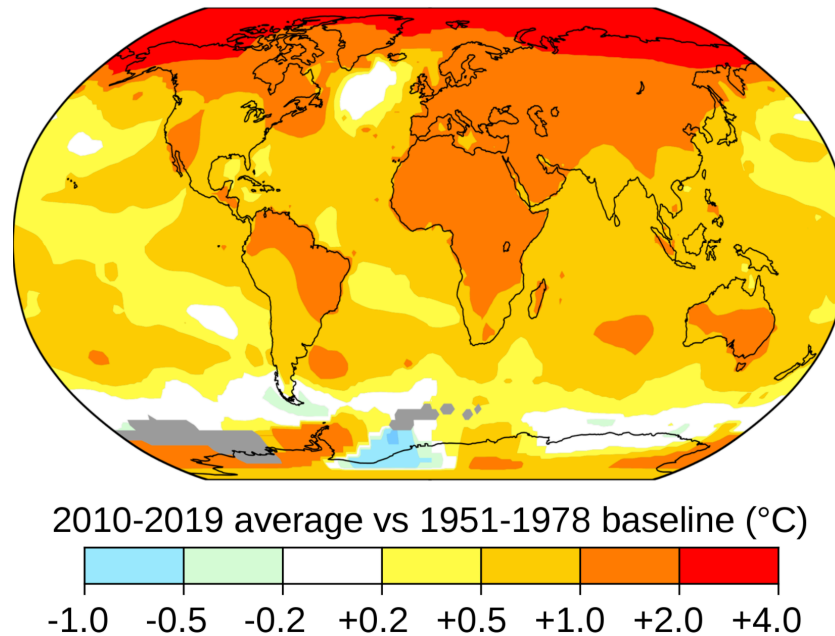


Figure 1.2: Increase in global average temperature range with respect to pre-industrial levels according to NASA's Goddard Institute for Space Studies [2]

1.2. CO_2 emissions: mitigating technologies

In order to reduce the carbon release in the atmosphere, different approaches are possible. Reducing the environmental impact of existing processes through the introduction of energy efficient technologies is a valuable way of dealing with the global warming problem without the necessity of disrupting the way we currently convert and utilize energy. On the other side, the capture of CO_2 from large emitting sources, gives the possibility to reduce the emissions either by storage of the captured CO_2 , carbon capture and storage (CCS) technologies, or by converting the captured gases into higher economic value products, carbon capture and utilisation (CCU) technologies. In this section, those three ways of reducing the environmental impact of human activities are briefly reviewed.

1.2.1. Energy efficient technologies

Energy efficiency can be defined as the ratio of a system's energy input to its output. As stated by the Industrial Development Report from the United Nations Industrial Development Organization (UNIDO) [28], in engineering, energy efficiency can be interpreted as the proportion of the energy input which is available as a useful output. Improving the energy efficiency of a certain process will reduce the necessary energy input for obtaining a certain output, thus reducing the overall energy consumption.

This CO_2 mitigation strategy can be applied to multiple sectors like residential, industrial and commercial. For example, the energy efficiency demonstration report from the Electric Power Research Institute (EPRI) [29], has identified six categories of technologies that can reduce the energy usage in U.S. buildings. Those include the use of heat pumps water heater, light-emitting diodes for street lighting and novel technologies for "white goods" like refrigerators and washing machines. Similar analysis exists for different industries like the iron and steel ones [30] or the automotive one [31]. Figure 1.3 shows emissions abatement scenarios up until the year 2035. It can be seen how CO_2 emissions will be above 36 Gt by that time and how the different abatement strategies are predicted to reduce this num-

ber below 22 Gt. Clearly, different technologies will contribute to that with energy efficient technologies accounting for almost half of the overall abatement between 2010 and 2035.

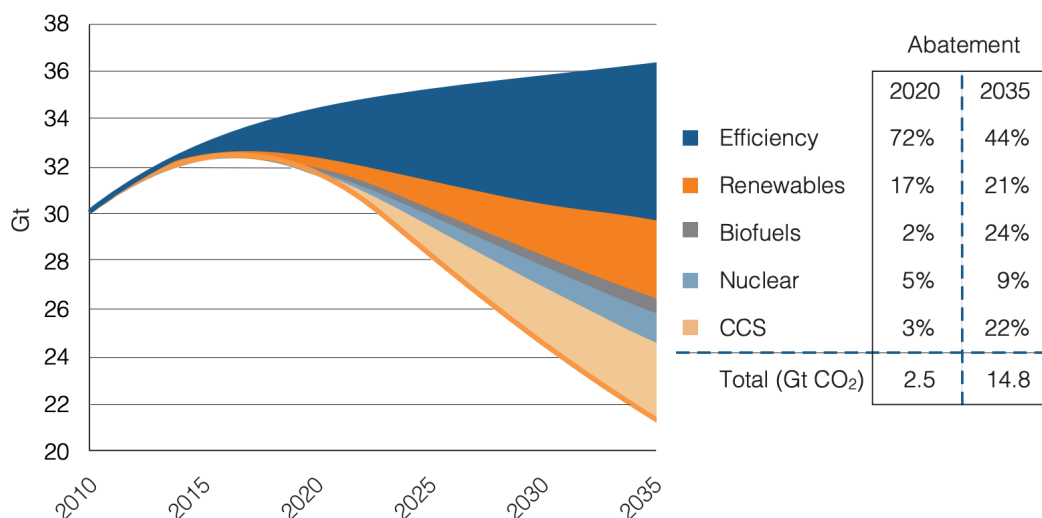


Figure 1.3: CO₂ emissions abatement scenario [3]

1.2.2. Carbon capture, storage and utilisation technologies

The ability of capturing and, eventually, using or storing CO₂ includes a series of different processes for CO₂ capture, separation, storage and monitoring [32]. Multiple technologies are, therefore, involved in this overall process.

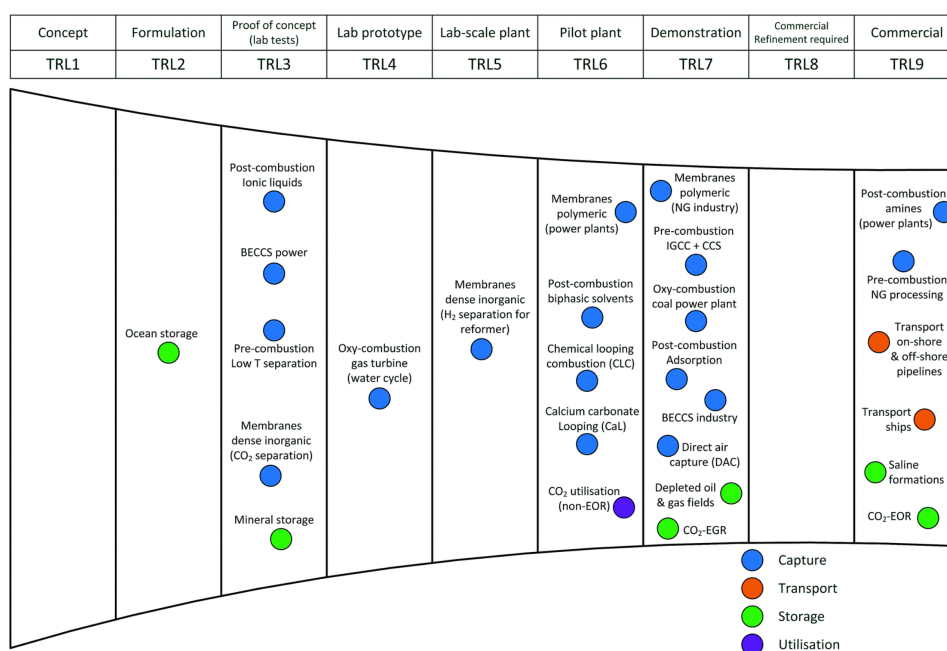


Figure 1.4: Overview of TRL for multiple technologies involved in CO₂ mitigation [4]

Figure 1.4 gives an overview of the current development in these technologies on the TRL (technology readiness level) scale. As it can be seen, multiple CO₂ capture technologies are already well established (TRL of 9) as well as ways for transporting the captured gases. The use of post-combustion amines is particularly relevant to this thesis project since amines are the sorbent used to pursue the investigation. Having a TRL of 9, multiple commercial-scale post-combustion facilities using amines to

capture CO_2 already exist like the Petranova facility in the U.S. [33].

Regarding the storage of carbon dioxide, an increasing interest is placed in using geological formation having otherwise no other practical use [32]. Prior to a proper selection, geological formations can hold up to tens of millions tonnes of CO_2 [34]. On the other side, some projects are focusing on using the captured flue gases to produce higher value products like in the production of urea and methanol [35] or to help with the cultivation of crops and algae [36].

1.3. The case of ZEF (Zero Emission Fuels)

This research project is conducted on behalf of Zero Emission Fuels (ZEF B.V.). This start-up, located in the Process & Energy laboratory of the TU Delft and in close collaboration with both the university and TNO, has the ambitious goal of engineering a micro process plant able to produce zero emission methanol using sunlight and air as its only inputs. The company is based on the concept of numbering up rather than scaling up. That allows the installation of multiple micro farms in convenient low cost locations where there is abundance of sun light [37].

The concept of the micro farm consists in a modular design of four different subsystems each one powered by electricity coming from solar panels. Figure 1.5 shows an overview of the micro plant conceptual design.

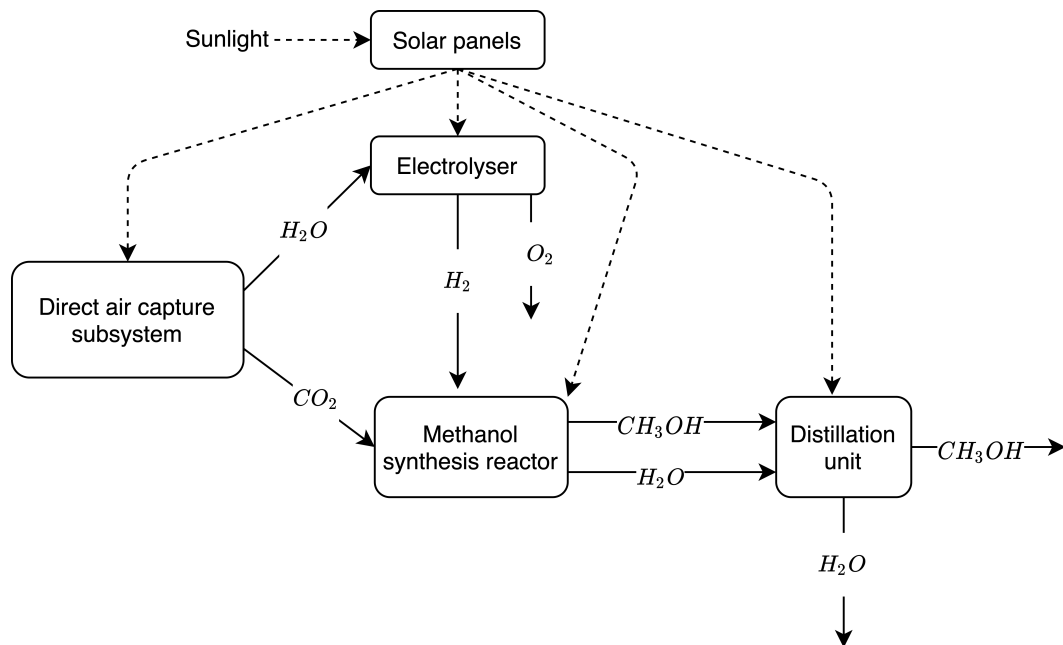


Figure 1.5: ZEF microplant concept [5]

A brief explanation of the four subsystems is given below:

- **Direct air capture subsystem:** This system is composed of an absorption and desorption part. CO_2 and H_2O are directly captured from air by an amine based absorber, while the desorption side separates the captured gases and sends them to a methanol synthesis reactor (CO_2) and an electrolyser (H_2O) for further processing.

- **Electrolyser:** The water captured by the absorption system is split into oxygen and hydrogen via the following reaction:



Oxygen is released into the atmosphere, while hydrogen is sent to the methanol synthesis reactor.

- **Methanol synthesis reactor:** This subsystem is capable of synthesising the main product methanol (CH_3OH) and by-product H_2O .

- **Distillation unit:** Finally, the products of the methanol synthesis are further processed by the distillation unit which separates methanol and water to obtain a methanol of up to 99.8% purity.

The research pertaining to this thesis is based on the Direct Air Capture (DAC) subsystem. Currently, ZEF is developing that system based on the temperature-swing-absorption principle. The process is carried with the use of two different subsystems: the absorption and desorption stages. This project is focused on the absorption part of the system.

The goal of the absorption stage is to capture a certain amount of CO_2 and H_2O using a specific type of amine: TEPA (Tetraethylenepentamine). This sorbent is flown over a plate at a certain mass flow rates. When TEPA is exposed to air, it will capture water and carbon dioxide.

Being a novel absorption process, different challenges were identified in previous research at ZEF [38], [14]. The main findings from ZEF's research, their systems and how that influences this research project are reviewed in greater detail in Chapter 2, but here is a collection of different aspects of the process that are currently being investigated:

- It seems that CO_2 diffusion into the amine happens with a very low diffusion coefficient. Therefore, the process seems to be diffusion limited. In particular, when the sorbent flows inside a channel, only the layer of sorbent in contact with the free air seems to be loaded with water and carbon dioxide. Therefore, it seems necessary to induce a form of mixing to change the layer of sorbent in contact with the stream of air.
- Very few channel geometries have been tried for the absorption process. Due to the huge surface tension effects on the flow, the absorption performance may vary significantly when changing the geometry of the channel. Therefore, an optimum channel geometry which reduces the amount of the sorbent necessary for obtaining a certain amount of CO_2 and H_2O should be investigated.
- ZEF is planning on installing micro plants in different regions in the world having very different atmospheric conditions. However, the effect of different environmental relative humidities and temperatures on the absorption performance are still to be investigated.
- The absorption subsystem has not been modelled yet. Ideally, the model would consist of a fluid dynamic part to describe how the sorbent is flowing on the plate and a mass transfer part to understand the absorption of water and carbon dioxide from ambient air. Eventually, coupling those two models, one could obtain a full description of the process.

The above-listed challenges constitutes part of the background of this thesis project. From those, a series of research questions and research goals are defined and mentioned in the following section.

1.4. Research goals and objectives

The aim of this thesis is to study, understand and improve a DAC absorption process. The research is based on a novel process developed by ZEF. The relevant research questions are collected below:

1. In a continuous absorption process where a viscous polyamine flow is driven by gravity on an absorption channel, **is it possible to circulate particles from the top surface of the channel into the bulk of the flow?**
 - **Are absorption performances of the channel improved because of that?**
2. Previous research underlined how the process is diffusion limited. **How is that happening at a molecular level?**

The listed research questions are answered by achieving certain goals in the experimental and modelling part of the thesis. These are:

- **Induce mixing in the absorption process.** That includes the design and fabrication of one or more experimental setups where mixing experiments can be performed.
- **Model the fluid dynamics and mass transfer aspects of the absorption process.**

Reaching the goals and answering the research questions is in the framework of **proposing an iteration of ZEF's current absorber** that satisfies the requirements collected in table 1.1.

Requirement	
Operational rich loading $[mol_{CO_2}/kg_{TEPA}]$	>2
CO_2 capture rate $[g_{CO_2}/8 hr]$	>825
H_2O capture rate $[g_{H_2O}/8 hr]$	>2475

Table 1.1: Absorption column requirements

1.5. Thesis overview & report outline

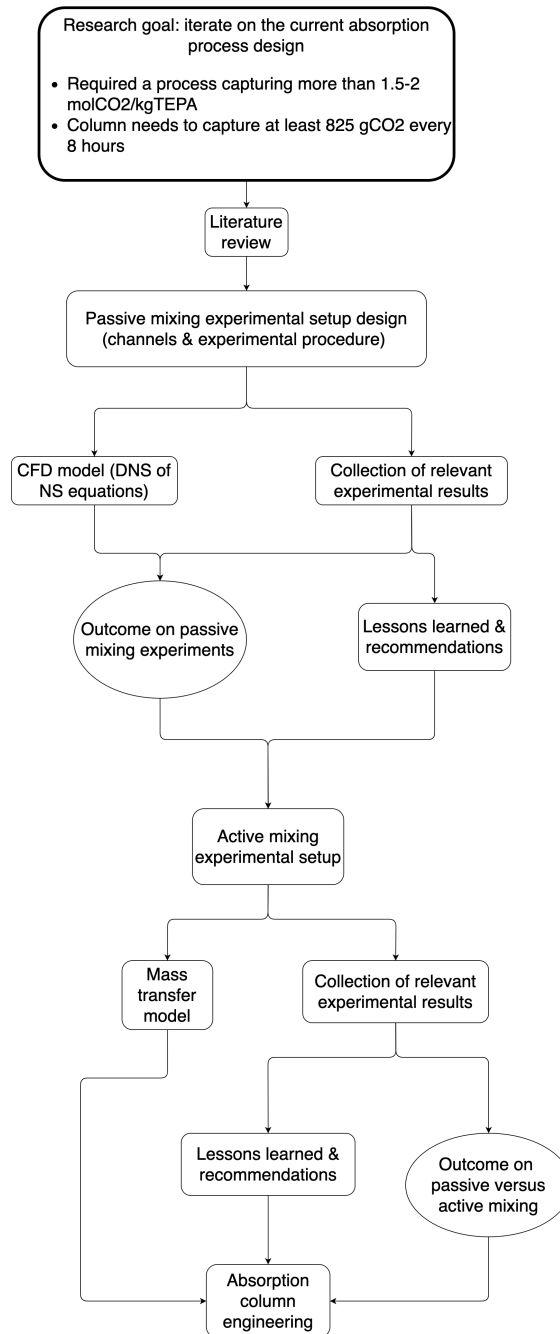


Figure 1.6: Thesis flow chart

This thesis project lasted several months, different models were developed and multiple aspects of the absorption process were investigated. **Figure 1.6 shows an overview of the different tasks of this project in the order they were tackled.**

After a literature investigation, passive mixing experiments were designed and performed in order to evaluate how absorption can be influenced by that. A CFD model based on direct numerical simulation (DNS) of Navier Stokes (NS) equations was coded in Matlab to simulate the fluid dynamic aspects of the flow of TEPA in channels engineered for passive mixing. That brought to an overall evaluation of this mixing strategy and, in turn, to the design of new experiments investigating active mixing instead. After that, a mass transfer model was developed based on a detailed theoretical framework: the "Ice Sheet Layer" theory. This mass transfer model was validated using data collected in active and passive mixing experiments and finally used to engineer an absorption column able to satisfy the original absorption requirements.

This report starts with a summary of relevant knowledge available in literature. Chapter 3 and 4 describe the experimental investigation and the models developed with it. The mass transfer model is based on a very specific physical interpretation that is described in chapter 5. Basically, justification of why the mass transfer is modelled in a certain way is given after the description of the model itself. Together with that, chapter 5 is all about collecting the main results and giving the main interpretations for the observed phenomena. Finally, in chapter 6, the engineering of the absorption column iteration is described and chapter 7 collects the main recommendations for continuing this research in the future.

Literature review

This chapter provides the review of relevant literature concerning this thesis project. In particular, focus is given on the problem of capturing CO_2 in industrial applications as well as how team ZEF has approached and is currently approaching that. Efforts from previous teams are described to give a framework on which this thesis is based. Firstly, a general overview on industrial CO_2 capture from flue gases is given and two technologies are described in more details: absorption and adsorption. The first one is particularly relevant for this project, therefore both the theory behind it and the industrial applications are reviewed. For the second one, only different industrial applications are considered.

After that, the specific problem of direct air capture (DAC) is reviewed both at industrial level and in the specific case of ZEF. With that, the main characteristics of the sorbent used in the experimental investigation, TEPA, are described. Finally, mixing strategies for very viscous flows at very low Reynolds number is reviewed. The chapter is concluded by listing relevant lessons learned.

2.1. CO_2 capture in industry

Even though the focus of this thesis project is placed on DAC technologies, that only constitutes one among the different methodologies for reducing the amount of carbon dioxide in the atmosphere. The broader picture involves the capture of CO_2 directly within the gas emitting power plant.

Since the idea of this thesis is to propose means for improving a novel CO_2 capture process, **looking also at technologies different than DAC is considered to be relevant to understand all the different ways with which ZEF's process could be improved.**

Sifat and Haseli provide an extensive overview of existing CO_2 capture technologies in fossil fuel-based power plants [39]. Their investigation can be summarized with figure 2.1.

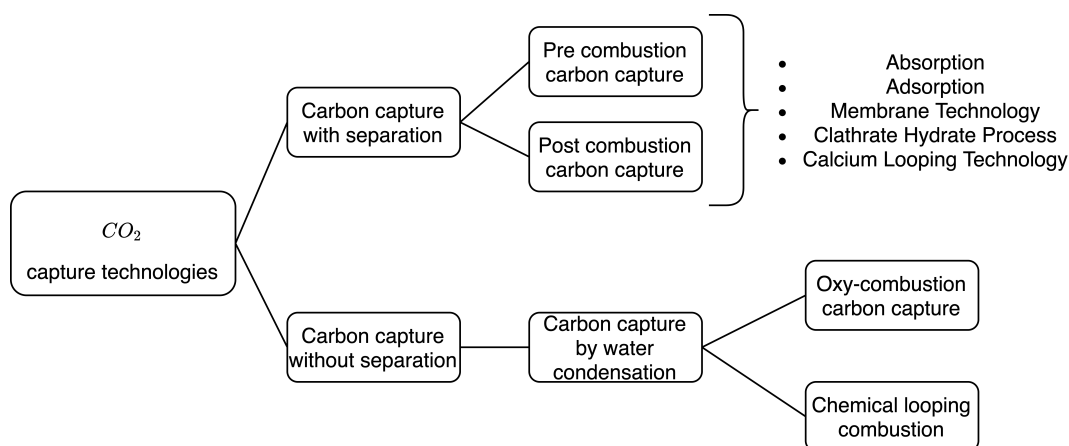


Figure 2.1: Overview of carbon capture technologies within power plants

Among the separation technologies, absorption is presented as the most mature one [39] [40],

although attention toward equipment's corrosion and solvent's regeneration cost still needs to be fully addressed. Moreover, the real environmental impact requires further studies.

In general, post combustion carbon capture technologies can be applied to already existing power plants, without the need of disrupting the existing plant layout. In pre-combustion carbon capture, the fossil fuel is further processed before combustion. That involves the formation of syngas (a mixture of mainly CO and H_2) at high pressure. The CO_2 that is formed in the process can be easily separated because of the high pressure [41]. Once that is done, a fuel containing mainly hydrogen is combusted, thus significantly reducing the formation of CO_2 as exhaust of the combustion process.

A novel approach in CO_2 capture during power generation consists in burning the fossil fuel with pure oxygen instead of air. The result is that the combustion products will mainly consist of CO_2 and steam. Eventually, by simple water condensation, it is possible to capture the exhaust CO_2 . Most commonly, pulverized coal is combusted together with (almost) pure oxygen and recycled flue gas [42].

Among all the different technologies for carbon capture with separation, it is believed that absorption and adsorption technologies are currently the most suitable ones for use in power plants [43]. In this framework, the challenges to integrate the carbon capture technology into the power plant mostly regards the type of sorbent to be used and/or the type of equipment to perform the CO_2 capture efficiently and at a reduced cost. Those type of challenges are present in the DAC case as well and, as a consequence, in this thesis project. Therefore, specific focus is placed in reviewing means for capturing CO_2 in power plants with the use of either absorption or adsorption technologies.

2.1.1. Absorption technologies - Theory & Industrial Application

Due to the nature of this thesis project, **it is crucial to understand how absorption of gases by liquids works.** Firstly, the physics and chemistry governing the problem are studied, then focus is given in reviewing the main types of industrial absorption technologies.

Theory Gas absorption is a topic which covers multiple disciplines of engineering like fluid mechanics, molecular diffusion and chemical reaction kinetics. Therefore, it is no easy task to underline all the relevant aspects in a typical absorption process.

A pioneer paper in convective mass transfer theory comes from W. G. Whitman in 1923 [44]. The author underlines the lack of a solid theoretical framework capable of handling the nature of every gas-liquid absorption process. Since then, multiple papers were published in this field. Danckwerts [45] propose to focus on the specific case of absorption of carbon dioxide since the kinetics of the reaction accompanying the process are relatively well understood.

Among the models available at that time, he chooses to focus specifically on two of them. The first one, the **"film" model**, was firstly introduced by Nernst in 1904 [46]. According to that model, a liquid flows over a surface while it is kept thoroughly mixed by turbulence in the bulk. However, in the immediate neighbourhood of the free surface (the surface where the gas contacts the liquid), turbulence is reduced enough to leave a very thin film which can be considered to be stagnant. Molecules can pass through that film only by molecular diffusion. On the other hand, a **"surface renewal" model** assumes that part of the liquid particles on the free surface are periodically replaced by fresh liquid brought up from the bulk of the layer [47]. The replaced surface absorbs faster since the concentration of the solute is smaller. Thus, this model assumes that the free surface on the liquid side is a mosaic of elements which have been in contact with the gas phase for different amount of time and which will have, therefore, different absorption rates. The distribution of the exposure times gives the distinction between the different surface renewals models [48] [49]. A particularly relevant one was proposed by Higbie and better known as the penetration theory [50]. Perhaps the most simple surface renewal theory, the model assumes that all the eddies reaching the surface are in contact with the interface for the same amount of time. These two main theories, the film theory and the surface renewal theory, are illustrated in figure 2.2.

These models can be applied to the two different absorption processes: physical and chemical absorption. The first one implies that absorption happens without any chemical reaction taking place, while, in the second one, gases are absorbed into liquids with which they chemically react. When dealing with a chemical absorption process, the situation suddenly becomes quite complex since the reactants concentrations are usually not uniform due to the fact that chemical reactions happen simultaneously with the diffusion process. Therefore, making useful predictions becomes quite a challenge [45]. **Modelling of the chemical absorption process is, therefore, considered to be outside the**

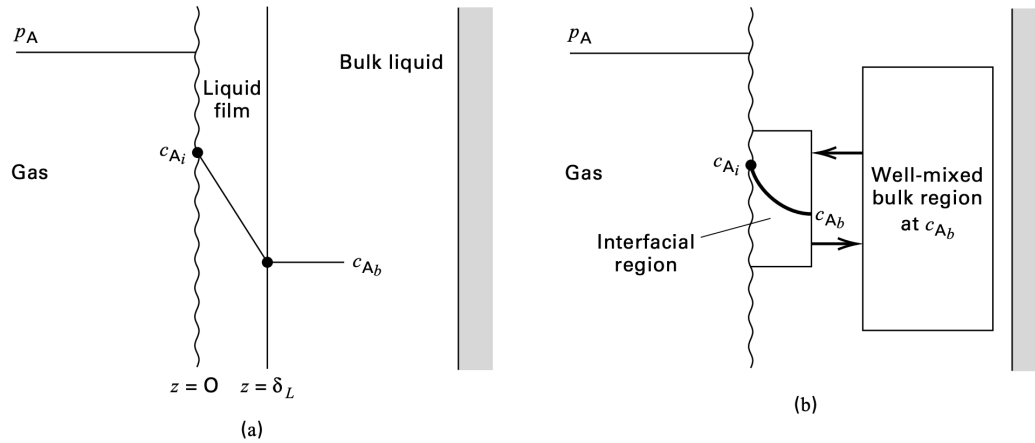


Figure 2.2: Mass transfer models: a) film model; b) surface renewal model [6]

scope of this literature review. However, it is **still interesting to look into mathematical expressions describing the physical absorption process instead.** According to the two models mentioned before, the physical absorption process can be described by the two equations below, the first one according to the film model and the second one to the surface renewal model:

$$N_A = \frac{D_{AB}}{\delta} (c_{A_i} - c_{A_b}) = \frac{cD_{AB}}{\delta} (x_{A_i} - x_{A_b}) \quad (2.1)$$

$$N_A = \sqrt{\frac{D_{AB}}{\pi\tau}} (c_{A_i} - c_{A_b}) \quad (2.2)$$

Where:

- N_a is the instantaneous molar transfer per surface area $\left[\frac{\text{mol}}{\text{m}^2\text{s}}\right]$
- D_{AB} is the diffusivity of specie A into specie B $\left[\frac{\text{m}^2}{\text{s}}\right]$
- δ is the film thickness $[\text{m}]$
- c_{A_i}, c_{A_b} is the concentration of specie A at the interface and bulk respectively $\left[\frac{\text{mol}}{\text{m}^3}\right]$
- x_{A_i}, x_{A_b} are dimensionless concentrations at the interface and bulk respectively
- c is a volumetric concentration factor $\left[\frac{\text{mol}}{\text{m}^3}\right]$
- τ is the characteristic time related to the exposure of particles at the interface due to surface renewals $[\text{s}]$

Referring to figure 2.2, mass is transferred from the gas phase A into the liquid phase B . Phase equilibrium is assumed at the interface so that c_{A_i} is related to the solubility of A in the liquid phase. Therefore, solubility relations like Henry's law can be used to estimate c_{A_i} :

$$c_{A_i} = H_A p_A \quad (2.3)$$

Equation 2.3 indicates that the concentration at the interface is related to the partial pressure of specie A in the gas bulk p_A times a solubility constant like, for instance, the Henry constant H_A . Looking at equation 2.1, it is general practice to replace the ratio $\frac{D_{AB}}{\delta}$ with an empirical mass transfer coefficient, k_c , in $\left[\frac{\text{m}}{\text{s}}\right]$ obtaining 2.4

$$N_A = k_c c (x_{A_i} - x_{A_b}) \quad (2.4)$$

In this thesis, k_c and c are grouped in a term referred to as the Space-Time Yield (*STY*) and having units $\left[\frac{\text{mol}}{\text{m}^2\text{s}}\right]$. Therefore, the general equation used to describe the mass transfer in the notation of this project is:

$$N_A = STY \cdot (x_{A_i} - x_{A_b}) \quad (2.5)$$

Both film theory and surface renewals theories assume a proportionality with respect to the diffusivity of the solute into the liquid solvent D_{AB} . Here the two models diverge since **the film model predicts the rate of mass transfer to be proportional to D_{AB} , while the surface renewals model to $\sqrt{D_{AB}}$** . Moreover, both models assume a proportionality with respect to the driving force $(c_{A_i} - c_{A_b})$.

Since gas-liquid absorption processes involve a multi phase contact, it is important to consider mass transfer resistances coming from both phases as suggested by Whitman in 1923 [44]. He proposes an **extension of the film theory that considers two films in series instead of a single one**.

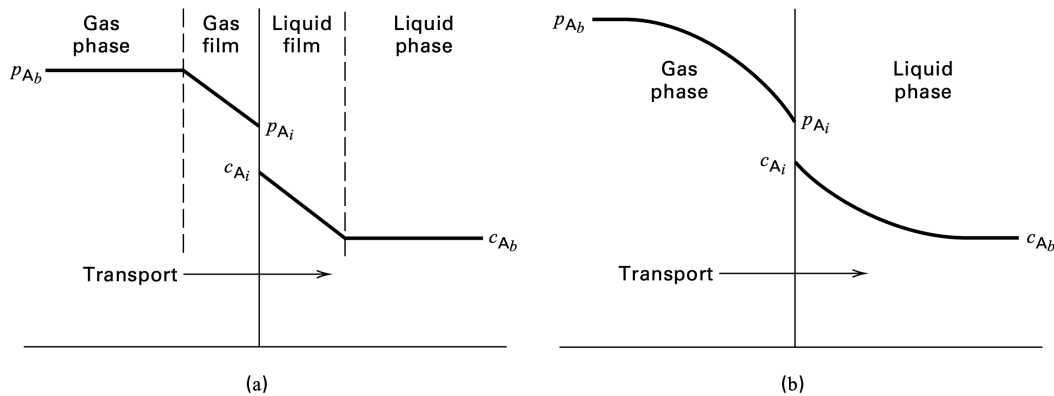


Figure 2.3: Two film theory with a) ideal and b) more realistic concentration gradients [6]

Looking at figure 2.3, one can write an equation including an **overall mass-transfer coefficient** which accounts for resistances coming from both the liquid and gas phases.

$$N_A = K_L (c_A^* - c_{A_b}) \quad (2.6)$$

$$\frac{1}{K_L} = \frac{H_A}{k_p} + \frac{1}{k_c} \quad (2.7)$$

where

- K_L is the overall mass transfer coefficient based on the liquid phase $\left[\frac{\text{m}}{\text{s}}\right]$
- c_A^* is a fictitious liquid phase concentration of A that would be in equilibrium with the bulk gas phase $\left[\frac{\text{mol}}{\text{m}^3}\right]$
- k_c and k_p are mass transfer coefficient driven by variations in concentration (for the liquid phase) and pressure (for the gas phase) respectively $\left[\frac{\text{m}}{\text{s}}\right]$
- H_A is the Henry's constant for relating the concentration of specie A at the interface with the partial pressure of specie A in the gas bulk

A similar expression can be obtained for an overall mass transfer coefficient based on the gas phase. Clearly, the equation for the mass transfer takes into account the difference in partial pressure of the gas phase as the driving force [6].

One can imagine a simplification of equation 2.7 when the conditions in the absorption process make one of the two films more relevant with respect to the other one. In this way, it is possible to simplify the mathematical treatment of the problem. **A year after proposing the two film theory, Whitman pointed out how the importance of the two films in the absorption process depends mainly upon the solubility of the solute [7].**

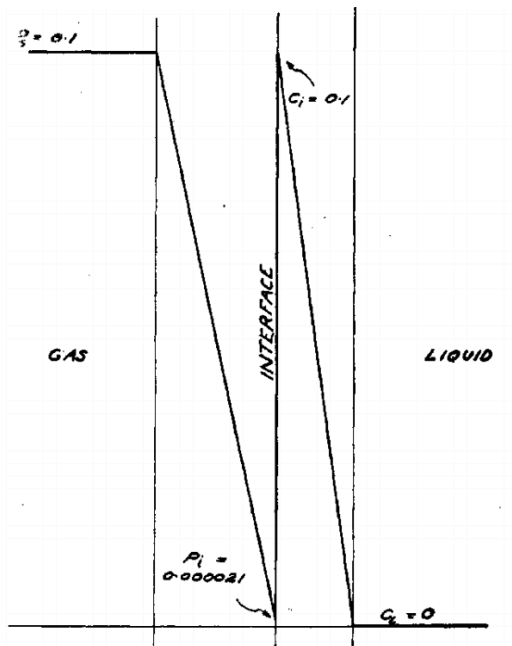


Figure 2.4: Very soluble gases [7]

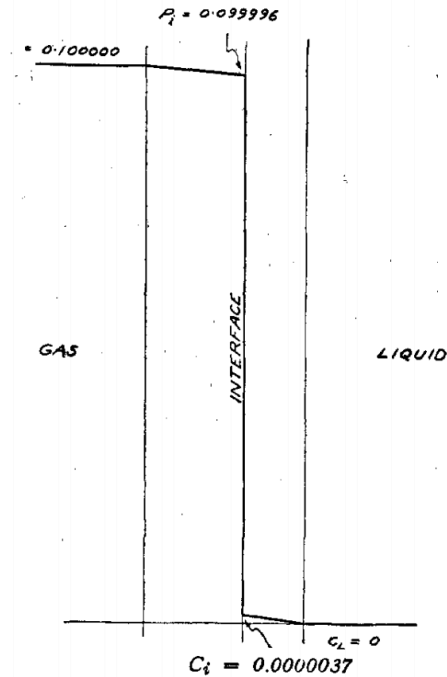


Figure 2.5: Low solubility gases [7]

He distinguishes three different cases:

- **Very soluble gases.** In this case, once it reaches the surface of the liquid, the gas is rapidly moved into the liquid film, thus generating a very high gradient of concentrations across the interface. In figure 2.4, a sudden rise in concentration at the interface is shown because even a very low partial pressure at the interface is in equilibrium with a quite high concentration in the liquid phase due to the great affinity of the gas with the liquid. In this case, the mass transfer through the gas layer is limiting the process and the resistance of the liquid film can be ignored.
- **Low solubility gases.** With this type of gases, the rate of absorption is low because of the low tendency of the gas to dissolve at the interface. For that reason, only small concentration differences can be established across the liquid film. Moreover, since a very low amount of particles are crossing the interface, the drop in partial pressure across the gas film is very limited as shown in figure 2.5. When that is the case, the gas phase can be ignored in the calculations since the limit to the process comes from the liquid phase.
- **Intermediate solubility gases.** There are cases where the solubility of the gas is not high enough to permit disregarding of the liquid phase, but not low enough to accept disregarding of the gas phase. In that case, one should refer to equations 2.6 and 2.7 for a mathematical treatment of the problem.

Absorption in industry The previously discussed theory can be applied to the absorption of any gas by a liquid. **In this section, the specific case of CO₂ absorption in industry is reviewed.** Once again, the different technologies for CO₂ absorption can be divided into two different classes: physical and chemical absorption [43].

In physical absorption, based on Henry's law, CO₂ is absorbed at high pressure and low temperature in order to increase the gas solubility, while desorption happens at the opposite conditions of low pressure and increased temperature. Chiesa et al. [8] propose a **re-engineering of an Integrated Gasification Combined Cycle (IGCC)** with minimal changes to the gas turbine (figure 2.6).

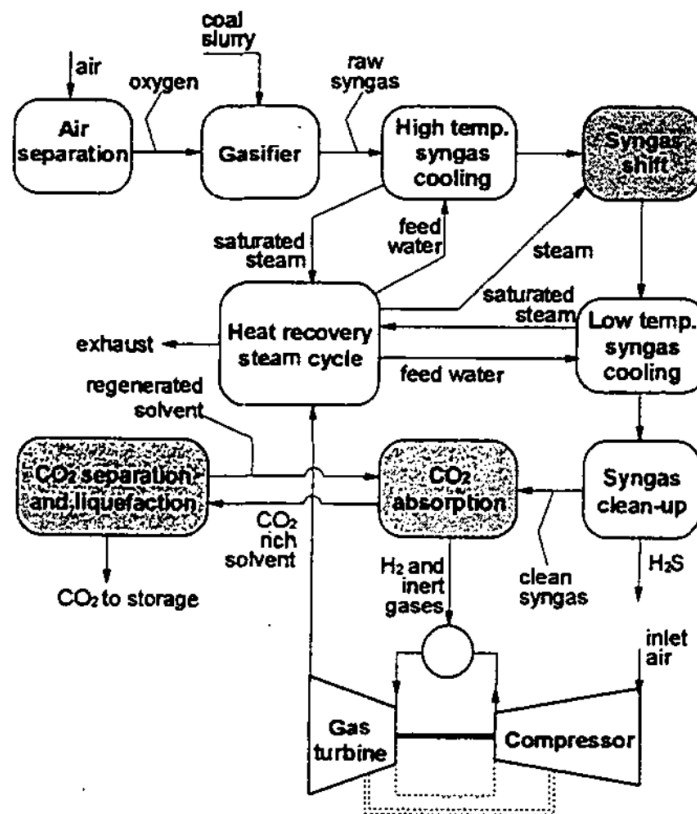
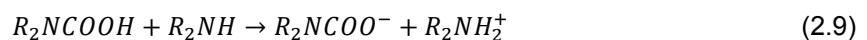


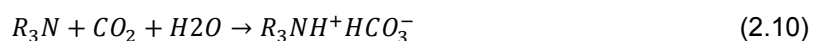
Figure 2.6: IGCC equipped for CO_2 physical absorption. The components added to the cycle are in black [8]

After cooling the syngas, the shift reactor converts almost all the CO into CO_2 so that the physical absorption unit can dissolve efficiently the gas with a Selexol process. When that is done, the gas can be prepared for transportation and storage into a separation and liquefaction unit. 90% CO_2 emissions reduction are predicted with, however, an overall increase of the electricity cost of about 45%. Even though many commercial physical absorption processes exist [43], Selexol process can be used to separate both CO_2 and H_2S under a low temperature operation [51].

On the other hand, for **post combustion CO_2 absorption**, an absorber and a stripper are used to chemically capture CO_2 from the flue gases. In this configuration, a CO_2 absorbent is used in a packed bed where the flue gases are sent counter-currently in order to remove the gas. When that is done, the CO_2 rich absorbent flows into a stripper for thermal regeneration and, after that, is pumped back into the packed bed for further absorption. **This type of technology generally uses alkanolamines as absorbent.** These include primary, secondary and tertiary amines and, among them, the more widely used are monoethanolamine (MEA) and diethanolamine (DEA). The chemistry of reaction between CO_2 and primary, secondary and tertiary amines has been extensively studied due to the huge potential of alkanolamines as an absorbent for CO_2 capture [52], [53], [54], [55]. Relevant publications regarding the reaction mechanism are from Caplow [56] and Danckwerts [57]. they explain how, in primary (RNH_2) and secondary (R_2NH) amines, a **two step reaction** occurs in the absorption of CO_2 . In the first one (eq: 2.8), an amine group reacts with a CO_2 molecule to form a zwitterion molecule. In the second reaction (eq: 2.9), the zwitterion will react with a free base (either water or another amine group) to form carbamate. The reaction equations are shown for secondary amine groups:



On the other hand, tertiary amines (R_3N) react differently with CO_2 . In fact, they cannot form carbamate due to the absence of a free proton [52]. Instead, bicarbonates are formed (equation 2.10):



Loading capacity is different for the different amines lying between 0.5-1.0 mole of CO_2 per mole of amine for primary and secondary groups and being 1.0 mole of CO_2 per mole of amine for tertiary amines [43]. Because of the different advantages of the various amine groups, mixed amines can be used to increase CO_2 loading capacity and reduce regeneration costs in the stripper.

More recently, other types of sorbent that can be used to capture CO_2 both physically and chemically, are Ionic Liquids (IL). Their usage has attracted a lot of attention due to their particular properties such as negligible vapor pressure and high affinity with the CO_2 gas [58]. For these reasons, research has focused on describing CO_2 solubility for different ILs studying the influence of temperature, the presence of other gases and trying to describe the various reaction mechanisms [59]. Particularly relevant is the use of IL in chemical absorption. In fact, Task-Specific Ionic Liquids (TSIL) able to act selectively in CO_2 absorption can be synthesized. Bates et al. [60] report that TSIL can chemically absorb three times as much CO_2 than a simple IL in a physical absorption process.

2.1.2. Adsorption technologies - Industrial Application

An alternative to aqueous amines absorption is the use of a solid adsorbent in order to achieve the wanted CO_2 loading. A huge advantage in using solid adsorbents is given by the high diffusion of the gas within the mesoporous adsorbent. That is reported to be three orders of magnitude higher than that for amine-based adsorbents [61]. However, before practical application of adsorption technologies becomes feasible, research still needs to address problems related to low CO_2 adsorption capacities at low pressure and contaminants' influence on the process [43].

Carbonaceous adsorbents are an example of physical adsorbent widely used due to their low cost, high thermal stability and wide availability [43]. As specified before however, this technology presents major drawbacks related to their ability of only treating high pressure gases. That makes it very difficult to use them in post combustion processes, thus severely limiting their application in treating flue gases. Of more interest are amine-based chemical adsorbents. Compared to aqueous based amines, they provide for a lower heat of regeneration due to the low heat capacity of the solid supports. Those types of adsorbents can be classified based on the interaction between the amine and the support as amine-impregnated and amine-grafted materials [62]. The first category exhibit a higher amine loading, while the second one performs better in terms of adsorption rate [43]. Moreover, a large diffusion resistance is reported for impregnated materials [63].

2.2. Direct Air Capture (DAC)

While capturing CO_2 directly from the source of emission like industrial power plants might seem a good solution, it must be considered that **about half of the anthropogenic CO_2 emissions come from small and distributed sources like houses and cars** [26]. Moreover, while the capture from high concentration sources can only decrease the carbon addition to the atmosphere, **capturing CO_2 from the air could potentially be used to achieve negative CO_2 "emissions"**. Finally, a Direct Air Capture (DAC) facility, could be installed in any part of the world since a local buildup of depleted CO_2 is very unlikely and no contaminants like NO_x and SO_x are present in air compared to flue gases [64].

For these and other reasons, companies like ZEF are looking with increasing interest in DAC technologies. **In this section, the main industrial solutions for CO_2 capture from the atmosphere are reviewed.** Special focus is given in describing the way that ZEF has approached the problem in past years to give a background on which this thesis project is based.

2.2.1. DAC in industry

Ambient air contains around 400 ppm (by volume) of carbon dioxide against 100,000 to 150,000 ppm by volume of an average coal power plant [65]. Therefore, it is reasonable to expect that, while for conventional capture from flue gases, it can be advantageous to modify the incoming flue gases for better CO_2 capture, that is not the case for DAC systems [66]. This excludes all capturing technologies that put energy into the air like heating, cooling or pressurizing.

Brohem et al. [67] divides the currently available DAC technologies in three different categories based on their operating mediums:

- Aqueous solutions of strong bases,
- Amine adsorbents

- Inorganic solid sorbents

It is specified how the first approach is the more developed one for near-term implementation compared to the other two. The same classification is used here to review DAC technologies.

Aqueous Solutions of Strong Bases Aqueous solutions suggested for DAC systems include strong bases like sodium hydroxide ($NaOH$), potassium hydroxide (KOH) and calcium hydroxide ($Ca(OH)_2$). In a so-called contactor, these solutions are brought into contact with a flow of air in order to take up CO_2 . Since the gas is chemically bonded to the solution, a regeneration process is needed to return the solution to its useful lean state [67]. In this way, three are the critical components in the system: the solution, the contactor and the regeneration system.

For example, a realistic design for a plausible DAC system using KOH as solution is provided by Keith et al. [9]. Their system consists of two cycles connected in a loop (figure 2.7).

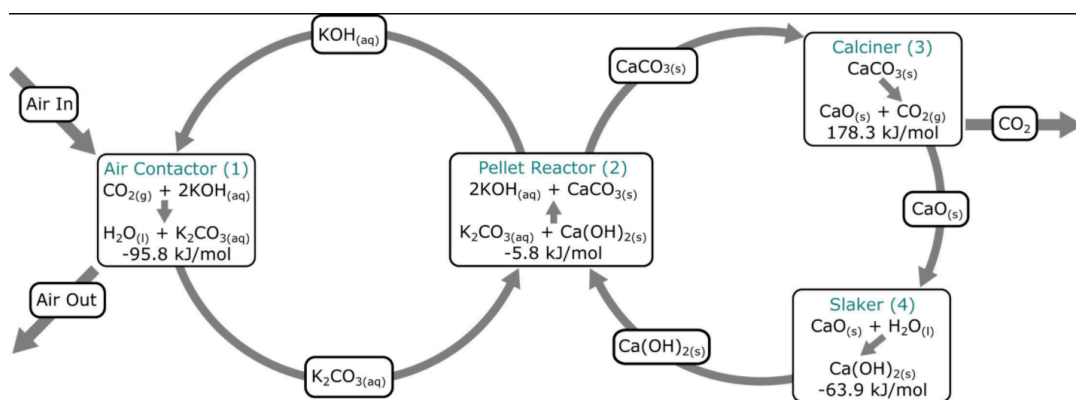


Figure 2.7: Example of a DAC system using a KOH solution [9]

The first cycle uses the alkali capture fluid to chemically bond CO_2 in an aqueous solution of K_2CO_3 . After that, the solution is sent to a causticizer reactor together with calcium hydroxide in order to recover the potassium hydroxide and to form calcium carbonate ($CaCO_3$). The now lean KOH is sent back to the air contactor for further absorption, while the $CaCO_3$ goes in a calciner for CO_2 release. The byproduct of the reaction is a solid calcium oxide (CaO) which is finally reacted with water in a slaker to produce the calcium hydroxide needed in the pellet reactor. The calciner unit needs temperature of up to 900 °C to release CO_2 . This contributes to an overall energy demand of 1420-2250 kWh per ton CO_2 for this system [10]. Moreover, oxygen is used in order to provide enough heat for the process introducing extra CO_2 that needs to be separated again [9]. This process bottleneck is present in systems using sodium hydroxide instead of potassium hydroxide as well [64].

Amine Adsorbents The use of amines for CO_2 capture is not only interesting for applications in large power plants, but also for DAC systems. In particular, their regeneration process follows different and advantageous thermodynamic rules compared to the aqueous bases. That is, they can be regenerated by multiple means including pressure, temperature and humidity and some of them do not require large temperature swings for regeneration [67].

In a typical system, ambient air is either naturally driven or moved through the CO_2 capturing device with the help of fans. This process occurs at ambient conditions and continues until the adsorption unit is fully saturated with the gas. CO_2 poor air leaves the system and, when this phase is over, the fans are switched off and the system is prepared for the regeneration step. Depending on the adsorbent, the system is generally heated to a certain temperature so that CO_2 and H_2O can be collected, transported and purified in a different section of the DAC plant. A good illustration of this process is shown in figure 2.8.

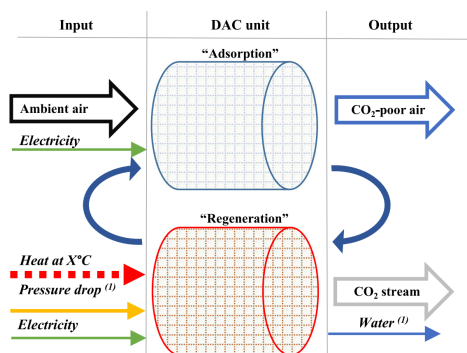


Figure 2.8: Example of a process using amine adsorbents [10]



Figure 2.9: The Climeworks DAC unit

Some companies are already actively proposing systems applying this type of solution. A Swiss company named **Climeworks** uses a composition of cellulose fibers and amines as a filter for the adsorption unit [68]. Being powered by renewable energy only, their collectors can be stacked to build machines solely powered by renewable energy (figure 2.9). Another company worth mentioning is the **American Global thermostat** [69] proposing a full cycle time of less than 30 minutes and a regeneration temperature below 100 °C.

Being novel technologies, a lot still needs to be addressed and skepticism exists related especially to the longevity of the amine used and the fact that a low concentration of carbon dioxide in the atmosphere massively increases the energy requirements of the DAC plant since a lot of unused gas still needs to be pushed through the system [70].

Inorganic Solid Sorbents The study of materials to be used in DAC systems under various conditions, includes also solid materials like zeolites and *Na* or *Ca* based solids [67].

In dry air, some zeolites can be used for CO_2 adsorption. For instance, a lithium low silica type X zeolite (*Li-LSX*) employed in a fixed-bed adsorber is shown to reach an adsorption capacity of up to 1.34 mol of CO_2 per kilogram of adsorbent [71]. In desorption, a combination of temperature swing adsorption (TSA) and vacuum swing adsorption (VSA) is used to achieve a CO_2 concentration higher than 93%. However, in line with what observed from zeolites, the same authors specify a huge decrease in adsorption capacity of the zeolite when increasing environmental relative humidity.

The use of sodium or calcium based inorganic solids is studied by the group of Nikulshina in multiple papers [72], [73]. All discussed processes involving the use of *Na*-based sorbents include a carbonation reaction when extracting the CO_2 gas. The slow reaction kinetics for carbonation is described as the main limiting factor in making the process technically and economically viable due to the very high sorbent mass flow rate that would be needed for capturing a reasonable amount of CO_2 per unit of time (1 mol per second). On the contrary, *Ca*-based cycles show a more favourable reaction kinetics at the expenses of a higher reaction temperature with respect to *Na*-based cycles. A solution proposed by the same research group involves the use of concentrated solar energy to drive the necessary reactions [73].

2.2.2. DAC at ZEF

Zero Emission Fuels has been actively researching the best way for capturing CO_2 and H_2O within their micro plant for methanol production. Over the years, multiple teams have produced a series of more or less successful prototypes that gave the opportunity for learning a series of important lessons that are reflected in the various iterations of the absorption system designs, including the latest one, which this thesis project aims to further improve.

In this section, an overview of the different prototypes is given in order to underline previous efforts relevant to this project.

ZEF's DAC prototype 1 As reviewed before, adsorption with solid materials impregnated by polyamines can be used for direct air capture. In the first prototype, developed by February 2018, **polyethylene-**

neamine (PEI) impregnated on a silica-based material constituted the adsorption packed bed. the prototype consisted of two of those packed bed to be used alternatively for desorption and adsorption in order to have a continuous capture and release of CO_2 and H_2O [74]. The process is based on a temperature-vacuum swing operation. During a 1 hour adsorption window, a fan is used to suck the air into one of the two chambers. After that, the impregnated material is considered to be fully loaded and the chamber is closed so that the desorption step can start. In that, the chamber is sealed, vacuumed to 0.1 bar and heated to about 120 °C in order to release the useful products [74]. Figure 2.10 shows an isomeric view of the prototype.

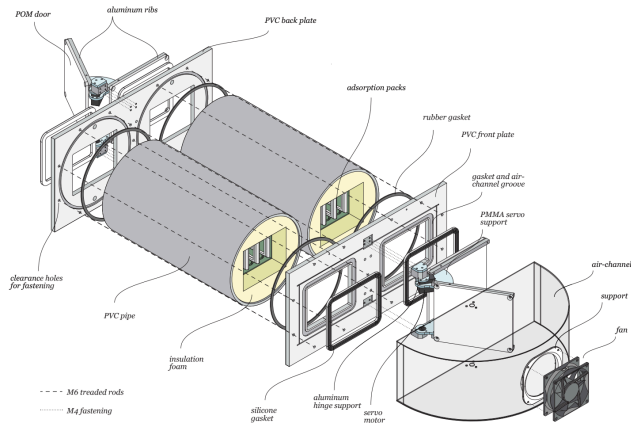


Figure 2.10: ZEF's DAC prototype 1 [11]

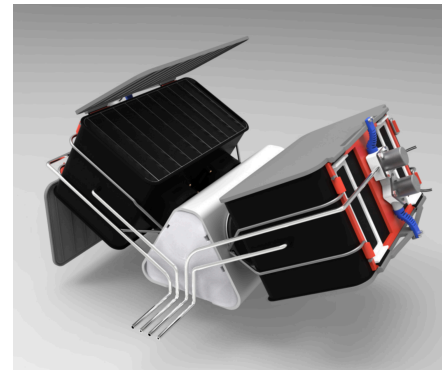


Figure 2.11: ZEF's DAC prototype 2 [12]

Evaluation of the first prototype underlined that **the volume of the system was excessively large for the amount of captured gases.** This is connected with a lot of unused volume in the final assembly. **Therefore, a monolith reactor was suggested as the next iteration [11].**

ZEF's DAC prototype 2 Together with the use of monoliths as support for the sorbent, two different polyethylenamines of high molecular weight 1,200 (PEI 1.2k) and 10,000 (PEI 10k) were evaluated during the design of the second prototype. Experimental results indicate that **the choice of an adsorbent is not straightforward** since the PEI 1.2k has faster adsorption kinetics, while the PEI 10k absorbs more CO_2 and is less easily degraded by oxygen [75]. The prototype 3 is shown in figure 2.11. Once again, a temperature-vacuum swing process was used in operation.

Despite the use of a better support structure, **the design showed a lot of flaws when being practically implemented.** Those included difficulties in correctly impregnating the monolith material due to the very high brittleness of the active carbon monoliths, leak tightness in the chamber was very difficult to be achieved as well and gravity made the sorbent distribution inhomogeneous in the prototype [75].

ZEF's DAC prototype 3 Due to the difficulties encountered when building and operating a DAC system serving both for CO_2 capture and release, **ZEF started the development of a system having separate units for absorption and desorption.** Moreover, for the absorber development, the use of amine-loaded solid sorbents (monoliths or silica-based materials) was abandoned in favour of **simply using bulk amines to be flown on a plate** for capturing CO_2 and H_2O . The new concept included the use of a fan blowing air counter currently to the amine flow. That marked the evolution from an adsorption-based DAC system to an absorption-based one. Moreover, the widely used batch sorbent DAC system was abandoned in favour of a system able to continuously capture and release CO_2 since the absorber and desorber are now developed and used separately. The idea was that **a continuous system would save energy by reducing the amount of active elements like pumps and valves [14].** Different experiments performed with test setups (figure 2.12) were used to develop this new concept and tackle the main encountered problems. Those mostly included difficulties in getting an homogeneous sorbent flow on the plate (figure 2.13) and the sorbent not being loaded until saturation [13].



Figure 2.12: Test setup for the novel absorption process [13]



Figure 2.13: Inhomogeneous sorbent flow (acrylic test) [13]

In this framework, huge steps forward were achieved with the work of Sinha [14]. **A uniform sorbent flow was obtained with the use of a channel to contain and guide the amine flow on the plate.** Moreover, the use of a new experimental setup (figure 2.14 and 2.15) gave insight into various aspects of the novel absorption process. **Results of this work constitute the baseline for this thesis project,** therefore, the most important ones are reported here.

The experimental setup used for the investigation consists in a PMMA plate fixed to an aluminium frame. The plate has a **channel milled at its center** along whole of its length. A **fan** provides the plate with the necessary air mass flow rate while a **syringe pump** is used to fix the sorbent mass flow rate. Eventually, a thermal imaging camera fixed to the aluminium frame is used to investigate thermal aspects of the absorption process. The investigation performed with the use of this setup gave multiple insights into the novel absorption process. The performance of the single absorption channel is investigated in terms of CO_2 or H_2O absorbed per sorbent used (weight ratio) and in terms of Space-Time Yield measured in $\frac{mol}{m^2s}$. This latter parameter, already introduced in this chapter, is a measure of the mass flux per unit area of CO_2 or H_2O .

Sinha [14] performed multiple experiments that showed the main characteristics of the process, the factors limiting the absorption and which type of sorbent yielded the best performances. It is found that increasing the mass flow rate of the sorbent in the channel will decrease the CO_2 and H_2O concentration measured at a certain distance on the plate, but the absolute captured amount of the two gases will actually increase. Changes in the mass flow rate of the air provided by the fan were investigated as well suggesting that the concentration of CO_2 and H_2O measured in the sorbent is affected by the depletion of the two gases in the air side. That is, when the mass flow rate of the fan is decreased too much, zones of the channel far away from the fan showed very little to none concentration of CO_2 and H_2O . Regarding the Space-Time Yield, the best performance was observed using a pure sorbent (0% CO_2 and 0% H_2O at initial concentrations). Moreover, the sorbent mass flow rate was not found to have an influence on the measured Space-Time Yield.

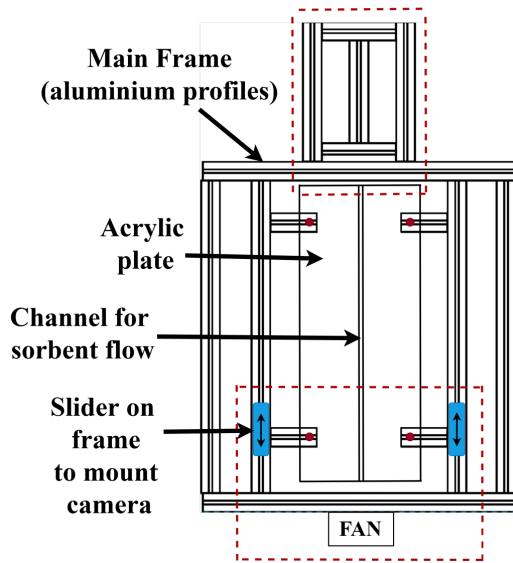


Figure 2.14: Schematic of test setup for single-channel absorption experiments [14]

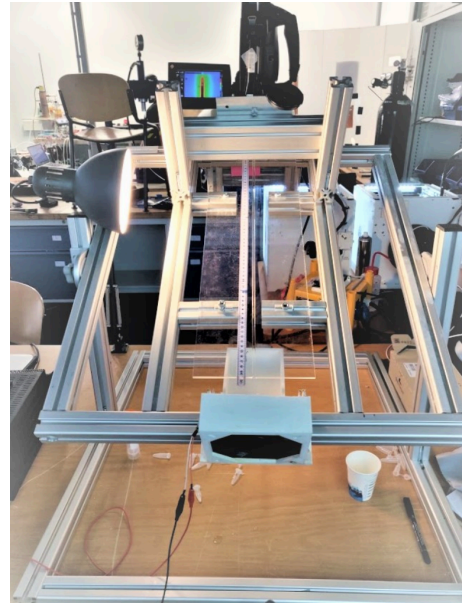


Figure 2.15: Test setup for single-channel absorption experiments [14]

Based on the experimental results, it was possible to describe the **limiting factors in the absorption process**. These are listed below [14]:

- **CO_2 diffusion in the sorbent layers.** Perhaps the most important phenomenon influencing the absorption of CO_2 is the gas diffusion into the sorbent layers. In fact, experiments showed that both water and carbon dioxide are absorbed on the free surface and then they slowly diffuse through different layers of the sorbent. Analysis of CO_2 and H_2O concentrations in the polyamine showed that a relevant part of the lower sorbent layers is not being used for capturing the gases. This brought to the conclusion that the absorption process is limited by the slow diffusion of the gases into the various layers of the sorbent. A further proof of this limitation was observed when the flow in the absorption channel was mixed using external elements in order to renew the free surface with fresh amine molecules. Indeed, as shown in figure 2.16, the relative loading of CO_2 is significantly higher in the mixed experiment. Moreover, also the Space-Time Yield was observed to be higher in the case of induced mixing meaning that the flux of CO_2 particles can be increased significantly when the top surface of the sorbent is renewed.

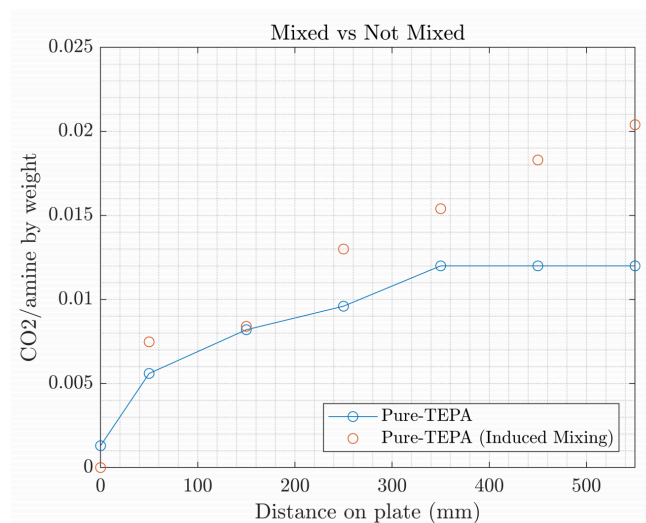


Figure 2.16: CO_2 over sorbent mass ratio with and without induced mixing [14]

- **Sorbent and air flow rate.** Figure 2.17 shows the CO_2 loading at different distances on the plate for two different sorbent volumetric flow rates. The conclusion is that an inverse proportionality exists between the sorbent flow rate and the amount of captured carbon dioxide gas per amine utilisation. This shows that the sorbent flow rate should be carefully chosen as it is another factor that could limit the absorption process.

Variations in the air flow rate were investigated as well and observed that they have an influence on the achieved loading at a certain distance on the plate. In fact, as shown in figure 2.18, the use of a fan increases the relative loading of the sorbent. Moreover, the figure shows that the CO_2 concentration, for an experiment where the fan is not being used, reaches a plateau after the sorbent has travelled a certain distance on the plate. That indicates a local depletion of air throughout the channel length. That is, the flow rate of air displaced by the fan should be high enough to avoid this effect [14].

- **Sorbent selection.** Another important aspect of the novel absorption process that was investigated regards the choice of the sorbent used in the process. Sinha [14] investigated the use of two different polyamines in the process: tetraethylenepentamine (TEPA) and polyethylenimine MW 600 (PEI-600). Based on experiments, it was concluded that TEPA performs better in the investigated absorption process since it showed a higher Space-Time-Yield as well as higher CO_2 loading per amine usage. **The use of TEPA as absorbent constitutes one of the starting point of this thesis investigation.**

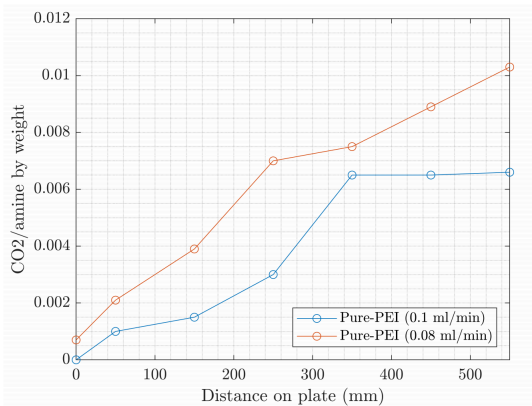


Figure 2.17: CO_2 loading at different sorbent flow rates [14]

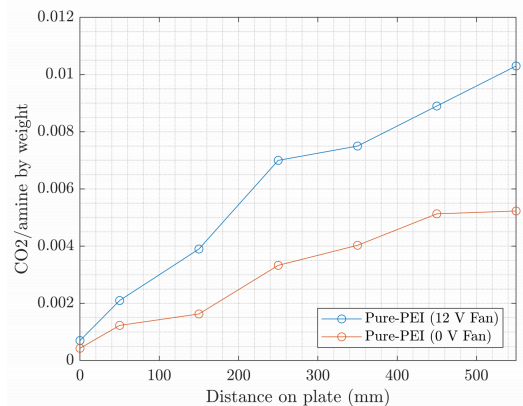


Figure 2.18: loading at different air flow rates [14]

The evaluation of the results from the experimental investigation were used to design what is currently the **last prototype for ZEF's DAC system (figure 2.19)**.

That consists of an absorption column formed by multiple channels where the sorbent is flown according to the specifications optimized via the single channel experiments. The column was designed in order to provide a certain mass flow rate of CO_2 . Constraints included the power consumption of the system as well as the total dimensions of the column according to ZEF's requirements.

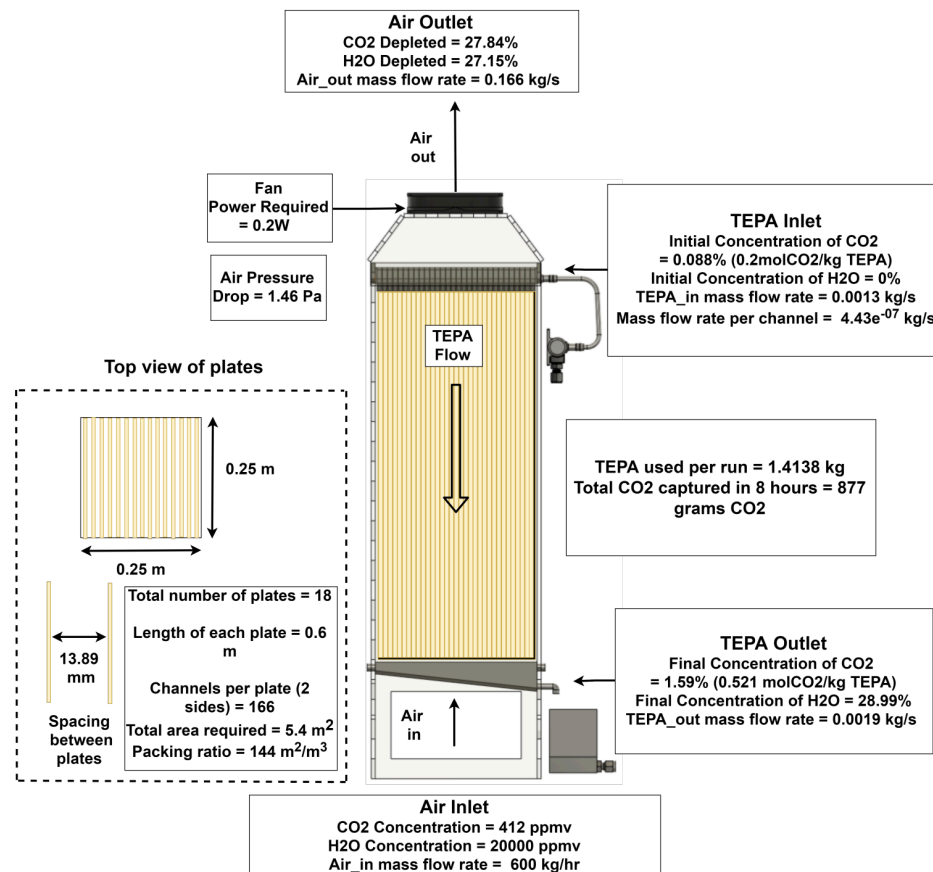


Figure 2.19: Design specification of ZEF's DAC prototype 3 [14]

2.3. TEPA as the working fluid

The sorbent chosen for the experimental investigation of this thesis project is a polyamine named tetraethilene-pentamine, or TEPA. Therefore, it is considered relevant to review its most important characteristics in order to understand its behavior during the investigation process.

TEPA contains primary and secondary amines. Therefore, as explained in section 2.2, the capture of CO₂ involves a two steps reaction where zwitterion is formed at first and later deprotonated to form carbamate. On the other side, the interaction with H₂O is different since the aminogroups do not react with it, thus generating a physical absorption process rather than a chemical one [52]. Figure 2.20 shows the structure of a typical molecule of TEPA while figure 2.21 shows a relationship between the viscosity of the polyamine and the applied shear rate. Since the measured shear stress and the applied shear rate follow a linear relationship, it can be concluded that **TEPA is a Newtonian fluid**.

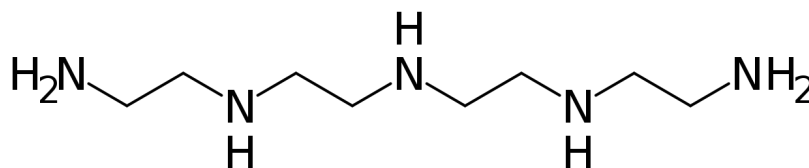


Figure 2.20: Structure of a molecule of TEPA [15]

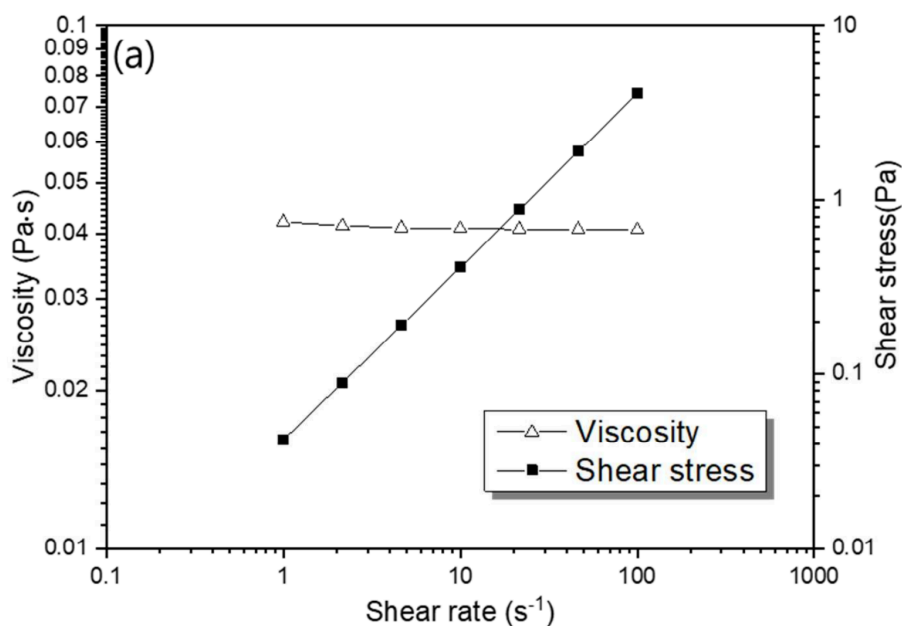


Figure 2.21: TEPA viscosity as a function of shear rate [16]

TEPA viscosity Apart from the newtonian/non-newtonian liquid behavior, **viscosity is an important sorbent characteristics for this thesis project**. In fact, since multiple experiments are performed giving different results in term of sorbent loading (concentrations of CO_2 and H_2O), it is important to realize how the viscosity of TEPA will change with that since the flow behavior will be strongly related to its viscosity. In a preliminary investigation at ZEF, **TEPA viscosity was measured at different ambient conditions and at different loadings**. Results are shown in table 2.1.

Gas concentration in sorbent			Viscosity ($pa \cdot s$)			
Sorbent	H_2O (wt%)	CO_2 (wt%)	11 °C	20 °C	29.2 °C	38 °C
TEPA	0	0	0.1981	0.09403	0.04877	0.02723
TEPA	10	0	0.4947	0.2227	0.1144	0.06534
TEPA	20	0	0.9484	0.3815	0.1822	0.09629
TEPA	30	0	0.9815	0.3836	0.1744	0.09114
TEPA	40	0	Crystal	0.2005	0.09762	0.05473
TEPA	10.32	2.32	1.84	0.7826	0.363	0.1811
TEPA	15.55	5.17	11.3	3.876	1.525	0.6904
TEPA	10.25	3.2	3.114	1.283	0.5714	0.2774
TEPA	20.195	2.46	2.645	1.008	0.4249	0.2016
TEPA	20.25	3.2	4.156	1.54	0.6433	0.2986
TEPA	30	1.56	1.417	0.577	0.2583	0.1273
TEPA	30	4	2.185	0.8728	0.3755	0.1855
TEPA	30	5.725	4.704	1.764	0.7335	0.3508
TEPA	30	9.43	17.35	5.438	2.102	0.9252
TEPA	31.27	16.03	41.08	14.44	5.779	2.544

Table 2.1: TEPA viscosity at different gas concentrations and different temperatures [14]

For no loading of CO_2 , at ambient temperature, an increase in H_2O concentration brings the viscosity of TEPA to a maximum at about 25 wt% of water. This interesting phenomena is confirmed by literature as well [76], [77] and it is associated to the fact that aqueous solutions of amines contains multiple polar species that can build or break hydrogen bonds. **The viscosity peak is associated with formation of hydrogen bonds within the solution**. On the contrary, an increase in CO_2 loading will exponentially

increase the viscosity of the sorbent of a degree depending on the water loading.

Influence of temperature Regarding the influence of ambient temperature on CO_2 absorption when using polyamines, it is reported that **the reaction of CO_2 with amine groups is an exothermic process** [52], [78] and the absorption temperature has an influence on the process' performance. In fact, when increasing the temperature of the liquid sorbent near the gas-liquid interface, two opposite effects are observed [79]. On the one hand, a temperature increase will influence the reaction kinetics, making the speed of absorption higher, on the other hand, the solubility of the gas will be reduced with an increase in temperature. For roughly understanding how temperature affects the process, one can look at experiments like the one performed by Mebane et al. [17]. That consists in loading a sample of a polyethylenimine (PEI) impregnated sorbent with H_2O and CO_2 via adsorption and desorption steps at different temperatures using as absorbed gas a mixture of inert nitrogen, CO_2 and H_2O at multiple relative concentrations.

Without the necessity of going into too many details, figure 2.22, shows how the CO_2 uptake varies when the temperature of the sorbent is changed and various dry mixtures (i.e. 0% H_2O) of CO_2 and N_2 are used in absorption.

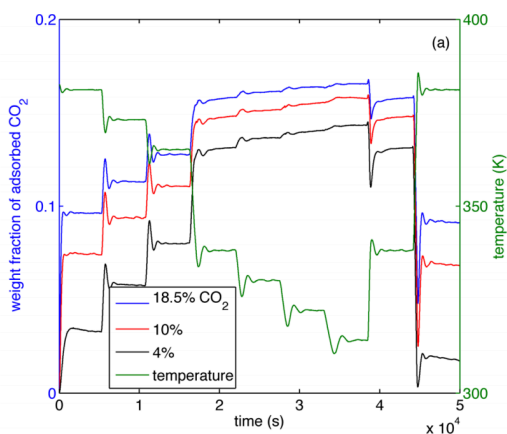


Figure 2.22: Results from the dry loading experiments [17]

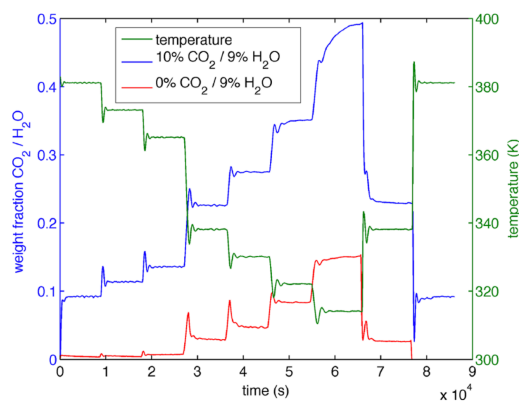


Figure 2.23: Results from the wet loading experiments [17]

From the picture, it is clear how the experiment is performed in steps that lasted 90 minutes each. For some of them, the weight fraction of adsorbed CO_2 is increasing (adsorption step), for some other is decreasing (desorption step). The figure shows that, independently on the concentration of carbon dioxide in the gas (black, red or blue line), **decreasing the absorption temperature (green line) will increase the weight fraction of adsorbed CO_2 .**

Influence of water An interesting result appears when a wet mixture is used for absorption instead of a dry one (figure 2.23). Upon the introduction of water, there is a weight gain in adsorbed CO_2 if one compares the loading curves at 10% CO_2 (red line in figure 2.22 and blue line in figure 2.23). This behavior is associated with an **increase in diffusion when water is present in the mixture** [17]. That is, the presence of water has an influence in the absorption performances of polyamine-based absorbents. As a consequence, in a DAC system, **the relative humidity of the absorbed air will have an influence on the CO_2 captured within the system.** In absorption from flue gases, the concentration of water in exhaust gases will have a similar effect. For these reasons, the effects of humidity on CO_2 absorption using primary, secondary and tertiary amine groups have been extensively researched [80], [81], [82], [83]. In tertiary amines, bicarbonate formation is observed in the presence of humid CO_2 even under supported amine sorbents. The bicarbonate formation is associated with a dramatic increase in CO_2 capture and, since the presence of water will eventually enhance its formation, a humid gas mixture will increase the CO_2 capacity. However, even accounting for that phenomena, the formation of bicarbonate in tertiary amine sorbents still shows a quite low CO_2 capacity over the formation of carbamate in primary and secondary amines [80]. Li et al. [81] underlines that, in the

two step reaction occurring in CO_2 absorption using primary and secondary amine groups, carbamate formation happens through a deprotonation of a zwitterion molecule via a free base. For that, both an amine group and a water molecule can act like a free base. Therefore, it is expected that water will decrease the sorbent consumption reducing the amine-carbon dioxide stoichiometric reaction ratio [81], [82]. In a recent investigation on TEPA-impregnated mesoporous carbon, this effect is explored even further and concluded that, together with the decrease of the TEPA- CO_2 molar reaction ratio, an excess of water molecules will occupy adsorption sites, thus decreasing the CO_2 adsorption capacity of the loaded solid sorbent [82].

2.4. Mixing at very low Reynolds number

As described in section 2.2, previous research on the novel absorption process strongly points toward a diffusion limited type of process [14]. That is, one of the main goal of this thesis project is to provide ways for mixing the sorbent while it flows on the absorption channel. This way, the free surface of the sorbent will be renewed, thus theoretically improving the absorption performance of the channel. Since that will be investigated in the experimental section of this project, it is found to be relevant to review the main ways with which mixing can be provided in channel flows. **Firstly, the fluid dynamic aspects of the flow specific to this project are studied to understand the flow behavior.** Then, multiple mixing strategies are reviewed.

2.4.1. Stokes flow theory

The **Reynolds number** is a dimensionless parameter used to define the regime of flow fields [84]. It is defined as the ratio of inertial forces to viscous forces:

$$Re = \frac{\rho u L}{\mu} = \frac{u L}{\nu} \quad (2.11)$$

Where:

- ρ is the density of the fluid of interest in $\left[\frac{kg}{m^3}\right]$
- u is the characteristic velocity of the problem in $\left[\frac{m}{s}\right]$
- L is the characteristic length of the problem in $[m]$
- μ is the dynamic viscosity of the fluid of interest in $\left[\frac{Ns}{m^2}\right]$
- ν is the kinematic viscosity of the fluid of interest in $\left[\frac{m^2}{s}\right]$

Reynolds number in ZEF's process The density of TEPA is $998 \frac{kg}{m^3}$ while the viscosity can be taken from table 2.1 in section 2.3. The flow velocity and relevant length scale of the absorption process can be taken from the experiments previously performed by Sinha [14]. The result is a Reynolds number on the **order of** 10^{-3} when a volumetric flow rate of about $5 \frac{mL}{hr}$ is used at the inlet of the channel. Since $Re \ll 1$, **the flow in the absorption channel falls in the dynamic regime usually referred to as Stokes flow or creeping flow.** The theory relevant to this type of flow is explained below and taken from the book of Childress [84].

Stokes flow governing equations Stokes flows are encountered when dealing with either extremely small length scales, very viscous liquids or very small velocities. Based on the definition of the Reynolds number, in a stokes flow field, viscous forces will dominate over inertial forces. That brings to the fact that **Navier Stokes equations can be significantly simplified** when mathematically describing this kind of flow.

$$Re \left(\frac{\partial \mathbf{u}}{\partial t} + \mathbf{u} \cdot \nabla \mathbf{u} + \nabla p \right) + \mathbf{F} = \nabla^2 \mathbf{u} \quad (2.12)$$

$$\nabla \cdot \mathbf{u} = 0 \quad (2.13)$$

Looking at the dimensionless Navier Stokes equations (equations 2.12 and 2.13), where vector fields are indicated with bold text, it is possible to reduce those equations to a much simpler form by taking the limit $Re \rightarrow 0$, i.e., by imposing the Stokes regime. Result is shown in equations 2.14 and 2.15.

$$\nabla p - \nabla^2 \mathbf{u} + \mathbf{F} = 0 \quad (2.14)$$

$$\nabla \cdot \mathbf{u} = 0 \quad (2.15)$$

It must be noted that it is chosen to keep the pressure in the equation since, even if the reduced Navier-Stokes equations without the pressure term are still a formulation of a Stokes flow regime, they do not encompass all the different Stokes flow of interest [84]. A huge advantage when mathematically solving the reduced equations is the disappearing of the non linear terms.

Having recognized the flow type for the problem of interest, the main ways to induce mixing in such a flow are reported below.

2.4.2. Micromixing: high Peclet number, slow diffusive mixing

. For low Reynolds number, looking at Stokes flow theory, the flow of sorbent proceeds along the channel in a laminar and uniaxial fashion. Therefore, mixing can only occur through molecular diffusion. However, this diffusive mixing can be extremely slow if compared to the advection of material along the channel. If the flow behavior can be understood by quickly estimating the Reynolds number, a glimpse of the mass transport behavior can be understood by computing the Peclet number:

$$Pe = \frac{\rho u L}{D} \quad (2.16)$$

Where D is here introduced as the diffusion coefficient in $\frac{m^2}{s}$. The Peclet number can be seen as the ratio of advective mass transport over diffusive mass transport. For problems where the flow proceeds at very low Reynolds number, the advective mass transport is very slow or almost non-existent and, when diffusion is very slow as well, **thus high Peclet number**, the result is **a flow with very low advection mixing and an even lower diffusion mixing**. In the case relevant to this thesis, Diffusion coefficient of CO_2 in the polyamine sorbent, as estimated in previous research at ZEF [14], [38], shows a very high Peclet number, thus slow diffusive mixing. The result is that the channel length required for complete mixing is prohibitively long. In this framework, mixing of the flow targets an increase in the advective mass transport rate.

The word "mixing" is used for describing a lot of different processes and can be applied to multiple physical transport phenomena like heat or mass transfer and can be done in multiple ways like by generating chaotic advection [85], [86] or by imposing a high Reynolds number to the flow [87]. In our case, mixing refers to a way for reducing as much as possible the time it takes for molecular diffusion to homogenize an initially inhomogeneous concentration gradient. Since the flow of interest has a Stokes flow behaviour, there is basically no advection (no bulk transport) and it takes a very long time for diffusion to "distribute" the absorbed CO_2 molecules until homogeneity is reached. Moreover, the region we are interested in mixing is the free surface of the sorbent flow. That is, **mixing in this case means to renew the sorbent particles on the free surface**.

Active Micromixing Mixing in Stokes flow behaviour is very common in very small geometries such as micromixers, microreactors or microchannels. **A way for classifying micromixers is as either passive or active mixers** [88]. In a passive micromixer, the specific geometry of the channel or of external elements is used to induce improvements on the mixing process. No external energy input is necessary for a passive mixer to work. On the contrary, active mixers are generally units that create disturbances in the flow by means of external pulsating energy fields.

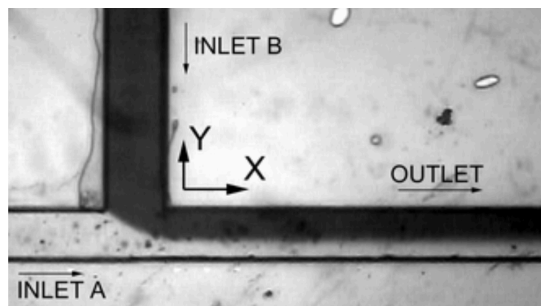


Figure 2.24: Example of two inlet channel segment [18]

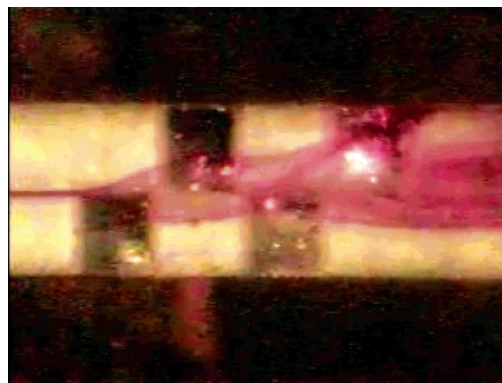


Figure 2.25: Ultrasonic micromixer [19]

Research shows that, when dealing with a multifluidic system as the one shown in figure 2.24, the higher degree of mixing is obtained when pulsating both inlets out of phase [18]. Another way of actively mixing two fluids is with the use of acoustic stirring created by ultrasonic waves [19]. As shown in figure 2.25, phenolphthalein (red) is mixed in a solution of sodium hydroxide and ethyl alcohol (yellow) with the use of transducers (black squares) able to introduce ultrasounds in the flow stream. The acoustic stream is induced perpendicularly to the flow direction and it is observed that, if the flow rate is increased, the power level of the transducers need to be increased as well in order to get a uniform mixing across the channel. Those are just two examples of active micromixing, multiple others exist like the use of fluctuating electric fields [89] or magnetic ones [90].

Passive Micromixing Differently from that, **passive micromixers do not rely on active elements**, but rather on very specific ways for engineering the channel geometry where the sorbent is flown. For example, channels are engraved with ridges of different shapes in order to create an anisotropic resistance to the viscous flow [20].

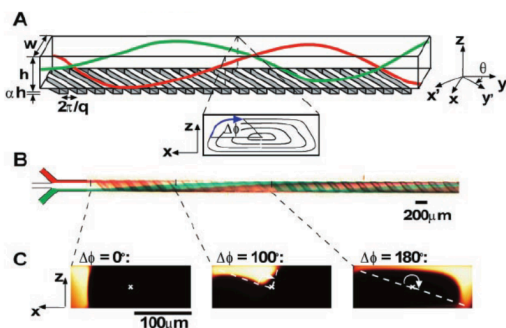


Figure 2.26: Channel with Obliquely Oriented ridges. A) Schematic diagram of the channel B) Optical micrograph showing mixing for a red and green stream C) Fluorescent confocal micrograph of different channel's cross sections [20]

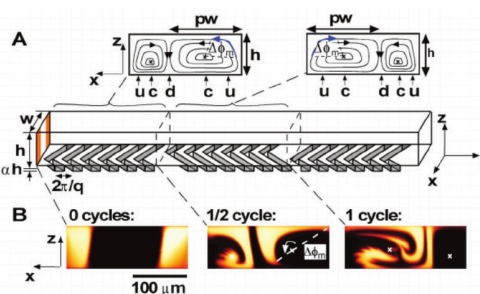


Figure 2.27: Channel with ridges shaped as Staggered Herringbones. First one-and-a-half cycles A) Schematic diagram of the channel B) Confocal micrograph of different cross sections of the channel [20]

Figure 2.26 shows the effect of the **anisotropic resistance on the flow**. In fact, by orienting the ridges at a certain angle with respect to the flow direction, there will be a reduced resistance on the flow in a direction parallel to the engraved ridges. As a result, the axial pressure gradient in the y' direction will generate a mean transverse motion (along x) of fluid particles. Those motion will make the fluid to circulate back across the top of the channel as shown in figure 2.26 A). It is reported that, within the Stokes flow regime, the form of the flow is independent of the specific Reynolds number [20]. That is, as it can be seen from figure 2.26 C), it is expected that the engraved ridges are able to twist the flow to the top of the channel and circulate it back at the bottom of it by creating helical streamlines as the fluid proceeds along the channel. This way of passive mixing can be further explored by designing the so-called Staggered Herringbone Mixer (SHM) as shown in figure 2.27. In this particular design, the

chaotic mixing is further enhanced by subjecting the fluid to local rotations in opposite directions. Looking at figure 2.27 A), a single mixing cycle is composed of two regions of ridges symmetric with respect to the centerline of the channel (y direction). This switch in the asymmetry of the single herringbones after every half cycle will further enhance chaotic mixing. The result is that the flow will exhibit a similar pressure gradient as the one described previously, both for the short and for the wide arms of the herringbone. That will generate a fluid motion in the z direction on both sides of the centerline. As shown by confocal micrograph of a mixing experiment done by injecting two streams of a fluorescent solution on both sides of a transparent solution (figure 2.27), after half cycles, ripples in opposite direction are being generated and chaotic mixing behavior is observed after a full cycle. Once again, **it is reported a non-dependence between the form of the flow in the SHM and Reynolds number in the Stokes regime**. That is, it is expected to observe similar mixing path also at $Re \ll 100$.

Reported micromixers for Reynolds numbers closer to zero value (0.2-75) include the use of sinusoidally shaped channel's side walls. As shown in figure 2.28 and reported by literature [21], phase-shifting the walls has the effect of generating Dean flows between the two fluids to be mixed. In this case, maximum mixing is observed for a phase shift $\phi = 3\pi/4$ and $\pi/2$. The authors also report that this mixing geometry works for a minimum Reynolds number of 0.2.

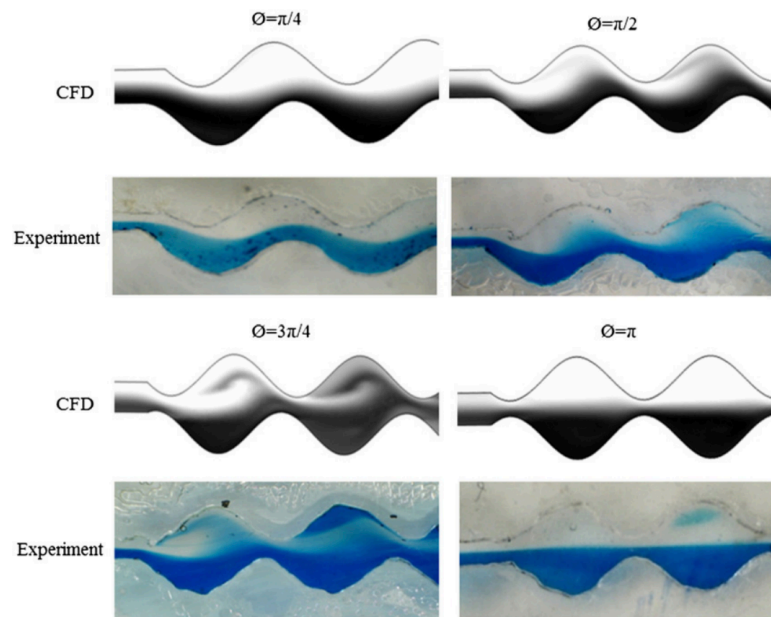


Figure 2.28: Micromixers with sinusoidally shaped side walls at different phase shifts (CFD and experiments) [21]



Figure 2.29: Kenics mixer geometry [22]

Perhaps of more interest is the use of an external passive mixer to be inserted inside the channel to generate chaotic advection in the flow. For example, a Kenics mixer is made of a long tube containing helical blades alternatively oriented clockwise and counterclockwise with respect to the flow direction as shown in figure 2.29. The blade connection is such that the fluid flowing through the mixing elements is separated in two parts after every change of blade. Computational Fluid Dynamics simulations of a Kenics Mixer at different Reynolds numbers indicate that identical velocity profiles are obtained in Stokes flow behaviour and deviation occurs only for $Re > 10$ [91].

2.5. Lessons learned

Sources of this literature review included books about general mass transfer theory, previous research projects part of ZEF's knowledge and papers about absorption of CO_2 and H_2O in polyamine sorbents. The most important insights from this literature research are reported below:

1. This project is mostly about the absorption of CO_2 . However, it is recognized how the presence of water might have a huge influence on that. Therefore, **water loading should always be kept in mind. That will be helped by monitoring the ambient relative humidity during every experiment.** Moreover, it is expected that experimental data will show very different loading curves for the two gases. In fact, apart from the differences in the absorption driving forces, they are also absorbed in two completely different ways since **H_2O is physically absorbed, while CO_2 is chemically absorbed when using polyamine absorbents.**
2. Absorption performances can be evaluated in terms of CO_2 captured per amine utilization ($CO_2/amine$) and in terms of Space-Time Yield (STY). The first parameter is related to decreasing the sorbent consumption, while the second parameter, equivalent to the flux of CO_2 within the sorbent, is related to reducing the size of the absorption equipment and the time needed to absorb a certain amount of gas.
3. From previous research at ZEF, **it is described how the process of CO_2 absorption is diffusion limited on the neighborhood of the free surface.** Therefore, it is suggested to renew the surface of the sorbent in contact with the air by mixing it as it flows downstream on the absorption plate. Moreover, **it is understood how the expected flow behaviour for this absorption process is a Stokes flow one with a characteristic Reynolds number of about 10^{-3} .**
4. Various mixing strategies have been analyzed for Stokes flow regimes and some channels geometries are found to be more interesting than others:
 - **Staggered Herringbone Mixer (SHM) and Obliquely Oriented Ridges (OR):** they could potentially provide for mixing since it is reported that they work independently on the Reynolds number value in Stokes regime
 - **Sinusoidally shaped walls** are of no interest since no mixing is reported when $Re < 0.2$ and mixing does not happen in a direction perpendicular to the channel floor (toward the free surface)
 - **Kenics Mixer:** it looks promising, but our specific process requires to always have a free surface on top of the channel. Therefore, it is not known how not entirely enclosing the mixer in a cylindrical shaped channel will influence the Kenics mixing performance.
 - **Active mixing** is interesting. However, it might be a challenge to use the same active mixing strategies as observed in literature. Coming up with creative ways for actively mixing the sorbent while maintaining a continuous flow on the plate might be necessary.

Most micromixing technologies work for $Re > 1$. The flow relevant to this thesis is several order of magnitude below that. Therefore, it might be that mixing is way more difficult to be achieved in that conditions.

5. **A clear theory describing mass transfer in this specific absorption method is still missing.** The reviewed mass transfer theory gives some insight into possibly applying one of the classic mass transfer theory like the two film theory or the penetration theory in order to explain the mass transport. However, it is not to be excluded the necessity of formulating a different physical theory for explaining this absorption process. This also applies in the formulation of a mass transfer model able to predict CO_2 capture performance for this novel absorption process.

3

Experimental investigation

In order to reach the research goals, an experimental investigation is necessary. This chapter describes the experimental setup and experimental methodology used for addressing the research questions relevant to this thesis. An experimental plan is proposed and assumptions specific to the setup are mentioned. Two different setups are used. The first one is used to investigate passive mixing in the novel absorption process, the second one deals with active mixing instead.

3.1. Previous work

The starting point of this work is a direct air capture setup developed in previous studies at ZEF. As reviewed in section 2.2, a setup was designed and built for performing experiments on CO_2 and H_2O capture when a polyamine sorbent is flown inside a single channel milled into a PMMA plate. In particular, the setup consists of an aluminum frame to allocate the plate and all the different equipment for performing the experiment. This aluminium frame was already shown in section 2.2 and can be seen in figures 2.14 and 2.15.

The mechanical robustness of the frame, together with the possibility of sliding the different beams relative to each other, make this setup perfect for pursuing the passive mixing experiments relevant to this thesis project.

Together with the **frame**, few other components, namely, a **fan** and a **syringe pump** are used. The first is an AD12038GP plastic fan of 120 by 120 *mm* from the company ADDA. It has a rated power of up to 20 Watts (at 12 Volts) and can provide a maximum air flow of 5.247 m^3/min at a max pressure of 1.8 *mbar* [92]. While the fan is used to provide continuous flow for the sorbate (air), a KDS100 syringe pump from KD Scientific is used to provide continuous flow for the sorbent (TEPA). The internal diameter of the used syringe is taken as the only input for the internal control of the pump. The used pump is rated to work with syringes having internal volumes ranging from 10 microliters to 100 milliliters [93]. For the purpose of this work, a 30 *mL* syringe from BD Plastic is used. The syringe pump can be used with two different dispense modes: dispense volume mode and run mode. Since continuous absorption is investigated in this thesis, the latter is used during the experiments. The syringe is clamped on the pump's syringe holder and a flexible plastic hose is connected to the syringe outlet in order to drive the sorbent flow rate to the inlet of the absorption channel. Basically, those two devices are used for providing and controlling the sorbent and the air flow rates necessary for the experimental investigation (figures 3.1 and 3.2).



Figure 3.1: The fan used to provide the air flow rate



Figure 3.2: The syringe pump used to provide the sorbent flow rate

Together with equipment for the collection of loaded samples, measurements equipment for checking the concentrations in the loaded samples are provided. In particular, a **Cary 630 FTIR** (Fourier Transform Infra-Red) Spectrometer [23] figure 3.3, is used for analyzing the different samples collected during the experiments. Such device is able to generate interactions between the matter and electromagnetic fields in the Infra-Red (IR) region. Molecules of the sample are excited by absorbing IR radiation. The radiation that goes back to the machine will contain information about the species present in the sample since various light wavelengths are absorbed by different species [94]. Peaks in the plot of the specific IR spectrum of the sample (measured IR intensity versus wavelength) can be used to identify the various molecules present in the sample and their weight concentration. However, in order to do that, it is necessary to obtain the spectrum of known samples and compare them to the unknown spectra of every collected samples. This was done during previous research at ZEF with the use of the software "TQ Analyst" to collect a database of "known spectrum" corresponding to different sorbent concentrations [14]. Basically, this database contains a collection of spectrum for TEPA at various relative concentrations of CO_2 and H_2O . This allows a direct comparison with unknown spectrum to obtain the concentrations in the collected samples.



Figure 3.3: Cary 630 FTIR Spectrometer [23]

3.2. Passive Mixing Experiments

The equipment described above is used as part of the equipment for performing the first set of experiments in this thesis project: the passive mixing experiments. In particular, the syringe pump, the aluminium frame and the fan are used in the same fashion of previous investigation at ZEF [14]. However, instead of the PMMA plate, **newly engineered mixing channels** are used in order to test the effects of different mixing elements. In this section, requirements of this first experimental investigation are defined. Those are considered when engineering the mixing channels geometries and in defining a solid experimental procedure. Finally, an experimental plan is proposed, together with the main assumptions that are considered during this investigation.

3.2.1. Requirements

Based on previous experiences of the DAC team at ZEF and on the research questions specific to this thesis project, different requirements of the experimental setup are defined. Engineering and manufacturing of the equipment used during the experiments is planned and executed based on those requirements.

1. Among the main difficulties traced when using TEPA as a CO_2 and H_2O absorption medium, there is the difficulty in **obtaining repeatable results** [14]. For example, collection of the loaded sample by manually using a spatula in the channel, constitute a source of uncertainty in the experimental result since the loaded gases will be influenced by the time it takes to collect the sample, the impossibility of properly collecting the sample without leaving any residue in the channel and the ability of the operator to collect the sample at the right location in the channel. As a consequence, the experimental setup is required to provide a reliable way for repeating the experiments via reducing as much as possible the influence of human error on the final result.
2. Connected to the requirement mentioned above is the necessity of **collecting samples at multiple distances on the channel** without interfering with the sorbent flow on the plate.
3. Since the absorption length is not known beforehand, it is necessary to have a **modular configuration** for the channel used to flow the sorbent. That gives the possibility of experimenting with channels of different lengths without the necessity of manufacturing new pieces, but simply by adding more sections to the channel assembly. This modularity requirement introduces the added challenge of providing for a complete **seal of the connection parts of the different modules** in order to avoid a flow rate reduction as the flow proceeds through the channel.
4. The approach of this passive mixing experiments is based on trying multiple type of channels to verify which one works better. For this reason, it is not known how many channels will have to be manufactured. Therefore, a requirement is that the **channels are easily produced within the equipment accessible at the university** to avoid as much as possible delays due to the manufacturing process. That is, rapid prototyping and low cost are requirements of the manufacturing process.
5. Regarding the specific design of the channel geometries, it is required to experiment at different sorbent flow rates. This means the geometry of the channel needs to be able to accommodate multiple volumetric flow rates without problems like flow separation or accumulation on the sides. This requirement is defined after previous investigation at ZEF underlined difficulties in obtaining a uniform flow with polyamine sorbents [13].
6. Reviewed literature underlined how variations in ambient relative humidity and temperature can have a massive influence in the outcome of the experiment. Therefore, it feels necessary to **measure ambient relative humidity and temperature** for this set of experiments due to the high variability in Dutch's weather conditions. Therefore, that is included as an experimental requirement as well.

3.2.2. Setup Description

The requirements mentioned before are fulfilled via engineering of the channel for sorbent collection with the use of the CAD software Fusion360 and selecting a suitable manufacturing technique. Results of that work are described in this section.

Multiple channels are designed and manufactured. Therefore, **for illustrating the main features of the design job, the so-called Empty Channel (EC) design is used.** That is the simplest channel used for the passive mixing experiments and it is supposed to give information about a base scenario where no mixing elements are present. In fact, the other channel containing passive mixing elements are made using this type of channel as the starting point with the addition of, for instance, engraved herringbones. The rest of the channels are described in this section in the experimental plan. An orthographic view of the channel made via the 3D CAD software is used for illustrations of the channel's features.

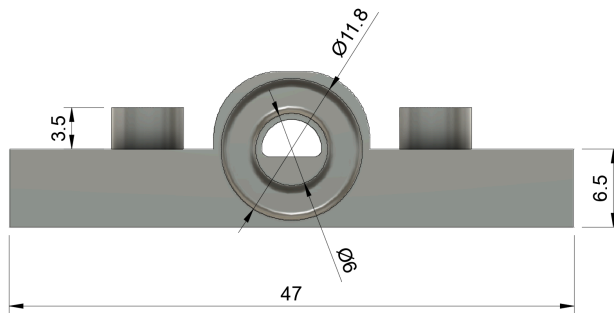


Figure 3.4: Empty Channel, front view

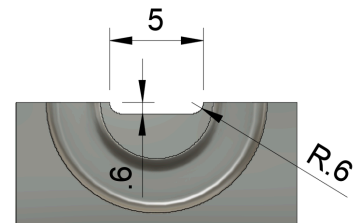


Figure 3.5: Detail of channel dimensions

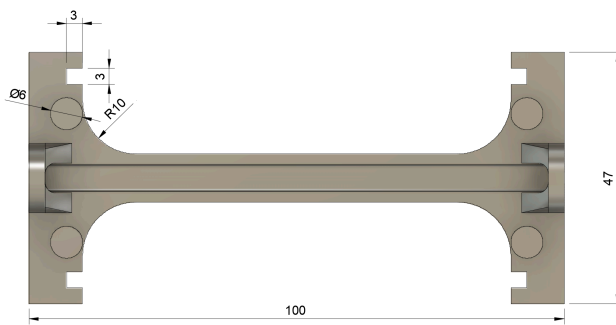


Figure 3.6: Empty Channel, top view

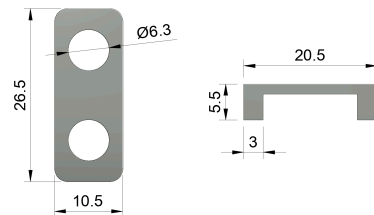


Figure 3.7: Clamps dimensions

The experimental setup is based on a modular configuration of 100 mm long modules to be connected in series. Figures 3.4 and 3.6 show a frontal and top view of the modules respectively, while figure 3.5 shows a detail of the module to highlight the dimensions of the channel. As it can be seen, the sorbent is flown on top of the module and a tunnel-like configuration at the end and beginning of each module allows the series connection. All dimensions are in millimeters and the technical drawings are obtained with the use of the software Fusion360. The relevant engineering features of the module are described below:

- Each module can be connected to the sequent one via the use of the clips shown in figure 3.7. The role of the two clips is exactly the same and two of them are used because of redundancy in order to make sure it is less likely that the whole connection fails during an experiment. To eliminate the inconvenience of the sorbent flowing out from the channel at the connection points, an O-ring groove is included at the beginning and end of each module. The groove dimensions are shown in figure 3.4 and they are based on specifics taken from the Eriks O-Ring technical handbook [95] for a 6x2 mm O-Ring. In order to obtain a high degree of compression, thus reducing as much as possible leakages, a **silicone O-ring** is used instead of a plastic one. Those silicone O-rings are **manufactured in-house** by using a 3D printed mold. Pouring silicone in the mold and waiting 8 hours for hardening, one obtains the desired result.
- In order to prevent the sorbent from accumulating on the sides of the channel due to viscosity effects, **fillets** of 0.6 mm of radius **are added on the lateral walls of the channel** (figure 3.5). The

aspect ratio of the channel (width/depth) is kept higher than 1 (8.3 in this case), to reduce once more the effects of sorbent accumulation on the sides of the channel. That is used to strengthen the assumption of a flat flow surface. This assumption is important especially when modelling the flow over the ridges via the Matlab model described in chapter 4.

- Regarding the influence of different ambient relative humidity and temperature on the experimental outcome, the measuring tool shown in figure 3.9 is used to perform measurements of relative humidity and temperature during an experiment. The device is a simple **analog psychrometer able to measure temperatures with a wet and a dry bulb**. Subtracting the temperatures and referring to a table coming with the device, one can find the ambient relative humidity.

Once the geometrical parameters of the channel are decided, the most suitable manufacturing technique for the purposes of this thesis is selected to be 3D printing technology. In particular, **Ultimaker 3D printers are used to manufacture the modules** and clamps for the experiments (figure 3.8). Poly-lactic acid (PLA) is used as the material for the 3D printer due to high availability and good mechanical strength. The choice of 3D printing the modules allows for rapid prototyping of different channel geometries both with respect to the specific channel dimensions (width, depth, fillet radius) and to allow for experimenting with multiple mixing strategies. Moreover, the high availability of 3D printers within the university, reduces lead times for production to the mere time required for the printer to actually complete the printing task. That is especially true since multiple printers can be used at once and overnight to significantly speed up the manufacturing process, thus allowing for multiple design iterations.



Figure 3.8: A Ultimaker 2+ 3D printer



Figure 3.9: Analog sling psychrometer

The final assembly for passive mixing experiments is shown in figure 3.10. It can be noticed how the different modules are assembled and how the fan and syringe pump are placed at two opposite ends of the aluminium frame. That is, **air will flow counter currently with respect to the flow of the sorbent**. Once the assembly is completed, a precise experimental procedure is followed for each and every experiment. Once again, defining this beforehand makes much easier to obtain repeatable results and, eventually, it also makes the whole experimental investigation much faster.

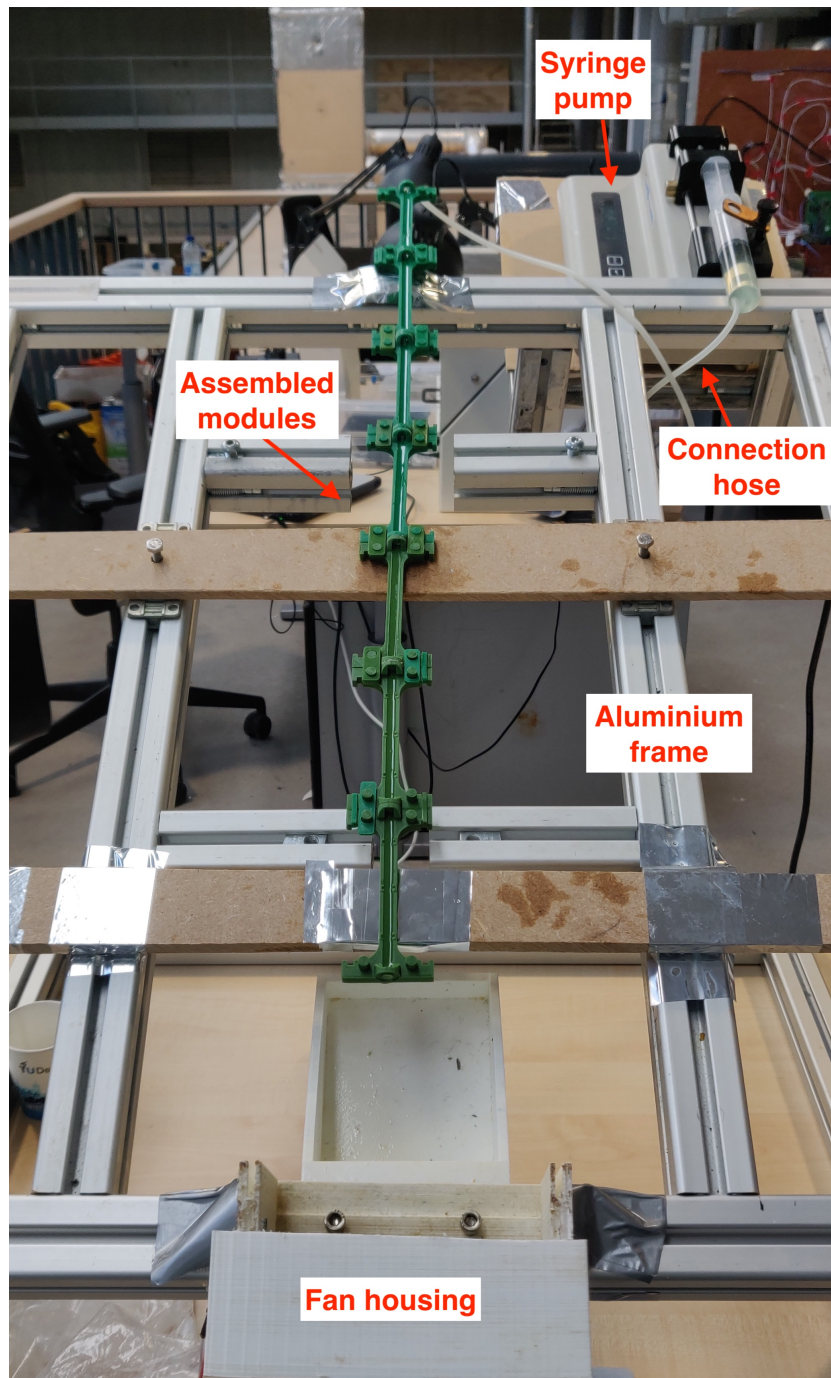


Figure 3.10: Final assembly of the experimental setup for passive mixing experiments

3.2.3. Methodology

In order to collect samples for data analysis that are repeatable as much as possible, **a very strict experimental procedure is defined** (appendix A.1). The goal of the experimental procedure is to give the researcher a structured way of collecting the samples which, together with the specific design of the setup, will increase the probability of obtaining reliable and repeatable data. For the passive mixing experiments, the selected experimental parameters are collected in table 3.1. After the parameters are selected, relative humidity and temperature are measured and the experiment is started. The residence time is measured with a stop watch and samples are collected as described in appendix A.1. The experimental plan relevant to this investigation is presented in the next section.

Parameters
Plate (or channel) inclination
Channel type
Channel length (or number of modules)
Sorbent initial conditions
Sorbent flow rate
Fan operating voltage

Table 3.1: Experimental parameters: passive mixing

3.2.4. Experimental plan

The main goals of this first experimental investigation is to **find out if passive mixing can be used to improve the performance of the absorber**. Following from the literature review, three different channels geometries are selected for this investigation:

- Empty Channel (EC) geometry
- Staggered Herringbone Mixer (SHM) geometry
- Bridges (BR) geometry

The first of these geometries, the EC one, is already described in this section when giving an example about a channel design. Therefore, only the description of the SHM and BR geometries follows.

Staggered Herringbone Mixer geometry The SHM geometry is selected because it is reported that, in a Stokes flow behavior, the mixing performance is independent on the specific Reynolds number [20]. Experimenting with this geometry serves to understand if engraving mixing elements into the channel floor can provide top surface renewals while the sorbent is flowing downstream in the channel. This geometry is chosen over simple diagonally engraved ridges because the presence of herringbones is expected to generate opposite sorbent circulation on both sides of the herringbone, thus enhancing mixing. Details about the design of the herringbones are shown in figure 3.11 and 3.12.

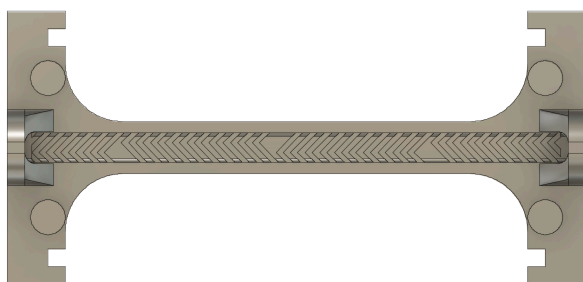


Figure 3.11: Staggered Herringbone Mixer, top view

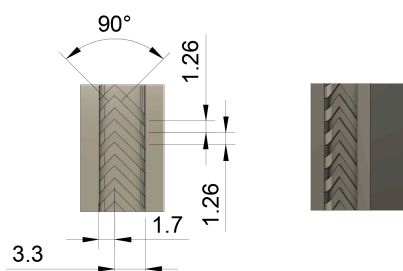


Figure 3.12: Staggered Herringbone Mixer, perspective view

Every dimension of the module design shown in figure 3.11 is exactly the same as in the Empty Channel case. In fact, the only difference between the two channels is the presence of herringbones engraved in the channel floor. The design of the herringbones is based on suggestions from Stroock et al. [20], in particular, the design parameters shown in figure 2.27 are selected. Those are reported in table 3.2.

Parameter	Value	Unit	Description
p	2/3	-	Herringbone's asymmetry
w	5	mm	Channel width
h	0.6	mm	Channel height
α	0.3	-	Herringbone's depth over channel height
q	$\frac{\pi}{\alpha h}$	mm ⁻¹	Herringbone's spacing
#	10	-	Number of herringbones per half cycle

Table 3.2: SHM geometrical parameters, refer to figure 2.27

It is suggested that selection of p and other geometric parameters like α is very important for controlling the efficiency of mixing. Once again, those are selected following suggestions from [20].

Bridges geometry The BR geometry is selected following suggestions from [14]. In fact, it was found that the presence of bridges stopping the top layer of the flow had a positive influence in the absorption performance. The channel designed following that suggestion is reported in figures 3.13 and 3.14.

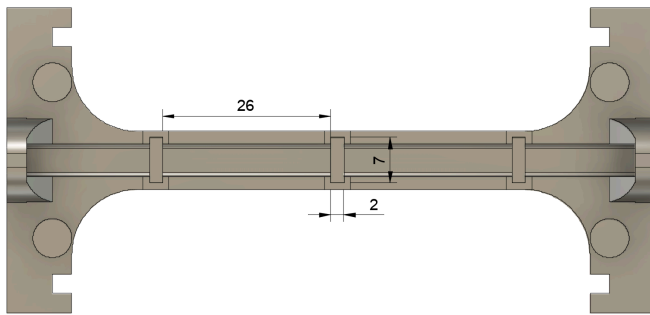


Figure 3.13: Bridges, top view

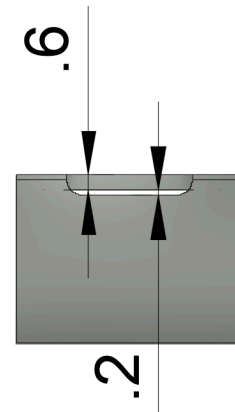


Figure 3.14: Bridges, cross sectional view

According to the writer of this report, increase in absorption performance can be associated with the creation of a pressure differential between the upstream and downstream flow over the bridge. In fact, by stopping the top layer of the sorbent, flow accumulation upstream the bridge will generate a higher pressure as compared to the pressure of the flow after the bridge. In theory, since the flow moves from a higher to a lower pressure, the lower pressure downstream the bridge should be able to move the sorbent from the bulk toward the free surface, thus providing for surface renewal. This effect should be enhanced by the pressure differential, therefore, by how much flow is accumulated before the bridge. For that reason, the clearance between the bottom of the bridge and the floor of the channel is chosen to be as small as possible, that is, 0.2 mm (figure 3.14). Clearly, in order to have surface renewals, there must be a difference of pressure between the free surface sorbent layers and the bulk sorbent layers. Therefore, even if the bridge is actually generating a pressure differential in the flow direction, that does not mean that there is a pressure differential in a direction perpendicular to the flow direction as well. That must be considered and verified with the experimental investigation.

After having defined which type of channels will be used in this first experimental investigation, the **experimental plan** is reported in table 3.3.

Experiment Number	Channel Type	Sorbent Flow Rate [mL/hr]	Channel Length [mm]	Sorbent Initial Conditions	Channel Inclination	Fan Voltage [V]
1	EC	0.3	500	Pure TEPA	45°	7
2		0.7	500	Pure TEPA	45°	12
3		1.5	700	Pure TEPA	45°	12
4		3	700	Pure TEPA	45°	12
5	BR	1.5	500	Pure TEPA	45°	7
6		3	500	Pure TEPA	45°	7
7	SHM	1.5	700	Pure TEPA	45°	12
8		3	700	Pure TEPA	45°	12

Measured Parameters:
Ambient relative humidity and temperature, sorbent residence time and sorbent composition at the end of each module

Table 3.3: Passive mixing, experimental plan.

3.2.5. Assumptions

The assumptions relevant to this experimental investigation are described below:

- The **main target** of the experiments is to **verify if passive mixing happens with the designed geometries and**, especially in the case of the Empty Channel, **understand the influence of varying the sorbent flow rate** in terms of Space Time Yield and CO_2 and H_2O loadings.
- The residence time is expressed by the time required by the first droplet of sorbent to flow through the different modules. **It is assumed that the average particle flowing in the channel will take the same time to reach the end of each module as the particles of sorbent in the first injected droplet.**
- All the experiments are performed in the same laboratory. Due to the climatized environment, it is observed that ambient temperature stays more or less constant around 21 °C. Therefore, **it is assumed that temperature variations have no effect on the experimental results.**
- Differently from temperature, ambient relative humidity is observed to change significantly depending on atmospheric conditions. **It is assumed that the ambient relative humidity has no effect on the absorption of CO_2** , but, for absorption of H_2O , the ambient relative humidity at which the experiment is performed is taken into account when interpreting data about H_2O absorption.
- Following recommendations from previous works at ZEF [14], **the fan is used at a voltage higher than 7 Volts in order to avoid air depletion.** Therefore, air is considered to be always well mixed in proximity of the sorbent interface.

3.3. Active Mixing Experiments

Passive mixing experiments use a single channel where the sorbent is flown at very low flow rates. For some of the experiments, the sorbent took hours to reach the end of the channel and mixing is only induced with the use of static elements.

Another approach of imposing mixing is by **actively stirring the sorbent after it flows on the plate and then re-pumping it back at the inlet of it.** Therefore, if passive mixing experiments were investigating absorption performance of a slow sorbent flow into a single channel where no energy input is used for mixing, the goal of the active mixing experiments is to investigate how absorption is affected when the sorbent flow rate is orders of magnitude higher and mixing is actively imposed by investing energy into the process.

3.3.1. Requirements

The requirements of the active mixing experiments are listed below:

1. The main requirement of this experimental setup is to **actively mix the sorbent** while the absorption process is happening. Moreover, it is required that data can be collected in a reliable way without stopping the experiment to do that.

2. The flow rate of the sorbent on the flowing plate, and, therefore, its residence time, must be controllable.
3. The same applies to the air flow rate.
4. The sorbent flow rate is expected to be higher, therefore, the use of a single channel is not of practical interest for this experiments and a **plate containing multiple channels is rather used**. That will increase the surface area of the experiment allowing to use way higher flow rates.
5. Due to variation in sorbent viscosity when absorption is happening, it is expected that the mass flow rate will vary as well. Therefore, the setup should allow for **measuring the sorbent mass flow rate** while the experiment is running.
6. Once again, the experiments are performed in the same laboratory where passive mixing experiments are performed. The variability in the weather conditions makes necessary to **measure ambient relative humidity and temperature**.

3.3.2. Setup Description

Once again, the assembly of the experimental setup is built in Fusion360 before production. Parts of this setup were designed during previous works at ZEF [96].

A schematic describing the experimental assembly is shown below in figure 3.15.

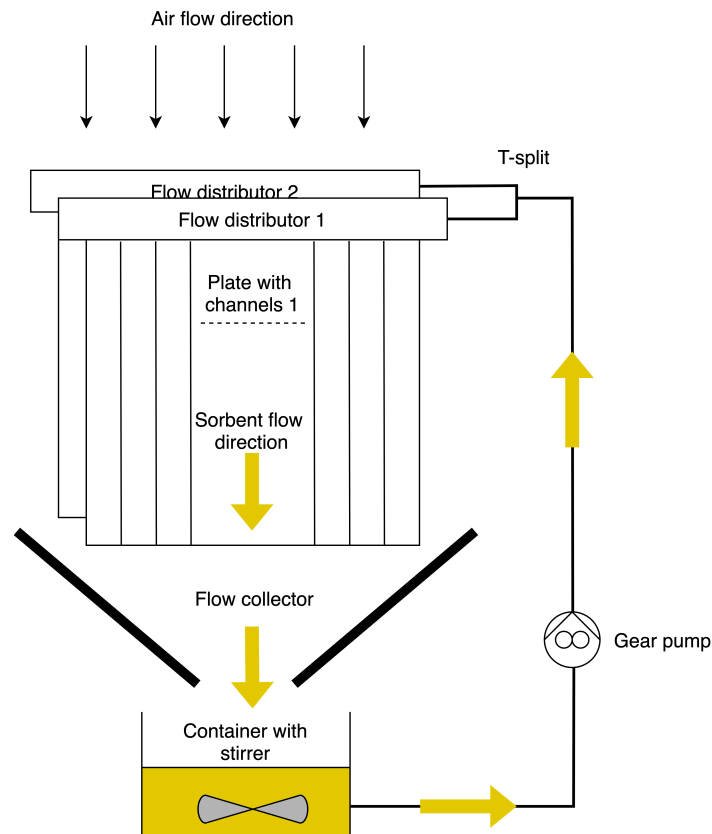


Figure 3.15: Schematic of the active mixing experimental setup

In order to explain the working principle of the setup, the main components are listed and their role in the assembly is described.

- **Gear pump** This component provides the flow of the sorbent in the setup. A simple 12 volts gear pump from Surflo (series KGP-001) is used for that [97]. The pump can reach an operating nominal power of 14.4 W. The low pressure side of the pump is connected to a reservoir where the sorbent ends up after flowing in the absorption plates. The high pressure side of the pump

is connected to a T-split junction to divide the flow in the two absorption plates. **The operational voltage of the pump is used to increase or decrease the sorbent mass and volumetric flow rate.** That can be easily done powering the pump with a power supply. A picture of the pump is shown in figure 3.16.



Figure 3.16: Surflo KGP-001 gear pump

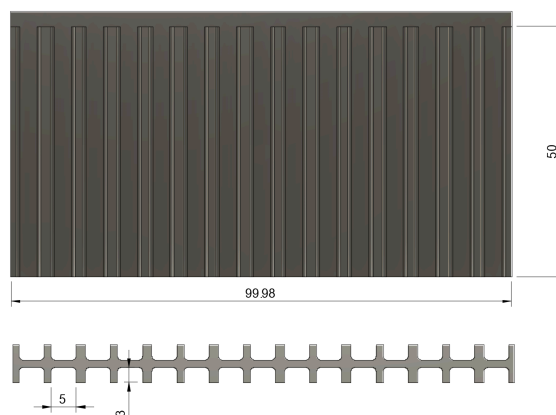


Figure 3.17: Absorption plate CAD model and dimensions (front and bottom view)

- **Flow distributors** This component has the role of distributing the sorbent flow rate into the various absorption channels. Describing the design of these distributors is outside the scope of this report. However, they are provided by ZEF and they are designed to have a single lateral inlet and multiple outlets in a direction perpendicular to the inlet. That is, the flow enters horizontally from the T-split junction and exits vertically divided into the different channels that are present in the distributor. Two distributors are used in this design so that to have two plates with channels in the assembly. That means absorption happens in a total of 4 faces in order to increase the absorption surface area and, therefore, speed up the experiment.
- **Plate with channels** Directly connected to the flow distributors are plates with channels shown in figure 3.17. As it can be seen from the picture, a total of 30 channels are present on the single plate (15 channels every face). Therefore, since two plates are used in parallel, **60 channels are present in the full assembly.** Those plates are 3D printed for reasons similar to the ones explained in section 3.2. Therefore, the flow coming from the pump is firstly split into the two distributors, then into all the various channels present in the two plates and, after absorption has happened, a flow collector drives the sorbent into the container with stirrer. The CAD model of the assembly containing the distributors, the plates and the collector is shown below in figure 3.18

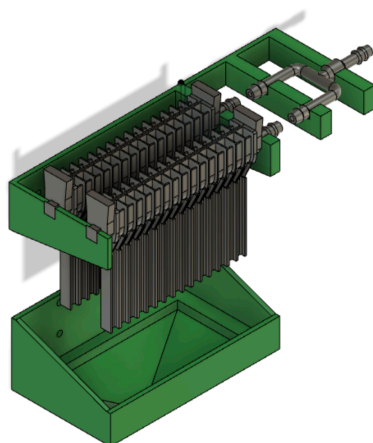


Figure 3.18: Distributors, plates and collector assembly

- **Container with stirrer** In order to provide for active mixing, the sorbent is collected in a laboratory graded glass beaker placed on top of a Dlab MS-H280-pro magnetic stirrer [98]. The stirrer will provide for active mixing before repumping the sorbent back at the inlet of the two distributors. This will allow for an experiment where the sorbent is continuously flown over the absorption plates, mixed and pumped back at the inlet of the cycle.

In the setup, the air flow rate is once again provided by the fan used in the passive mixing experiments (section 3.2). Figure 3.19 shows how the active mixing experimental setup looks during an experiment. It can be noticed the dark yellow colour of loaded TEPA and also that some liquid was dripping from the end of the absorption plates into the flow collector. This problem was later solved by increasing the wall height of the flow collector.

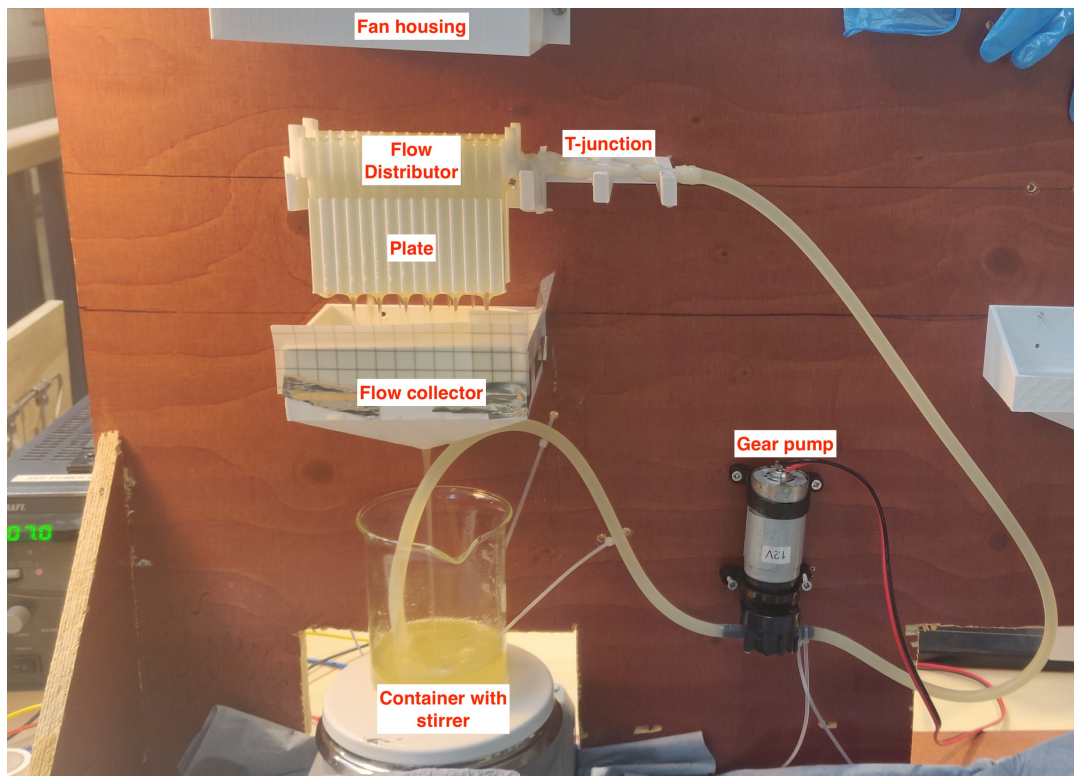


Figure 3.19: Working active mixing experimental setup

Finally, similarly to the passive mixing experiments, spectrometry is used to measure the weight concentrations of the collected samples.

3.3.3. Methodology

The methodology of the active mixing experimental investigation includes the selection of the following parameters:

Parameters
Plate inclination
Sorbent initial mass
Plate length
Sorbent initial conditions
Sorbent flow rate (or pump power)
Number of plates
Fan operating voltage

Table 3.4: Experimental parameters: active mixing

The sorbent is collected at the outlet of the flow collector at specified time intervals. Moreover, once every couple of hours, the mass flow rate generated by the pump is measured. At the end of the day, the experiment is stopped by collecting the sorbent in a sealed container. For a more detailed and complete overview of the active mixing experimental methodology, please refer to appendix A.2. Once again, the experimental plan follows below.

3.3.4. Experimental plan

The main goals of the active mixing experimental investigation is to understand the absorption performance of the setup and the effects of the sorbent flow rate and the air flow rate. The full experimental plan is described in table 3.5.

Experiment number	Pump voltage (affects sorbent flow rate) [V]	Fan voltage (affects air flow rate) [V]	Sorbent initial condition	Plate inclination	Plate length [mm]	Number of plates	Sorbent initial mass [g]
1	7	7	Pure TEPA	vertical	50	2	140
2	7	4	Pure TEPA	vertical	50	2	164
3	11	7	Pure TEPA	vertical	50	2	183.8

Table 3.5: Active mixing, experimental plan.

3.3.5. Assumptions

The assumptions relevant to this experimental investigation are described below:

- As for the passive mixing experiments, **the change in ambient temperature is assumed to have no effect on the experiment results** and variation in ambient relative humidity is assumed to only affect H_2O absorption, but not CO_2 one.
- When interrupting the experiment, it is impossible to completely collect all the sorbent inside the container. That is, some sorbent will continue to drip from the collector during the night. This sorbent amount is collected in a glass and put back into the collector when the experiment is started again in the morning. A sample is collected before stopping the experiment and another one after the dripped sorbent is put back in the bulk. It is observed that the concentrations of these two samples are exactly the same. That is, **it can be assumed that no further absorption happens during the night and also that the sorbent which drips in the glass overnight can be put back in the sorbent bulk without altering the experimental results.**
- Collecting the samples will eventually reduce the overall amount of sorbent present in the experiment. However, since less than 1 mL is collected, **it is assumed that the initial amount of sorbent is conserved during the experiment.**
- While measuring mass flow rate, 10 mL of sorbent are momentarily removed from the overall sorbent amount. The process of measuring lasts for a maximum of 2 minutes. Therefore, since the removed amount is very small and the sorbent removal only lasts a couple of minutes, **it is assumed that measuring the mass flow rate has no effect in the experimental outcome.**

4

Modelling

This chapter describes the models developed during this thesis project. Emphasis is placed on assumptions and models' relevance. Based on the specific research questions, the developed models are focusing on the fluid dynamics aspects of the passive mixing experiments and on the mass transfer aspects of the absorption process. Some of the proposed models are independent on the data collected during the experiments, some others rely on measurements done and experimental results.

4.1. Stokes Flow DNS Solver

Together with the CFD model developed in AutodeskCFD (appendix B), a Matlab DNS solver is used to model the sorbent flow in the Staggered Herringbone Mixer channel. The goal of the model is to have a structured and reliable way for simulating the effects of the ridges that are engraved on the channel floor for mixing purposes. Results from the model are used to interpret experimental ones. Since the considered flow has a Stokes' flow behavior (creeping flow), it is possible to **develop a Direct Numerical Simulation (DNS) of a simplified version of the Navier Stokes (NS) equations** that do not include the advection terms (bulk transport of matter). In fact, since the Reynolds' number of this specific problem is of the order of 10^{-3} , the viscous forces are dominant over the inertial ones, thus allowing for the simplification of the NS equations:

$$\rho \frac{\partial \mathbf{U}}{\partial t} = -\nabla P + \mu \nabla^2 \mathbf{U} + \mathbf{F} \quad (4.1)$$

$$\nabla \cdot \mathbf{U} = 0 \quad (4.2)$$

Where vector fields are indicated in bold text and:

- \mathbf{U} is the velocity field in $[m/s]$
- P is the pressure field in $[pa]$
- μ is the dynamic viscosity of the fluid of interest in $[pa \cdot s]$
- ρ is the fluid density in $[kg/m^3]$
- \mathbf{F} is the vector field of external forces like, for instance, due to gravity acceleration

Equation 4.1 is the momentum NS equation simplified for the Stokes' problem and written in vectorial form, while equation 4.2 is mass conservation. Both equations are solved with a DNS model **coded in Matlab**. The starting point of the DNS solver is an old group assignment for the course "Modelling of Thermo and Hydrodynamic systems (ME45155)" [99].

It must be noted that, apart from being a dimensional equation, 4.1 is different from the typical stokes flow momentum equation shown in section 2.4. In fact, for a generic creeping flow, the unsteady term (left-end side of the equation) is usually neglected. However, as it will be explained later, this model is built on an Adam-Bashfort time discretization scheme and it solves the flow iterating in time until

a steady state solution is reached. Therefore, for coding purposes, the unsteady term needs to be present in order to provide for the above-mentioned iterative scheme. It is recognized that solving the equation including a term that could be neglected could mean to add unnecessary complexity to the problem. However, since that term is necessary for the chosen discretization scheme, it is also recognized how the added complexity pays off when writing the model's algorithm. Since the extra term does not make the solution less valid (as it would happen when doing the opposite, i.e., removing a term which is necessary), it is chosen to consider the unsteady equation for this model.

4.1.1. Model description

The flow over the **SHM has no exact analytical solution** due to the complexity of the grooves. However, the same research group that proposed the experimental investigation relevant to the SHM geometry [20], also published another paper describing a simple analytical model to simulate the flow over such geometry [100]. **The fully three-dimensional flow can be decoupled into an unperturbed open channel flow (YZ plane) and a lid-driven cavity flow in the cross section of the channel (XY plane).** This simple physical model can yield an approximate solution for the three-dimensional problem. The model is justified by the observation that the net effect of the diagonal grooves is to generate a slip velocity at the flat boundary located at the average position (along y) of the grooved surface.

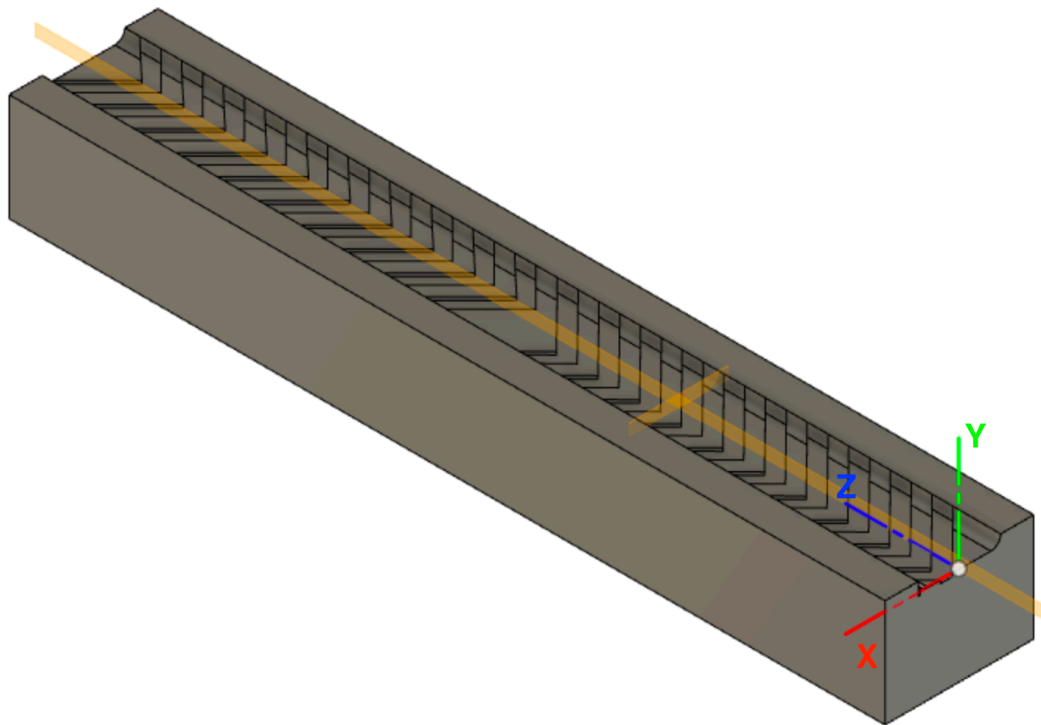


Figure 4.1: Staggered Herrinbone Mixer, CAD model view with axis

Figure 4.1 shows a representation of the simulated geometry including the two perpendicular XY and YZ planes where the physical model is represented. The geometry of the channel is the same one described in chapter 3. That strategy turns out to be quite advantageous since both the open channel flow and the lid-driven cavity flow in Stokes regime can be solved numerically by discretizing the NS momentum equations in the X , Y and Z directions.

The nomenclature for the velocity projections in the various directions is as follow:

- u , velocity component in the X direction
- v , velocity component in the Y direction
- w , velocity component in the Z direction

Before describing the model in greater details, an overview of the model inputs and outputs is shown in figure 4.2.

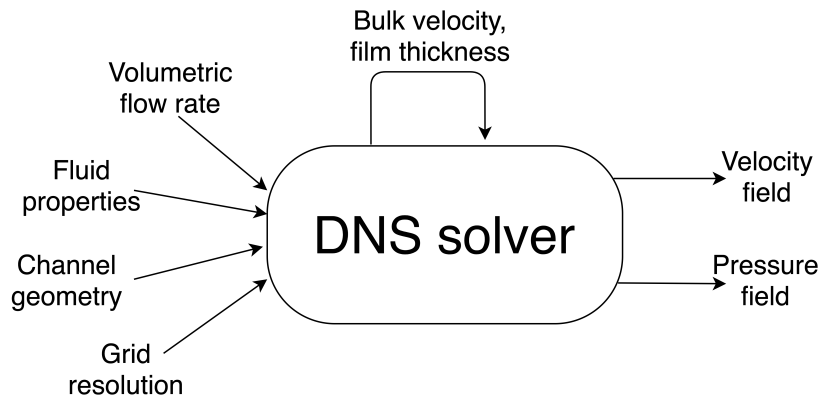


Figure 4.2: "Black box" view of the DNS solver

The considered fluid properties include density and viscosity, while the channel geometry is described with the channel width and channel length. Bulk velocity and film thickness are calculated based on the input conditions and then they are used internally during the evaluation of the Stokes flow equations. The following equations are used to calculate those two parameters [101]:

$$w_{bulk} = \frac{\dot{Q}}{L_x \cdot L_y} \quad (4.3)$$

$$film\ thickness = \sqrt{\frac{2\mu w_{bulk}}{\rho g \cos \alpha}} \quad (4.4)$$

where:

- μ is the dynamic viscosity of the sorbent in $[Pa \cdot s]$
- L_x and L_y are the channel width and channel height respectively in $[m]$
- \dot{Q} is the sorbent volumetric flow rate in $[m^3/s]$
- ρ is the sorbent density in $[kg/m^3]$
- g is the acceleration of gravity in $[m/s^2]$
- α is the plate inclination
- w_{bulk} is the sorbent average bulk velocity

The next subsections describe the domain and governing equations of the two solved flow: the open channel and lid-driven cavity flow. After that, it is illustrated how the DNS solver is built in Matlab.

Open channel flow (YZ plane) Figure 4.3 shows the geometry and the various surface types for the open channel flow (YZ plane).

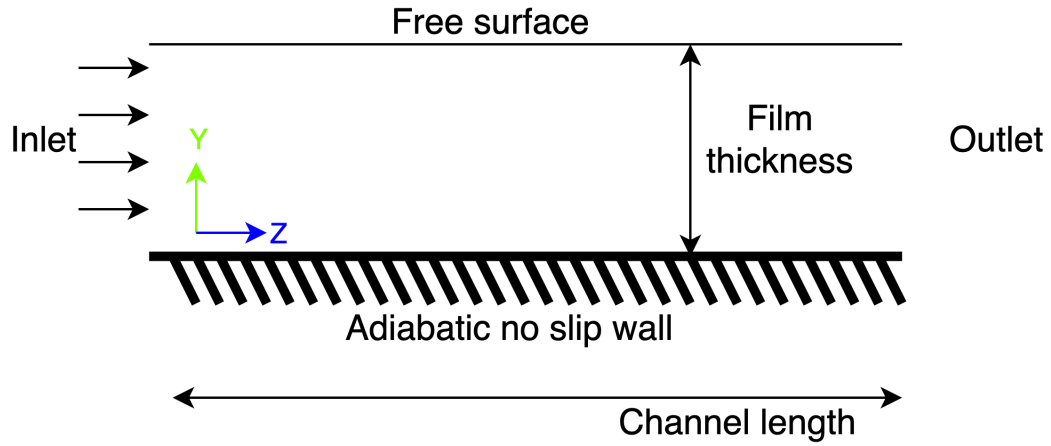


Figure 4.3: Open channel flow problem illustration

As it can be seen from the picture, the inlet boundary condition is a uniform velocity in the Z direction. This velocity is the bulk flow velocity and it is calculated using equation 4.3. On the adiabatic no slip wall, a zero velocity in the Z and Y direction is imposed, while for the free surface, zero shear stress is imposed for the velocity component in the Z direction. The governing equation for zero shear stress is the following one:

$$\tau = \mu \frac{dw}{dy} = 0 \quad (4.5)$$

The free surface is located at the interface between the liquid sorbent and the surrounding air. The location of this interface in the Y direction is equal to the film thickness calculated with equation 4.4. As explained in the assumptions of the model, it is assumed that the free surface is completely flat. This is necessary since this is not a multiphase flow simulation, but just the fluid dynamics of the sorbent is considered.

For the inlet and free surface boundary, velocity in the Y direction is imposed to be zero. Before applying the boundary conditions, the governing equations (4.1 and 4.2) are expanded:

$$\frac{\partial w}{\partial t} = -\frac{1}{\rho} \frac{\partial P}{\partial z} + \nu \left(\frac{\partial^2 w}{\partial z^2} + \frac{\partial^2 w}{\partial y^2} \right) + \frac{g \cos \alpha}{\rho} \quad (4.6)$$

$$\frac{\partial v}{\partial t} = -\frac{1}{\rho} \frac{\partial P}{\partial y} + \nu \left(\frac{\partial^2 v}{\partial z^2} + \frac{\partial^2 v}{\partial y^2} \right) - \frac{g \sin \alpha}{\rho} \quad (4.7)$$

$$\frac{\partial w}{\partial z} + \frac{\partial v}{\partial y} = 0 \quad (4.8)$$

These equations are discretized and numerically solved on a staggered grid. The approach, together with the various steps and methodologies which are used in the code are described in a later subsection. An argument similar to the one made for the open channel flow is made for the lid-driven cavity flow.

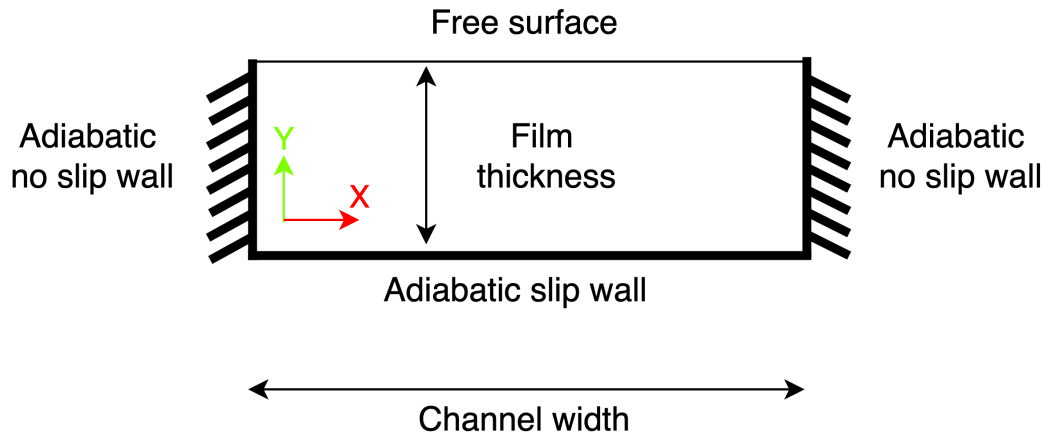


Figure 4.4: Lid-driven cavity flow problem illustration

Lid-driven cavity flow Similarly to the open channel flow case, figure 4.4 shows the geometry of the problem, together with the various surface types, for the lid-driven cavity flow problem. The height of the two adiabatic no slip walls is once again given by the calculated film thickness. Zero velocity in the Y and X direction is imposed on those walls. Regarding the free surface, a zero-shear stress condition is imposed. On the other side, at the bottom of the domain, a slip velocity is used as boundary condition. The value of this slip velocity depends on the geometry of the ridges on the floor of the channel and it is a projection of the velocity at the average height of the grooved surfaces which is calculated after the open channel flow is solved.

The equations governing this problem are shown below:

$$\frac{\partial u}{\partial t} = -\frac{1}{\rho} \frac{\partial P}{\partial x} + \nu \left(\frac{\partial^2 u}{\partial x^2} + \frac{\partial^2 u}{\partial y^2} \right) \quad (4.9)$$

$$\frac{\partial v}{\partial t} = -\frac{1}{\rho} \frac{\partial P}{\partial y} + \nu \left(\frac{\partial^2 v}{\partial x^2} + \frac{\partial^2 v}{\partial y^2} \right) \quad (4.10)$$

$$\frac{\partial u}{\partial x} + \frac{\partial v}{\partial y} = 0 \quad (4.11)$$

As it can be observed from the governing equations, the v component of the velocity field (Y direction) is calculated once again. Eventually, the magnitude of this velocity component will be added to the magnitude of the v component calculated for the open channel flow case. This can be done since the simplified NS equations considered for this problem do not have the nonlinear components from the advection contribution, thus making it possible to add up the velocity components from the open channel flow problem and the lid-driven cavity flow problem.

This concludes the description of the physical model for the three-dimensional flow in an open channel with a grooved surface. Next is proposed the description for a mathematical model coded in Matlab and used to obtain a solution for the two problems resulting from the physical model.

4.1.2. DNS solver

The equations and methodology reported in this section are used to numerically solve in Matlab the simplified Navier Stokes equations for the case of a creeping flow applied to a lid-driven cavity flow and an open channel flow. The two DNS solvers developed are identical to each other, with the only difference being the location on the grid where the boundary conditions are applied and the velocity components of the three dimensional flow that are solved (u and v for the lid-driven cavity flow and w and v for the open channel flow). Eventually, **the two solvers are using the same structure and assumptions**. Therefore, for the sake of brevity, **only the DNS solver built for the lid-driven cavity flow problem is extensively described**.

The solver is built on a staggered grid as shown in figure 4.5. The **staggered grid is selected** since it allows to avoid the pressure-velocity decoupling that is necessary in a collocated grid where the pressure and the velocity components are all computed in the same location. This grid is defining

the domain of the problem. Therefore, whenever indexing a certain variable, please refer to figure 4.5 for understanding the location of the variable in the domain.

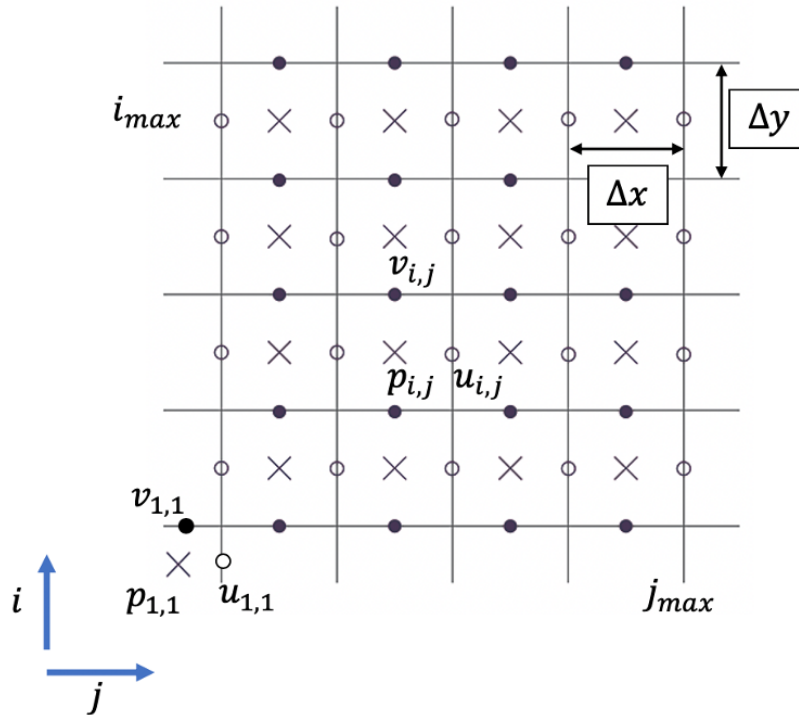


Figure 4.5: Staggered grid

The two velocity components u and v are represented by white and black dots respectively, while each element of the pressure field is represented by a cross in the center of each cell. The user decides the number of elements on the grid by specifying the values i_{max} and j_{max} . A finer grid will give more precise results in terms of numerical error but requires longer computational time. The algorithm describing the DNS solver is schematically represented in figure 4.6.

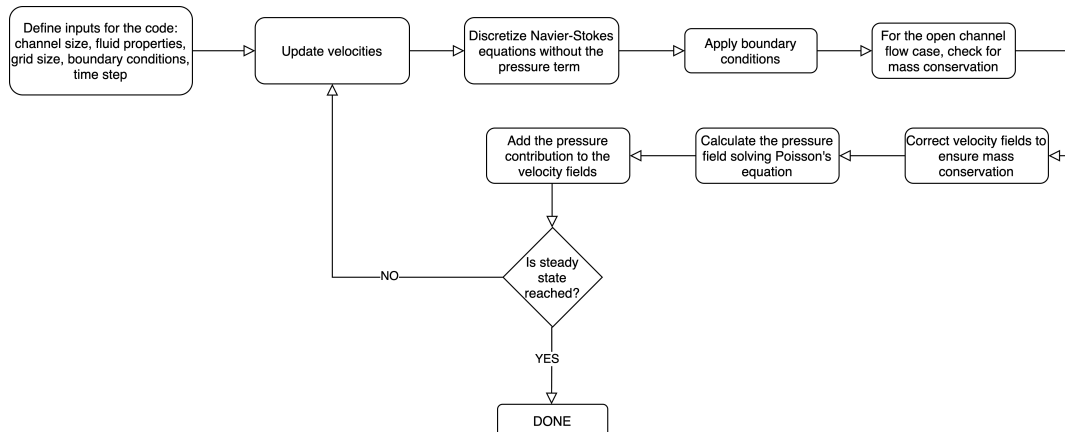


Figure 4.6: DNS solver algorithm

Initially, the unsteady equations for the velocities (equations 4.9 and 4.10) are discretized without the pressure term (u^* , v^*). **The time discretization is done using an Adam-Bashforth discretization scheme, while spatial derivatives are computed using a second-order central difference discretization.** Applying those, one obtains the following equations for the time discretization of the

momentum equation in the X and Y direction:

$$\frac{u_{i,j}^{*n+1} - u_{i,j}^{*n}}{\Delta t} = \frac{3}{2}RHS_{i,j}^n - \frac{1}{2}RHS_{i,j}^{n-1} \quad (4.12)$$

$$\frac{v_{i,j}^{*n+1} - v_{i,j}^{*n}}{\Delta t} = \frac{3}{2}RHS1_{i,j}^n - \frac{1}{2}RHS1_{i,j}^{n-1} \quad (4.13)$$

Where RHS and $RHS1$ are obtained via the second order central difference spatial discretization of the velocity terms:

$$RHS_{i,j} = \nu \left(\frac{u_{i,j-1} - 2u_{i,j} + u_{i,j+1}}{\Delta x^2} + \frac{u_{i-1,j} - 2u_{i,j} + u_{i+1,j}}{\Delta y^2} \right) \quad (4.14)$$

$$RHS1_{i,j} = \nu \left(\frac{v_{i,j-1} - 2v_{i,j} + v_{i,j+1}}{\Delta x^2} + \frac{v_{i-1,j} - 2v_{i,j} + v_{i+1,j}}{\Delta y^2} \right) \quad (4.15)$$

At this point, the boundary conditions for the velocity fields are imposed following the geometry of the two problems as described before (figures 4.3 and 4.4). The boundary conditions are imposed by overwriting the velocity profiles obtained after the discretization.

In the case of the open channel flow, **mass conservation needs to be ensured** since the geometry of the problem contains an inflow and outflow of matter. This is done by calculating the difference between the mass flow at the inlet cells and the mass flow at the outlet cells. Eventually, the outlet velocity is modified according to the value of the mass deficit calculated before. The following two equations describe this procedure:

$$\Delta M = M_{in} - M_{out} \quad (4.16)$$

$$u_{i,j,max}^* = u_{i,j,max}^* + \Delta M \cdot \frac{u_{i,j,max}^*}{M_{out}} \quad (4.17)$$

Looking at the algorithm presented in figure 4.6, the next step in the DNS solver is to solve the poisson equation in order to determine the pressure contribution in the velocity fields. Please note that, up to now, only the momentum equations have been treated in the solver. That is, the divergence equation is not satisfied by the velocity fields up to this point. Therefore, the next step includes the calculation of the pressure field by imposing a divergence free velocity field. Substituting into the divergence free equation the velocity fields corrected with the pressure contribution, one obtains a poisson equation:

$$\nabla^2 p = \frac{\rho}{\Delta t} \left(\frac{\partial u^*}{\partial x} + \frac{\partial v^*}{\partial y} \right) \quad (4.18)$$

Discretization of the poisson equation yields to the following one:

$$\frac{p_{i,j-1} - 2p_{i,j} + p_{i,j+1}}{\Delta x^2} + \frac{p_{i-1,j} - 2p_{i,j} + p_{i+1,j}}{\Delta y^2} = \frac{\rho}{\Delta t} \left(\frac{u_{i,j}^* - u_{i,j-1}^*}{\Delta x} + \frac{v_{i,j}^* - v_{i-1,j}^*}{\Delta y} \right) \quad (4.19)$$

Equation 4.19 can be used to obtain the following linear system of equations:

$$Ap = B \quad (4.20)$$

In this way, a direct solver can be built to calculate, with a simple matrix operation, the pressure field. Since the value of B has already been calculated when finding u^* and v^* , only the matrix A needs to be specified. Moreover, since the boundary conditions for the velocities have been included in the calculation of B , the matrix A only needs to include the boundary conditions for the pressure. Those simply are zero gradient for the pressure across the walls of the domain defined by the staggered grid in figure 4.5.

When p is found, velocities can be finally corrected adding the pressure contribution via the following equations:

$$u_{i,j}^{new} = u_{i,j}^* - \frac{\Delta t}{\rho} \cdot \frac{p_{i,j+1} - p_{i,j}}{\Delta x} \quad (4.21)$$

$$v_{i,j}^{new} = v_{i,j}^* - \frac{\Delta t}{\rho} \cdot \frac{p_{i+1,j} - p_{i,j}}{\Delta y} \quad (4.22)$$

This procedure is repeated until the difference between the velocities for a certain time step and the velocities for the previous time step are negligible. That is, until steady state is reached.

4.1.3. Model assumptions

This model is built upon a set of assumptions that is worth mentioning:

- As described in chapter 5, **the DNS model is validated by computing an analytical solution for the open channel flow and comparing that with the predicted results.** Since the lid-driven cavity flow uses the same code with different boundary conditions only, the validation is assumed to hold for that code as well.
- The **grooves** present on the floor of the channel are assumed to **have no influence when solving the open channel flow.** As specified by Strook et al. [100], the perturbation of the flow due to the grooves could be represented by imposing a slip velocity that counteracts the axial displacement of the flow. However, it is also specified that the magnitude of this slip velocity is very weak when compared to the open channel flow. Therefore, when solving the open channel flow, it is assumed that the floor of the channel is flat.
- The cross-section of the channel (XY plane) used to perform the experiments is not perfectly rectangular since the 3D printing manufacturing process will not deliver a perfectly flat surface. Moreover, in the design, fillets are present between the vertical walls and the floor to avoid flow accumulation on the vertical walls of the channel (see section 3.2). The irregularities due to the 3D printing process are neglected since the resolution of the 3D printer used for the experiments is on the order of 20 microns [102], thus smaller than the relevant distances in the problem. Regarding the meniscuses on the lateral walls, those are neglected as well since the aspect ratio of the channel (width over height) is much bigger than one. Those assumptions result in a **perfectly rectangular domain for the DNS solver.**
- **The free surface of the flow (that is, the gas-sorbent interface) is considered to be flat.** This assumption is needed to build the whole solver. In fact, assuming a non-flat surface means to build a solver for a multiphase flow simulation that would add a considerable amount of complexity to the proposed solver. That is considered to be outside the scope of this model.
- The fluid properties are considered to be constant in each and every part of the domain. This assumption is quite a strong one because it is known from previous experiments (see section 2.3), that the properties of the sorbent change considerably in the absorption process, especially regarding the viscosity of the fluid. In fact, as the sorbent flows over the channel, it will absorb CO_2 and H_2O . This means that the viscosity of the fluid near the end of the channel will be higher than the viscosity at the beginning of the channel. Moreover, since absorption only happens on the free surface, viscosity will vary both in the Z and Y direction. **Constant fluid properties are assumed for the sake of simplicity.** In the future, it would be interesting to couple a mass transfer model to the fluid dynamics model and simulate how the flow field is affected by the variation in fluid properties due to mass transfer between the sorbent and air.

4.2. Mass transfer model

One of the main research goals of this thesis project is to build and validate a mass transfer model able to describe how absorption is happening in this novel process. In this section, that model is described.

Its goal is to have a tool for predicting the absorption of CO_2 molecules and, as a consequence, being able of making predictions about the performances of the engineered absorption column. Similarly to the fluid dynamic model, this one is nothing else than a mathematical description of a certain physical interpretation. **For the fluid dynamic model, the physical interpretation is provided by a paper [100] and the mathematical description is coded in Matlab via a DNS solver. For the mass transfer model, both physical and mathematical interpretations are provided by the author of this report.** The physical interpretation of the absorption of CO_2 molecules is perhaps the strongest statement of this thesis project and an extensive description of that is provided in chapter 5 when talking about the main results and conclusions of this project. As a consequence, this section is only intended to describe how the model is built, list the governing equations and provide an overview of the most important assumptions. **It is not a goal of this section to justify why the model is built in this way nor to prove its validity. That will happen in chapter 5 where the physical interpretation backing up this model is explained and the results of the model are compared with the experimental results.**

4.2.1. Model description

From the literature review, it is described how absorption of CO_2 molecules into a polyamine absorbent involves the reaction of the gas molecules with the amines present in the sorbent. To understand how the model is built, it is enough to assume that, before the CO_2 molecules can react with the amine molecules, they **have to diffuse through a layer of heavily loaded sorbent which we will refer to as the "Ice-Sheet" (IS)**. That is, the modelled absorption process is a Unimolecular Diffusion (UMD) of CO_2 molecules into this layer. According to that, an image showing the stated problem is reported in figure 4.7.

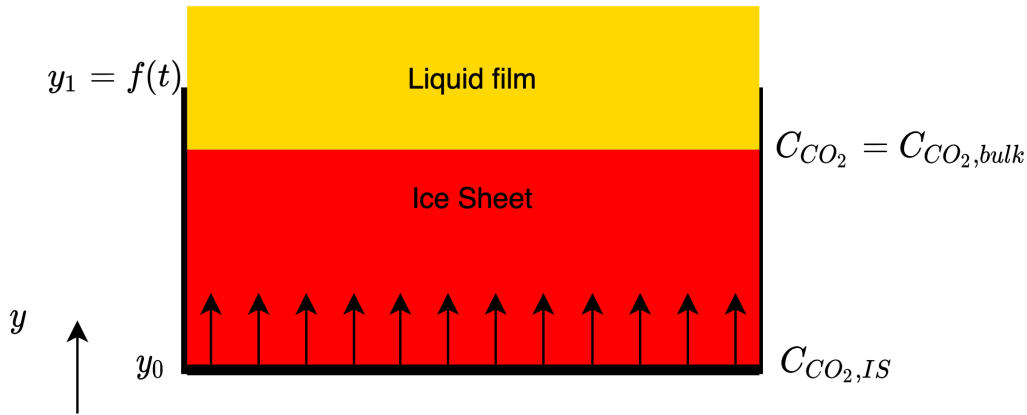


Figure 4.7: Unimolecular Diffusion (UMD) model

Looking at the picture, few things need to be clarified:

- y is a measure of a distance. The thickness of the ice layer (y_1), is not constant, but a function of time t because, while absorption is happening, **the thickness of the "Ice-Sheet" is increasing**. In fact, as soon as a CO_2 molecule is able to diffuse through the layer, it will react when in contact with the Liquid Film, and start to be itself part of the "IS", thus contributing to its growth.
- In the "Ice-Sheet", the concentration of CO_2 molecules is indicated by $C_{CO_2,IS}$, while, in the liquid film, that is $C_{CO_2,bulk}$.

The relevant theory used to define the governing equations of this problem is taken from section 3.1 of the book "Separation Process Principles, Chemical and Biochemical Operation" [6]. It is reported here for clarity.

Relevant theory When considering a binary system, one can write the molar average mixture velocity, v_M as:

$$v_M = \frac{N_A + N_B}{\rho} \quad (4.23)$$

where N is a molar flux $\left[\frac{mol}{m^2s}\right]$ and ρ is the total molar (volumetric) concentration of the system formed by specie A and B $\left[\frac{mol}{m^3}\right]$. In general, one can write the velocity of species i in terms of its molar flux and molar concentration ρ_i as:

$$v_i = \frac{N_i}{\rho_i} \quad (4.24)$$

Where the relative and overall (volumetric) concentration are related by the molar concentration C_i :

$$\rho_i = \rho C_i \quad (4.25)$$

Combining equations 4.23, 4.24 and 4.25, one obtains another expression for the molar average mixture velocity:

$$v_M = C_A v_A + C_B v_B \quad (4.26)$$

Defining the diffusion velocity of species i as v_{iD} , one can write the velocity of species i as the sum of the average mixture velocity and the diffusion velocity:

$$v_i = v_M + v_{iD} \quad (4.27)$$

Combining 4.24 and 4.27,

$$N_i = \rho_i v_M + \rho_i v_{iD} \quad (4.28)$$

Fick's law of diffusion can now be introduced as:

$$J_A = -\rho D_{AB} \frac{dC_A}{dy} \quad (4.29)$$

This equation describes the molar flux of A to be proportional to a diffusion coefficient of species A in B , D_{AB} in $\left[\frac{m^2}{s}\right]$ and to the variation of the molar concentration of specie A in the direction of diffusion (y). The minus sign is present since diffusion happens from a region of higher concentration to a region of lower concentration (similarly to the Fourier law of heat conduction). Combining equations 4.23, 4.24, 4.28 and 4.29, one can obtain an expression for the molar flux of both the specie present in the binary mixture:

$$N_A = C_A N - \rho D_{AB} \left(\frac{dC_A}{dy}\right) \quad (4.30)$$

$$N_B = C_B N - \rho D_{AB} \left(\frac{dC_B}{dy}\right) \quad (4.31)$$

Where the first right-hand side terms are fluxes resulting from bulk flow and the second terms are the diffusion fluxes.

At this point, the theory defines two main important cases:

- Equimolar counterdiffusion (EMD)
- Unimolecular diffusion (UMD)

Referring to figure 4.7, it is assumed that the mass transfer of CO_2 happens in a stagnant "IS". Therefore, $N_B = N_{IS} = 0$ and $N = N_A = N_{CO_2}$ and only the second of the two cases is relevant in this case.

Unimolecular Diffusion of CO_2 in the "Ice-Sheet" From equation 4.30, one can write:

$$N_{CO_2} = -\rho D \frac{dC_{CO_2}}{dy} + C_{CO_2} N_{CO_2} \quad (4.32)$$

Where:

- N_{CO_2} is the molar flux in $\left(\frac{mol}{m^2 s}\right)$
- ρ is the molar density of the entire system. In our case, that is the density of the "Ice-Sheet" in $\left(\frac{mol}{m^3}\right)$
- D is the diffusion coefficient of CO_2 into the "Ice-Sheet" in $\left[\frac{m^2}{s}\right]$
- C_{CO_2} is the dimensionless carbon dioxide concentration

Equation 4.32 can be rearranged in:

$$N_{CO_2} = -\frac{\rho D}{1 - C_{CO_2}} \frac{dC_{CO_2}}{dy} \quad (4.33)$$

Integrating this equation in space between $y_0 = 0$ and $y_1(t)$ and in concentration between $C_{CO_2,bulk}$ and $C_{CO_2,IS}$, one obtains:

$$N_{CO_2} = \frac{\rho D}{y_1(t)} \ln\left(\frac{1 - C_{CO_2,bulk}}{1 - C_{CO_2,IS}}\right) \quad (4.34)$$

So far, the encountered equations are quite general and they can be applied to solve countless diffusion problems. With respect to that, giving an equation for $y_1(t)$ means to go into more details in the solution of our specific problem. In this framework, $y_1(t)$ can be seen as the average distance that our average CO_2 molecule has travelled after a certain time t . Since diffusion is a random process, $y_1(t)$ can be referred to as a spacial extent of a random motion. In statistical mechanics, the most common measure of spacial extent of random motion is the **mean square displacement (MSD)**, defined as:

$$MSD := \frac{1}{N} \sum_{i=1}^N |x^i(t) - x^i(0)|^2 \tag{4.35}$$

Where:

- $x(t)$ is a position of particle i at time t
- N is the number of total particles

In our case, we are interested in the MSD for a diffusion motion, i.e., a Brownian motion [103]. That is, particles that are randomly moving suspended in a fluid medium. Using statistical mechanics, it can be shown that the MSD for a brownian particle in n dimensions is [103]:

$$MSD = \langle (x(t) - x_0)^2 \rangle = 2nDt \tag{4.36}$$

Where:

- n is the number of dimensions
- D is the diffusion coefficient
- t is time
- $\langle \rangle$ brackets are indicating an average

Following equation 4.36, because we are looking at a one-dimensional problem, we can write $y_1(t) = \sqrt{2Dt}$. Substituting this expression into equation 4.34, integrating in time and multiplying by the overall surface area of the process of interest A , one can find the moles of CO_2 that are captured in a certain time t as:

$$mol_{CO_2} = A \int_0^t N_{CO_2} dt = A\rho\sqrt{2Dt} \ln\left(\frac{1 - C_{CO_2,bulk}}{1 - C_{CO_2,IS}}\right) \tag{4.37}$$

According to the author, it is interesting to note that, for the process of interest, the model predicts a direct proportionality with respect to \sqrt{D} for the flux of CO_2 molecules. This is in accordance with information found in papers like the one from Dankwerts [45] and in theories like surface renewals or penetration theory [6].

Once again, this model is coded in Matlab and validated with experimental results coming from both the passive mixing (EC only) and the active mixing experiments. The algorithm used in the Matlab code can be summarized by figure 4.8

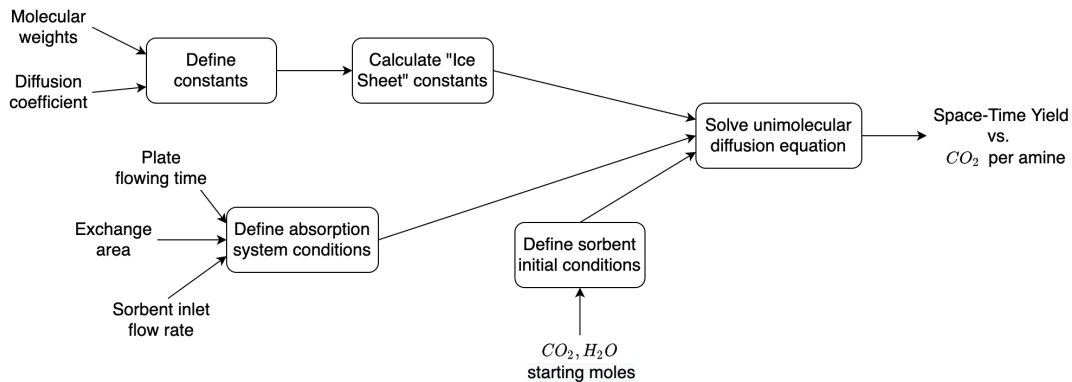


Figure 4.8: Unimolecular Diffusion (UMD) model: code algorithm

In calculating the "Ice-Sheet" constants, it is necessary to know the composition of it. It is assumed here and explained in chapter 5 that **the "Ice-Sheet" is nothing else than a layer of fully-loaded TEPA sorbent**. The composition of this layer is taken from an old experiment performed at ZEF where an amount of TEPA was loaded until saturation with CO_2 and H_2O . The resulting composition of the loaded sample was:

- $C_{CO_2,max} = 0.19$ [wt%]
- $C_{H_2O,max} = 0.33$ [wt%]
- $C_{TEPA,max} = 0.48$ [wt%]

Two other things are worth mentioning:

- Equation 4.37 is solved having time as variable and the amount of absorbed CO_2 is given by simply solving that equation. For the passive mixing experiments (EC), that is the time necessary for the sorbent to flow past the different modules, that is, the residence time measured during the experiments. On the other side, for the active mixing experiments, that is the time necessary for the sorbent to flow past the absorption plates. That time is measured as well during the experiments.
- **No data is fitted to the model, except for a starting condition.** In fact, the model assumes that the process is driven (limited) by the CO_2 diffusion in the ice layer. That is, **the model can be compared to experimental data if, and only if, the data point is limited by the liquid phase of the process**. For the Empty Channel experiments, that is always the case and the starting point is the first available data point (at 100 mm distance). On the other hand, for the active mixing experiments, as it will also be observed and explained in the results section, initially, it is the air phase that is driving the rate of absorption. Therefore, the first fit point is the first data point recognized not to be air side limited.

4.2.2. Model Assumptions

The assumptions relevant to this model are the following ones:

- The "Ice-Sheet" theory is assumed to hold for this model. That is, **it is assumed that the mass transfer of CO_2 occurs through stagnant, but growing ice**. That is, diffusion of CO_2 molecules in the "IS" is much faster than diffusion of "IS" molecules in TEPA molecules.
- Molar densities and diffusion coefficient in the "Ice-Sheet" are not influenced by the presence of diffusing CO_2 molecules
- In a real process, the absorption of CO_2 molecules happens together with the absorption of H_2O molecules. This model aims at describing only the former. Therefore, **it is assumed that the "IS" has reached a full loading of H_2O and also that the liquid film of the sorbent is fully loaded with water**. This assumption is considered to be quite strong in the case of modelling the active mixing experiments. In fact, experiments show that the first modelled data point (that is, the first one to be liquid phase limited), is already close to water saturation. Regarding the empty, single channel experiments, it is not necessary to consider the presence of water in the bulk of the sorbent because, since there is no mixing involved, the concentration of CO_2 in the bulk (that is, $C_{CO_2,bulk}$ in equation 4.37) is independent on how many water molecules are present in the bulk simply because $C_{CO_2,bulk} = 0$ always.
- **It is considered that the sorbent properties stay constant during absorption.** That will have a direct influence on the residence time (t) in equation 4.37 since t will always stay constant as a consequence of viscosity staying constant. In reality, it is observed that the sorbent viscosity is changing during absorption. However, for the passive mixing experiments, it is observed that the residence time is almost linearly increasing with the distance on the channels. That could be explained by the fact that the sorbent molecule in contact with the channel are actually pure sorbent since CO_2 molecules will never diffuse through the entire film thickness during the experiment, therefore, the friction between the channel and the sorbent does not change so much. Regarding the active mixing case, during the experiments, it is observed that the residence time

on the plate will firstly increase and then decrease again as a consequence of a first increase in viscosity and then decrease of viscosity when the loading of CO_2 increases. Therefore, t is taken as a mean value between the different ones measured during the experiments. Moreover, it is observed that the oscillation of the residence time is not so significant (± 2 seconds) and, also, that within that oscillation, the results given by the model are not diverging so much.

- When modelling active mixing experiments, it is assumed that **mixing happens instantaneously**. That is, after equation 4.37 is used to calculate how many moles of CO_2 are captured, those moles are assumed to be immediately and uniformly distributed in the bulk of the sorbent. That is, C_{bulk} is immediately updated every time the sorbent has flown over the plate (with a residence time t).

5

Results

The main goals of this research project include to find a way of inducing mixing in a novel absorption process. The idea is that mixing can improve the process in terms of Space-Time Yield (STY), i.e., the flux of absorbed gases and in terms of relative loading of CO_2 and H_2O . Moreover, research goals and objectives include the investigation of the fluid dynamics and mass transfer dynamics of the process via the formulation of a CFD and Mass Transfer model. Finally, all the different answers obtained with the investigation have to be used for engineering an absorption column able to capture a certain required amount of CO_2 and H_2O in the most efficient way.

In this chapter, all the relevant obtained results are collected. That includes **results from the experimental investigation as well as results from the developed models**. Eventually, the **theoretical framework behind the formulation of the mass transfer model is proposed and validated** by comparing the model's results to the experimental ones and looking at confirmations from literature.

Figure 5.1 is intended to give an overview of the main results discussed in this chapter. As it can be seen, three main sections are proposed: mixing experiments, modelling and a formulation of the process' physical interpretation. In general, results are shown and discussed/validated. Finally, it is underlined what is the contribution of these research topics to the main research questions, goals and objectives.

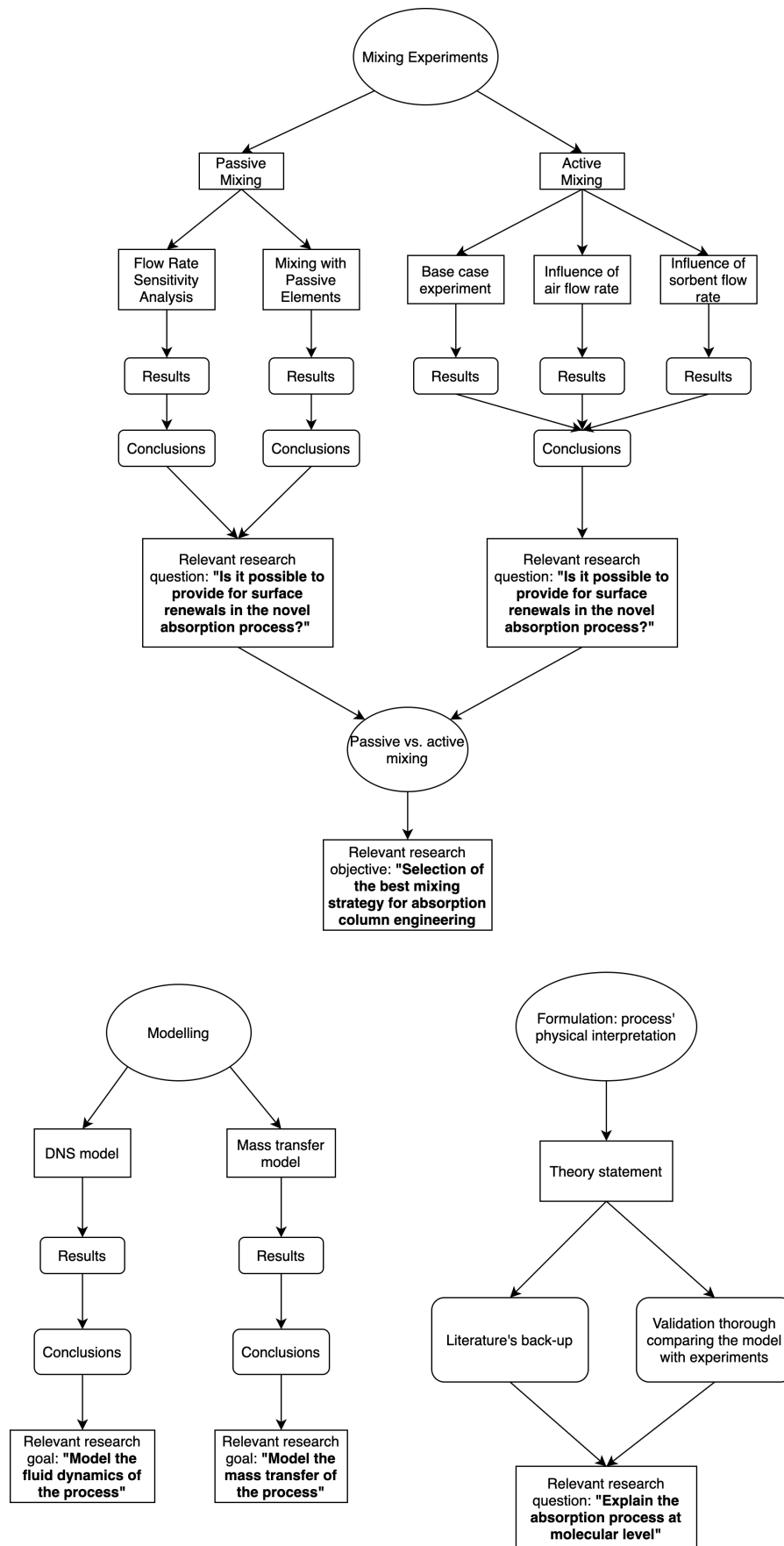


Figure 5.1: Overview of the main results presented in chapter 5

5.1. Mixing Experiments

This section presents the main results obtained with the experimental setups and experimental plans presented in chapter 3. Results are collected and discussed in separate paragraphs with one section dedicated to the passive mixing experiments and another one to the active mixing experiments. It must be noted how **results and conclusions are presented in two separate paragraphs in order to distinguish between the measured experimental results and the interpretation that is given to them**. Finally, a third section is included to compare the two mixing strategies in order to justify the selection of the one used for the absorber design.

5.1.1. Passive Mixing Experiments

For the passive mixing experiments, the collected results include a flow rate sensitivity analysis performed on the Empty Channel (EC) geometry and results from passive mixing using the Staggered Herringbone Mixer (SHM) and the Bridges (BR) geometries. It is shown how **no mixing is observed when using passive elements and how flowing the sorbent at different flow rates can influence the experimental outcome** in terms of Space-Time Yield and relative CO_2 and H_2O loading.

Regarding the Space-Time Yield calculation, multiple ways exist for doing that. Therefore, as a matter of clarity, it is important to specify which way of calculating the Space-Time Yield is used to interpret the results coming from the different experiments. This is especially important when comparing results or when using the STY for design purposes. In the following results plots, the STY is calculated as a cumulative one with the following equation (please note that, for H_2O , the same equation holds):

$$STY_{cumulative} = \frac{\dot{Q}_{sorbent} \cdot \rho \cdot CO_2/amine}{MW \cdot d \cdot w} \quad (5.1)$$

Where:

- $\dot{Q}_{sorbent}$ is the volumetric flow rate used in the experiment in $\left[\frac{m^3}{s}\right]$
- ρ is the density of the sorbent in $\left[\frac{kg}{m^3}\right]$
- $CO_2/amine$ is the measured gas concentration in $\left[\frac{kg_{CO_2}}{kg_{TEPA}}\right]$
- MW is the molar weight of CO_2
- d is the distance on the channel where the sample is collected in $[m]$
- w is the width of the channel in $[m]$

Flow rate sensitivity analysis (EC only) Figure 5.2 and 5.3 show the relative loading of CO_2 and H_2O at different distances on the plate for the different volumetric flow rates used during the experiments.

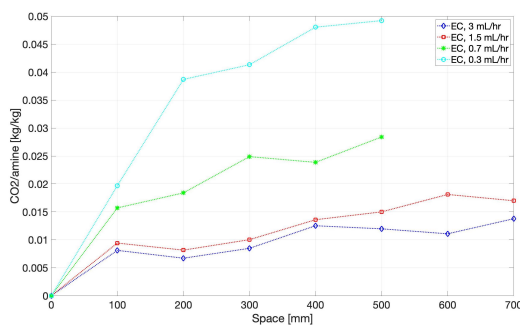


Figure 5.2: CO_2 per amine loading at different distances in the channel, for different volumetric flow rates

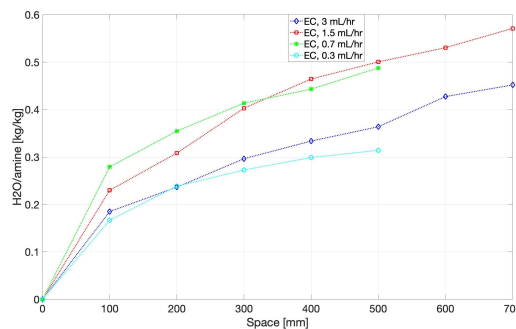


Figure 5.3: H_2O per amine loading at different distances in the channel, for different volumetric flow rates

The two figures show that the CO_2 and H_2O loadings are increasing at longer distances on the channel. Moreover, for CO_2 , it looks like the lower is the flow rate, the higher will be the relative loading

at the same distance in the channel. That is not observed to always be the case for the H_2O case, where it seems that there is no clear correlation between the flow rate and the relative water loading at a certain distance on the plate.

Regarding the Space-Time Yield, figures 5.4 and 5.5 show the STY calculated at different distances on the channel for different flow rates in the case of CO_2 and H_2O .

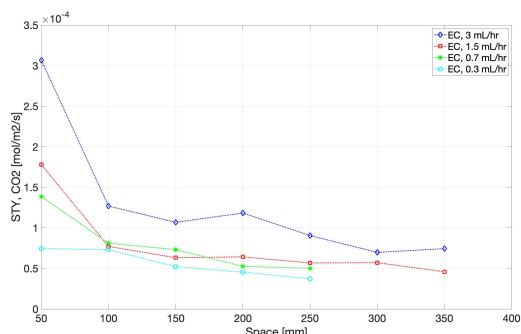


Figure 5.4: CO_2 STY at different distances in the channel, for different volumetric flow rates

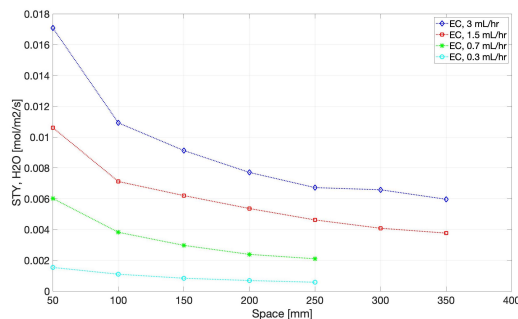


Figure 5.5: H_2O STY at different distances in the channel, for different volumetric flow rates

It can be seen how the Space-Time Yield is decreasing as the sorbent proceeds in the channel. That is, the flux of water and carbon dioxide molecules is decreasing for longer distances on the plate. Moreover, opposite to the loading vs flow rate plots, a generally higher Space-Time Yield is observed at higher volumetric flow rates.

Conclusions on flow rate sensitivity analysis Looking at the experimental results presented in figures 5.2, 5.3, 5.4 and 5.5, the following conclusions can be made:

- For every flow rate, the loading curves obtained in figure 5.2 show that the concentration of CO_2 in the samples reaches a plateau after a certain distance in the channel. Moreover, the higher is the flow rate, the lower is the relative loading at a certain channel distance. **A higher flow rate means a higher film thickness and, as a consequence, higher dilution of CO_2 in the bulk.** This suggests that layers sufficiently distant from the free surface are not reached by diffusing CO_2 and are not contributing to the absorption process. That is, **the process is diffusion limited at the sorbent side.** That is in agreement with previous research at ZEF [14]. Since it can be assumed that for equal residence times, the penetration of gas molecules is the same, the effects of different film thicknesses can be seen also when plotting the relative loading with respect to the residence time. Figure 5.6 shows that, **for the same residence time (same penetration), the lower is the flow rate (the lower is the film thickness), the higher is the relative sorbent loading.**

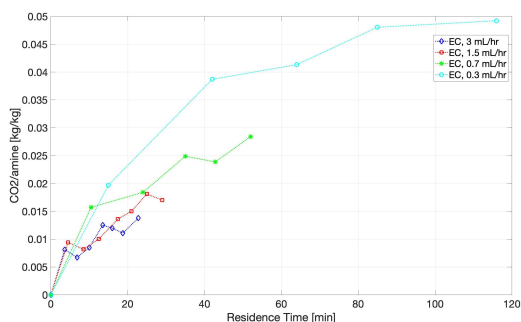


Figure 5.6: CO_2 per amine loading as function of the measured residence time and sorbent flow rate

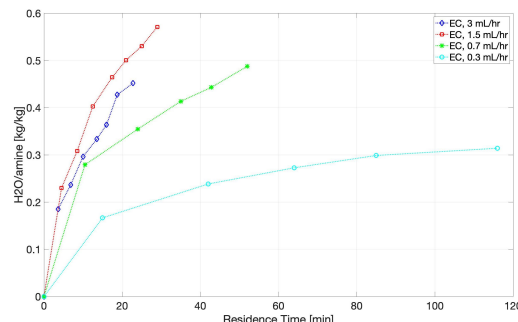


Figure 5.7: H_2O per amine loading as function of the measured residence time and sorbent flow rate

- Concerning water loading (figure 5.3), differently from carbon dioxide loading, it looks like there is no direct correlation between the sorbent flow rate and the relative loading. That could be explained

by the fact that the relative loading does not depend only on the flow rate of the experiment, but also on the driving force, that is, the ambient relative humidity, present in the room the day of the experiment. The higher relative humidity was measured for the 3 and the 1.5 mL/hr experiments (70%) while a 30% humidity was measured for the 0.3 mL/hr experiment and 43% for the 0.7 mL/hr experiment. Looking at 5.7, the higher relative loading corresponds to a higher relative humidity, thus higher driving force, measured the day of the experiment.

- On the other side, the plots for the Space-Time Yield in figure 5.4 and 5.5, are showing a decrease in the flux of the gases at longer distances on the channel. However, the shape of the curve is substantially different for the two gases. In fact, for CO_2 , the STY suddenly decreases after the first 100 mm and then the curve reaches an almost flat shape, with STY staying almost constant at different locations on the plate. For H_2O , the decrease is more linear and continues up until the last collected data point. Moreover, the magnitude of the STY for water and carbon dioxide is orders of magnitude different. That suggests that **the absorption of CO_2 and H_2O are two, very different, processes**. That is in agreement with reviewed literature describing the former as a **chemical absorption process** and the latest as a **physical absorption process**. The physical interpretation of the absorption of CO_2 presented in this chapter will shine some light on the way the absorption of that gas is happening. Regarding the influence of the flow rate, it can be seen how, in general, a higher STY is observed at a higher flow rate (same distance on the channel). For CO_2 , the STY calculated for the 3 mL/hr experiment is relevantly higher than the STY calculated for the other flow rates. That could be explained by the fact that, being a chemical absorption process, the reacted CO_2 on the free surface of the sorbent stream will have less time to prevent further absorption of CO_2 when the flow rate, therefore the sorbent travel speed, is higher. Figure 5.2 and 5.4 underlines a trade-off between a higher relative loading and a lower average CO_2 flux when the sorbent is flown at different flow rates in the channel.

Mixing with passive elements Figures 5.8 and 5.9 show CO_2 and H_2O loading at different distances on the channel, for the different mixing geometries at 3 mL/hr sorbent flow rate, while 5.10 and 5.11 show the same at 1.5 mL/hr flow rate.

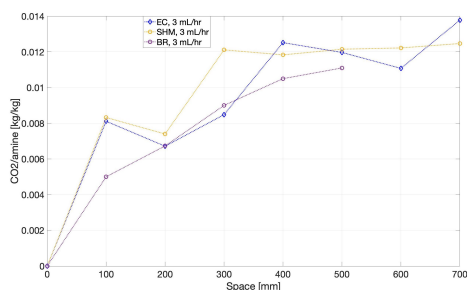


Figure 5.8: CO_2 per amine loading at different distances in the channel, for different channel geometries, at 3 mL/hr flow rate

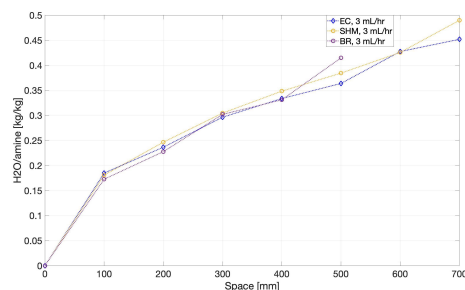


Figure 5.9: H_2O per amine loading at different distances in the channel, for different channel geometries, at 3 mL/hr flow rate

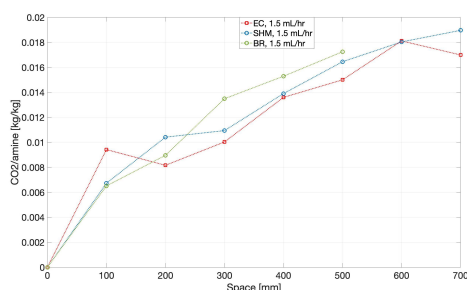


Figure 5.10: CO_2 per amine loading at different distances in the channel, for different channel geometries, at 1.5 mL/hr flow rate

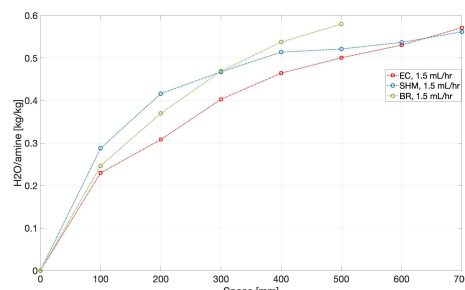


Figure 5.11: H_2O per amine loading at different distances in the channel, for different channel geometries, at 1.5 mL/hr flow rate

In those figures, the **EC geometry is used as a base case channel where no mixing elements are present**. Therefore, comparing the EC geometry with the mixing geometries (SHM and BR), one can understand if passive mixing can be achieved with the proposed channels' designs. However, looking at the loading curves for both H_2O and CO_2 , **no significant divergence is observed between the different channel geometries**. That is, it looks like the channel with bridges and the channel with engraved staggered herringbones are diffusion limited in the same way as the base case channel. That can be said of all loading curves obtained with either 3 or 1.5 mL/hr flow rate. Due to that, **also the Space-Time Yield curves show similar results for all the different passive mixing geometries**. That is shown in the following pictures:

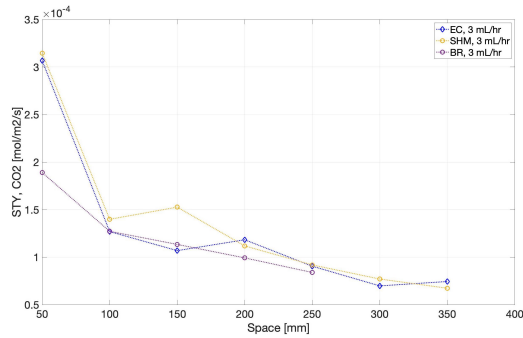


Figure 5.12: CO_2 STY at different distances in the channel, for different channel geometries, at 3 mL/hr flow rate

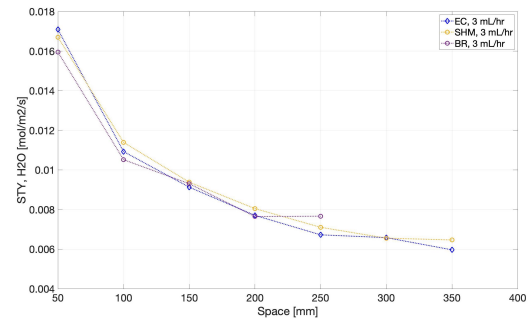


Figure 5.13: H_2O STY at different distances in the channel, for different channel geometries, at 3 mL/hr flow rate

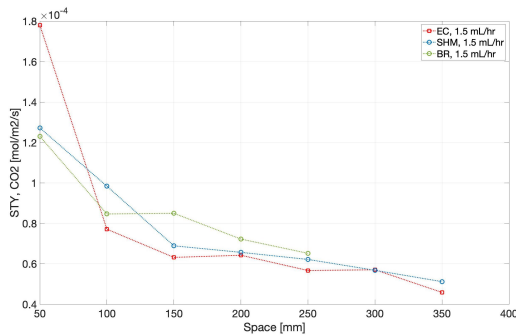


Figure 5.14: CO_2 STY at different distances in the channel, for different channel geometries, at 1.5 mL/hr flow rate

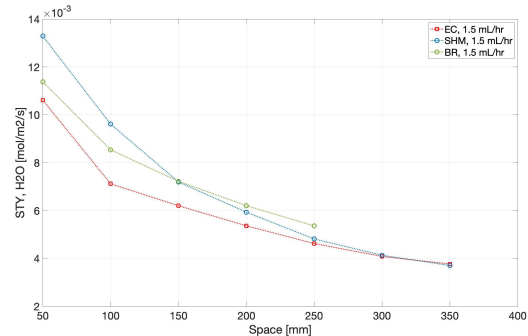


Figure 5.15: H_2O STY at different distances in the channel, for different channel geometries, at 1.5 mL/hr flow rate

In the next paragraph, the results of the passive mixing experiments are commented and possible reasons explaining the observed behaviors are presented.

Conclusions on mixing with passive elements Following the results shown in the last paragraph, it is possible to draw the following conclusions about improving the novel absorption process via mixing with passive elements:

- Regarding the SHM geometry, one could be tempted to say that mixing is not happening because the grooves are present on the floor of the channel. Therefore, since the downstream flow velocity is zero at that location, the velocity projection (in the ridges direction) of a zero velocity equals, of course, zero. However, this explanation does not cope with the fact that the grooves in the channel have a certain depth and, as specified as well by Stroock et al. [100], **the effective slip velocity generated by the grooves is located at the average vertical position of the grooved surface**. At that location, the axial velocity (in the flow direction) is very small, but not zero. Therefore, it rather looks like some slip velocity is being generated, but since we are talking about a projection of an extremely small velocity (axial flow has $Re = 10^{-3}$), it comes with no surprise that also **the magnitude of the projected velocity is extremely small**. Therefore, it can be concluded that the induced mixing effect is too small to be appreciated in the experimental

results. The DNS model will shine some light on the magnitude of the slip velocity that one could expect when having such flow condition. It will be observed that, even projecting the highest observed velocity, the lateral slip velocity is extremely small.

- The bridges geometry is not showing any mixing as well. Figure 5.16 highlights a close up view of the flow over a single bridge during an experiment.



Figure 5.16: Detail of a BR geometry during an experiment

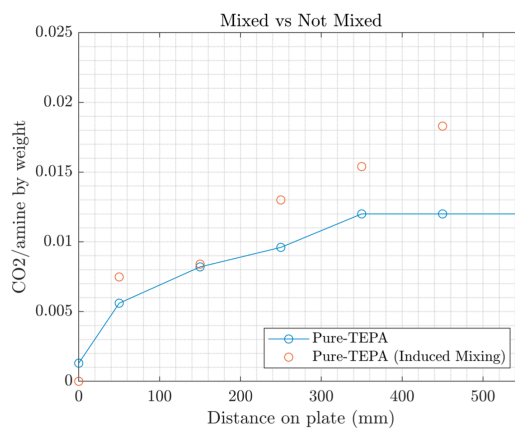


Figure 5.17: CO_2 per amine loading when mixing is induced using bridges at different distances on the channel, per [14]

As predicted, it looks like the presence of a bridge is generating flow accumulation upstream of it and, therefore, a pressure gradient in the flow direction. Still, no mixing is observed. A reason could be that, **even if a pressure drop is present in the flow direction, there is no pressure drop generated in a direction perpendicular to that, that is, from the bulk of the stream toward the free surface.** Therefore, it looks like the effect of the bridge is simply to accumulate some of the top surface flow upstream of it. It must be underlined how this result is in opposition with the one described by previous work at ZEF [14]. In fact, previously, it was found that the presence of bridges will generate an (almost) linear increase of the loading with respect to the distance on the channel (figure 5.17). That clearly diverges from the results observed in those experiments. However, as of today, it was not possible to develop a satisfactory explanation for that. It might be that the results are diverging because the experiments were performed in slightly different ways, especially the collection of the samples. In fact, in [14], a sample consisted of all the sorbent collected in between each bridge, while, in this case, only the sorbent flowing at the end of each modules is collected. Also, it could be that the bridges designed in [14] were more effective in inducing mixing.

- Despite for the reasons behind, it can be concluded that, for the novel absorption process, **passive mixing is not a promising solution for significantly improving the absorption rate.** That is, **it is not possible to provide for top surface renewals with the designed passive mixing geometries.** That answers part of the first research question. In the next subsection, the same question is answered using active mixing instead.

5.1.2. Active mixing experiments

For the active mixing experiments, the collected results include plots of Space-Time Yield as a function of the CO_2 and H_2O per amine concentration in the sorbent bulk. Following table 3.5, results are shown for the three performed experiments.

In this subsection, the Space-Time Yield is calculated as a cumulative STY in the following way:

$$STY_{cumulative} = \frac{\sum_{t=0}^t CO_2, moles(t)}{t \cdot A} \quad (5.2)$$

Where:

- $\sum_{t=0}^t CO_2, moles(t)$ is the total amount of moles captured up until time t in [mol]
- t is the time at which the sample is collected in [s]
- A is the surface area of the collection plates used in the experiment in [m^2]

Active mixing, experiment #1: reference Figures 5.18 and 5.19 show the results obtained for CO_2 and H_2O absorption in the first experiment using the active mixing setup.

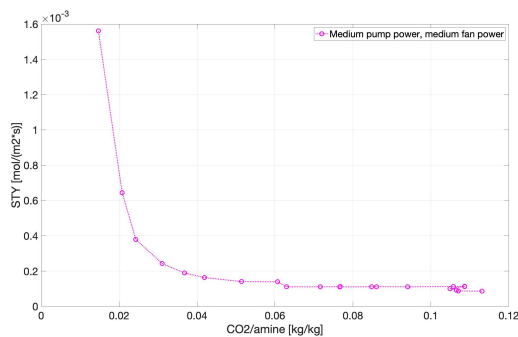


Figure 5.18: STY in function of CO_2 per amine loading, reference active mixing experiment

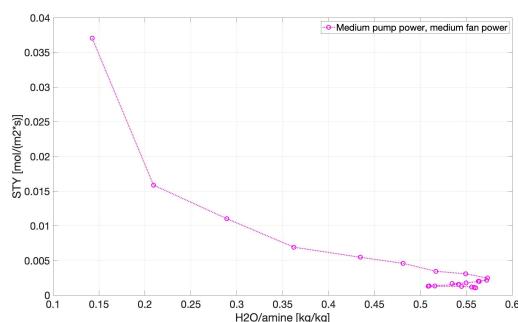


Figure 5.19: STY in function of H_2O per amine loading, reference active mixing experiment

In both pictures, it is clear how a lower STY (thus, lower flux) is experienced when the concentration of CO_2 and H_2O are increasing within the bulk of the sorbent. Moreover, **it looks quite clear how the rate of decrease of the STY is very different between the CO_2 and H_2O cases**. In fact, for H_2O , the STY is steadily decreasing up until an equilibrium is reached (sorbent saturation) at about 0.5 H_2O per amine [kg/kg]. On the other side, the STY for CO_2 experiences a sudden drop in the first part of the graph (very low loading) and then the STY stays almost constant (it is still slightly decreasing) until the end of the experiment. Conclusions from those results are presented in the next paragraph.

Conclusions on active mixing, experiment #1: reference Results from the first active mixing experiment already show some interesting insights in the absorption process. Those are collected in this paragraph.

When referring to a "limitation", example: mass diffusion in the liquid side, it means that is the slowest phenomenon happening in the process, that is, the one deciding the rate of absorption. For example, when the limitation comes from diffusion in the liquid side, it means that the gas molecules are diffusing much slowly in the liquid phase than in the gas phase. Being the slowest among the different phenomena, the rate of absorption (or STY), will be decided by how long it takes for the gas molecules to diffuse in the liquid molecules. **The active mixing experiments were designed with the goal of reducing the absorption limitations coming from the liquid side.** That is done by actively mixing the sorbent in order to provide for fresh amine molecules at the interface.

Since it is known that the single channel experiments are diffusion limited, it is interesting to compare the results of this first active mixing experiment with the single channel, passive mixing experiments to see whether actively mixing the sorbent can actually reduce the diffusion limitation coming from the liquid side. Figures 5.20 and 5.21 are used to show that.

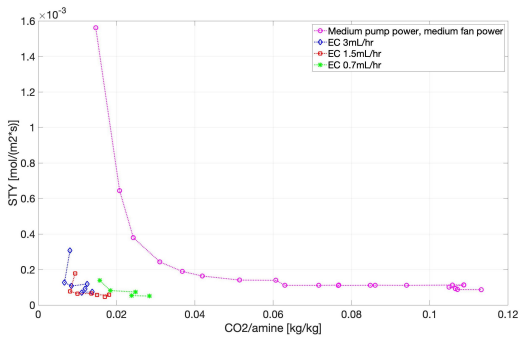


Figure 5.20: STY in function of CO_2 per amine loading, comparison between the reference active mixing experiment and single channel experiments

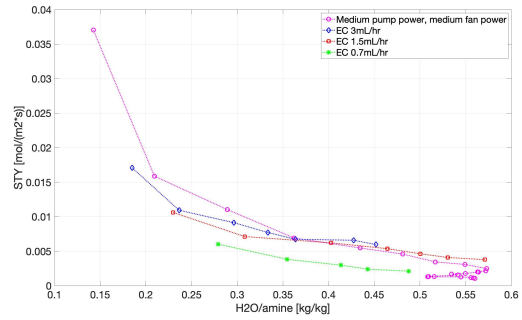


Figure 5.21: STY in function of H_2O per amine loading, comparison between the reference active mixing experiment and single channel experiments

For the CO_2 case (figure 5.20), it can be seen how, for low amine relative loading, the STY value observed for the repumping (active mixing) experiment is significantly higher than the one observed for the single channel (passive mixing) experiments. After the initial drop, the STY of the repumping experiments reaches values comparable to the ones reported in the passive mixing experiments. It can be concluded that, **for the initial part of the graph, the active mixing experiment is not limited by diffusion in the liquid phase, but from transport in the gas phase instead.** That is, the rate of absorption is decided by how quickly the molecules of CO_2 can reach the proximity of the gas-liquid interface. **This hypothesis is tested in the second active mixing experiment** by repeating it with reducing the air flow rate generated by the fan. Regarding H_2O , figure 5.21, shows similar trends for the STY of both passive and active mixing experiment. It can be concluded that, differently from the CO_2 case, **the water absorption is still limited by diffusion in the liquid phase from the start to the end of the experiment.** The averagely lower STY observed for the EC, 0.7 mL/hr flow rate can be explained with the fact that the relative humidity measured that day was 43 %, lower than the one during the other experiments. Therefore, the driving force was lower as well.

Active mixing, experiment #2: changing the air flow rate Once again, **the goal of this experiment is to observe the effect of decreasing the air flow rate while actively mixing the sorbent.** It must be underlined that this experiment was designed after comparing the results of active mixing, experiment #1 with the results coming from the passive mixing experiment. Therefore, the goal is to verify if, at the beginning of the experiment, limitations are coming from the air side and not from the liquid side.

Figures 5.22 and 5.23 show a comparison of results obtained for CO_2 and H_2O absorption between the reference and lower air flow rate active mixing experiment.

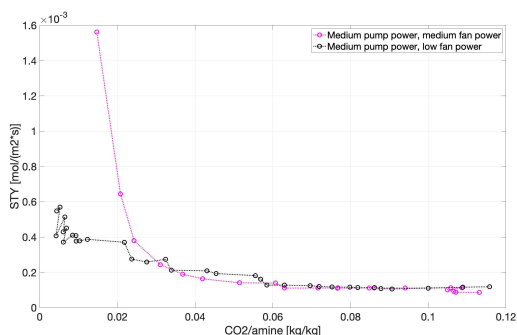


Figure 5.22: STY in function of CO_2 per amine loading, comparison between the reference and lower air flow rate active mixing experiment

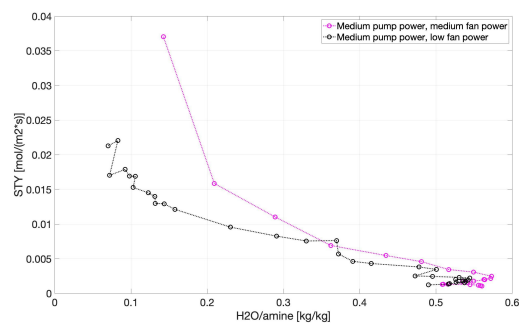


Figure 5.23: STY in function of H_2O per amine loading, comparison between the reference and lower air flow rate active mixing experiment

For the CO_2 case, it must be underlined the substantial difference of reported STY values for the initial part of the graph (low relative amine loading). A similar behavior is observed for the H_2O case. Conclusions traced from that follows below.

Conclusions on active mixing, experiment #2: changing the air flow rate Before diffusing into the liquid phase, CO_2 and H_2O molecules have to be transported into the gas phase toward the interface. Figures 5.22 and 5.23, underline how, **if the air mass flow rate is reduced enough, transport in the gas phase can actually be slower than diffusion in the liquid phase**. When the two curves merge again, it means that the liquid phase starts to be a limit for the process. In fact, due to the increase in concentration, diffusion in the liquid sorbent stream will slow down until not all the molecules reaching the interface can be dissolved in the liquid phase. That is, until the (possible) flux of molecules in the gas phase is greater than the (possible) flux of molecules in the liquid phase. Due to mass conservation, the lower flux will be the one "deciding" the rate of absorption.

It must be underlined that, increasing the air mass flow rate indefinitely, does not mean that the STY will keep increasing indefinitely. In fact, there will be a certain air flow rate for which the liquid phase will start again to be a limit even at very low concentrations. A third experiment using a higher air flow rate would be interesting to find out about this "upper bound".

Active mixing, experiment #3: changing the sorbent flow rate After having discussed about the limitations coming from the gas phase, one last active mixing experiment is performed to shine some light on the limitations coming from the liquid phase instead. Figures 5.24 and 5.25 compare the results from this last experiment with the results from the reference experiment.

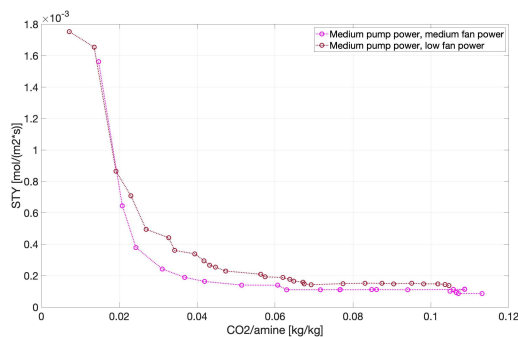


Figure 5.24: STY in function of CO_2 per amine loading, comparison between the reference and higher sorbent flow rate active mixing experiment

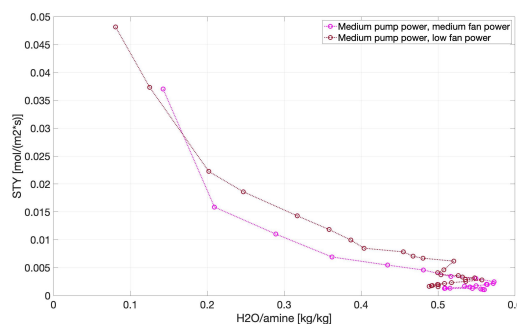


Figure 5.25: STY in function of H_2O per amine loading, comparison between the reference and higher sorbent flow rate active mixing experiment

For the pictures, it is clear how the effect of increasing the sorbent mass flow rate is an averagely higher STY at a certain CO_2 loading. Moreover, for both H_2O and CO_2 , the two curves diverge only after a certain concentration is reached.

Conclusions on active mixing, experiment #3: changing the sorbent flow rate The main conclusions from figures 5.24 and 5.25 are collected in this paragraph.

- At the beginning of the curves, that is, **for low loading, the curves are basically the same**. Since the only difference between the two experiments is the sorbent mass flow rate, it means that, at the beginning of the experiments, it is not absorption in the liquid phase which is deciding the rate of capture of gas molecules. That is, this is in agreement with the statement that the process is limited by the gas phase in that region.
- The curves diverge when the limit to the absorption process is influenced by an experimental parameter which is different between the two experiments. That is, **the curves diverge when the process is liquid phase limited and a variation in the sorbent flow rate is able to affect this limitation**. In particular, it looks like a higher sorbent flow rate is able to increase the resulting STY.

Describing the specific way a higher sorbent flow rate is able to affect the flux of captured gases is not a straightforward task. One could be tempted to say that, looking at the two film theory, a higher sorbent flow rate decreases the liquid film thickness in proximity of the gas-liquid interface and, as a consequence, it decreases the time needed for the gas molecules to cross this film. However, that would assume some sort of turbulent flow region in the liquid phase and we

know that, in this specific process, the flow in the liquid phase is completely laminar. Therefore, no turbulent region is present in the absorption plate. Therefore, there is no point in talking about a film thickness for the liquid phase. Please note that this is a film generated by the fluid dynamics of the process. **What if one assumes that a resistance layer is being formed not because of the fluid dynamics of the process, but because of the chemical absorption behavior of the process?** In particular, if one assumes that there is a layer of heavily loaded sorbent near the gas-liquid interface and that diffusion in this heavily loaded sorbent layers is what is limiting the process; it is reasonable to imagine that a higher sorbent flow rate will decrease the sorbent residence time on the plate and, as a consequence, it will decrease the time this heavily loaded layer can grow before active mixing happens. That will, in turn, decrease the thickness of the layer and also the time needed for gas molecules to diffuse within it. That is, it will speed up diffusion in the liquid phase. **This thought is at the basis of the physical interpretation given to the process and presented at the end of this chapter.**

5.1.3. Selection of the mixing strategy

The main results of this section, related to the relevant research questions and goals are presented below:

- Due to the way the active mixing experiments were performed, it can be concluded that **the designed mixing strategy is able to provide for surface renewals. Moreover, that is associated with an increase in the performance of the absorption process.**
- In fact, since the active mixing experiments performed way better than the passive mixing ones in terms of Space-Time Yield at the same CO_2 per amine loading and also in terms of relative loading that can be reached with that specific absorber design, **it can be concluded that, for the specific active and passive mixing strategies selected in this project, active mixing performs better.**
- As a consequence, for reaching the goal of engineering an optimization of the absorption column, **the active mixing strategy is selected for the design.**

5.2. Modelling

This section contains a collection of relevant results from the models presented in chapter 4. Firstly, results from the DNS model are commented and used to evaluate the performances of the passive mixing channels. In particular, **the SHM geometry is simulated and results from the model are used to explain results observed during the experiments.** After that, results from the unimolecular diffusion mass transfer model are presented and compared with the experimental results of both the active mixing experiments and the passive mixing ones.

5.2.1. DNS Model

The model for solving the Navier-Stokes equations applied to the SHM channel was developed following a physical interpretation of the flow in the channel. As extensively described in chapter 4, **the flow in the SHM channel geometry is decoupled as a flow in an open channel plus a lid-driven cavity flow.** That is, **results from the open channel flow are used to give the slip-velocity boundary condition for solving the lid-driven cavity flow.**

The results presented in this section are from a simulation run with the input conditions collected in table 5.1. These input conditions are the same of experiment #8 in table 3.3 for the passive mixing experiment with the SHM geometry.

Parameter	Value
Channel height [mm]	0.6
Channel width [mm]	5
Inlet flow rate [mL/hr]	3
Sorbent type	Pure TEPA

Table 5.1: Input conditions CFD model

Flow in an open channel has a very well known parabolic profile. Here, **we are interested at the velocity magnitude** in order to define a boundary condition for solving the lid-driven cavity flow problem.

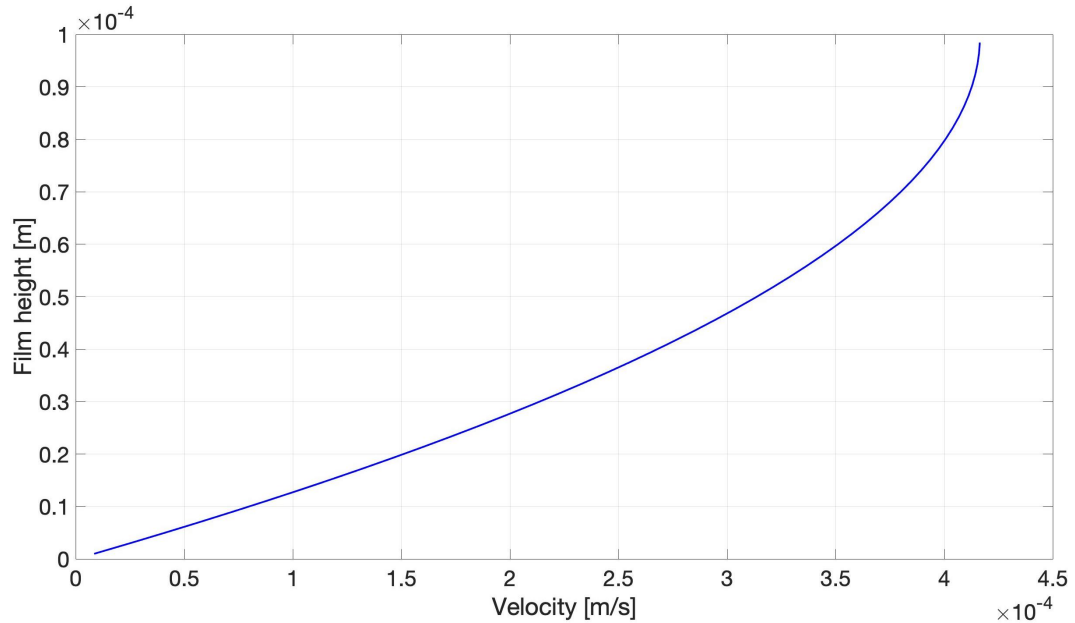


Figure 5.26: Velocity profile for the open channel flow in the Y direction with validation

Figure 5.26 shows the velocity profile for the simulated experiment. Validation of this profile, thus of the DNS solver, is done by computing the residuals between an analytical solution and the predicted profile. Details are collected in appendix C.

It can be seen how the (maximum) predicted velocity is on the order of $10^{-4}m/s$. This velocity value can be used to define a slip boundary condition for the lid-driven cavity flow. When that is done, The same DNS model (with different boundary conditions) is used to solve the lid-driven cavity flow problem.

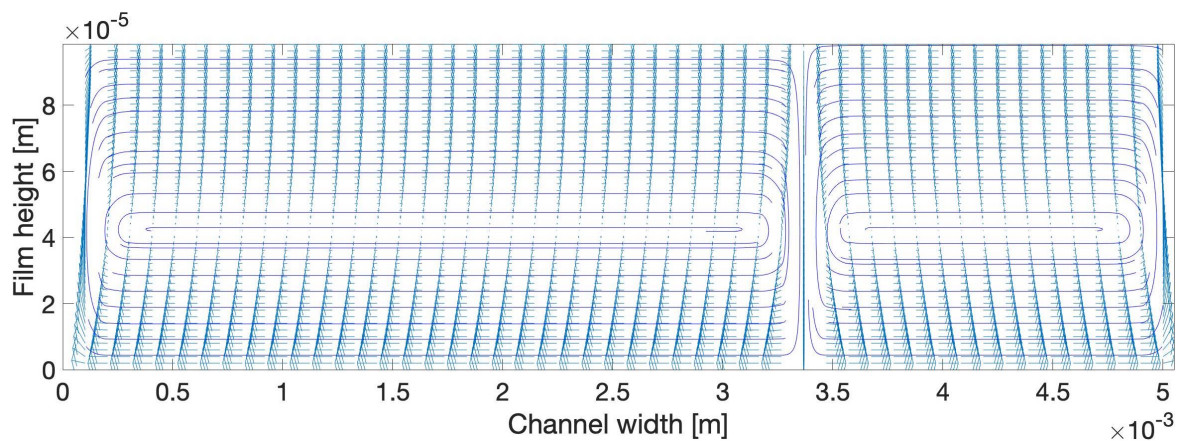


Figure 5.27: Velocity vectors and streamlines for the lid-driven cavity flow

Figure 5.27 shows a plot of the velocity vectors and the streamlines for the lid-driven cavity flow problem solved for the case of the SHM. In fact, since the herringbones have two branches in opposite directions, the result is that two circulations in opposite directions are generated within the cross section of the channel. Clearly, the model is predicting that a circulation is being generated because of the specific boundary conditions when solving the lid-driven cavity flow problem. With the assumption that

the model is reproducing what is happening in the experiment, the following conclusions can be traced:

- **The order of magnitude of the predicted circulation velocity is 10^{-5} m/s.** That is, with the channel dimensions specified in table 5.1, the average circulation time for a particle which is theoretically moved from the top of the channel to the bottom and then back on top of the channel is about 16 minutes. That is, if one considers that the residence time of the experiment for a 700 mm channel was about 23 minutes, only a single circulation is predicted during the entire time of the experiment.
- Moreover, figure 5.27 shows another reason why the passive mixing strategy is far from being an optimum one. In fact, due to the stokes flow behavior, **the particles will have the tendency of remaining within their trajectory over and over again.** That is, even if circulation is present, assuming constant fluid properties, always the same particles will be subjected to the "usefull" circulation path. That is, the one which brings sorbent molecules in contact with the gas-liquid interface and then back into the bulk.

Therefore, even if far from being able to exactly simulate the flow in the SHM mixing channel, this model is still able to show why no significant mixing was observed when using a staggered herringbone mixer for passive mixing purposes. In fact, according to the model, it can be concluded that **no mixing is observed with the SHM channel geometry because of a very small circulation velocity coupled with a tendency from particles subjected to a stokes flow behavior of always remaining within their fixed trajectories. That is, no chaotic mixing can be generated in this way.**

5.2.2. UMD mass transfer model

Results from the Unimolecular diffusion (UMD) mass transfer model are presented in this section. As specified in chapter 4, this model is directly linked with the physical interpretation for the absorption process of CO_2 molecules within the investigated DAC process. In fact, **this model is nothing else than the mathematical formulation of the physical interpretation.** That is, testing the validity of the proposed model is also a way of testing the validity of the proposed theory. Therefore, the physical interpretation, its mathematical equivalent and data from experimental results are directly linked. Figure 5.28 shows the way they are connected with each other.

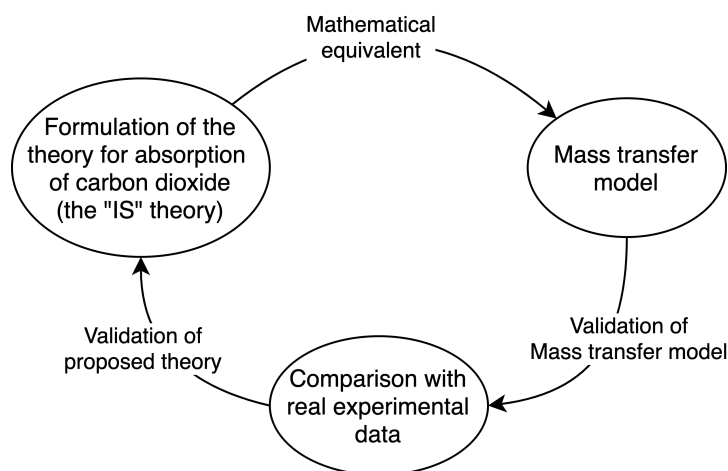


Figure 5.28: Connection between physical interpretation, mass transfer model and experimental results

Model validation Comparison between results from the model and the experiments is shown both by plotting the results together and by calculating the coefficient of determination, R^2 and the mean absolute error, MAE . Table 5.2 shows a list of the modelled experiments with respective values for R^2 and MAE .

Experiment Type	Experiment #	R^2	MAE
Active mixing	1	0.7953	$9.3 \cdot 10^{-6}$
Active mixing	3	0.9619	$1.1 \cdot 10^{-5}$
Passive mixing	1	0.9293	$1.6 \cdot 10^{-6}$
Passive mixing	2	0.9646	$3 \cdot 10^{-6}$
Passive mixing	7	0.9613	$1.6 \cdot 10^{-6}$
Passive mixing	4	0.9418	$2.3 \cdot 10^{-6}$

Table 5.2: Coefficient of determination and mean absolute error for the UMD mass transfer model

Together with table 5.2, a direct comparison between the model results and the experimental results is shown in the pictures below. For comparison with the active mixing experiments, results are shown in figures 5.29 and 5.30. Please note that, **once again after showing the experimental results, a cumulative STY is considered:**

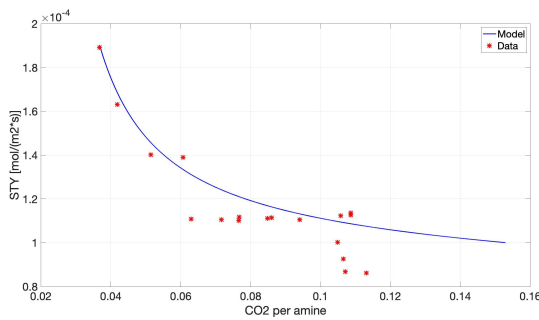


Figure 5.29: UMD mass transfer model validation: active mixing experiment #1

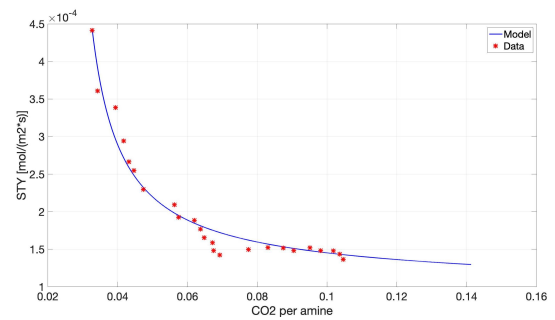


Figure 5.30: UMD mass transfer model validation: active mixing experiment #3

Regarding the passive mixing experiments, results are shown below:

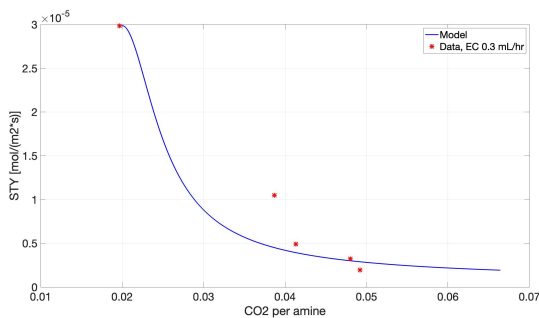


Figure 5.31: UMD mass transfer model validation: passive mixing experiment #1

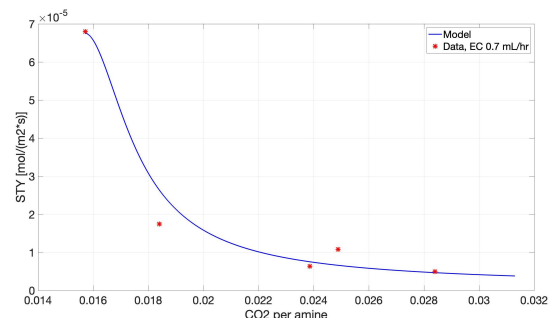


Figure 5.32: UMD mass transfer model validation: passive mixing experiment #2

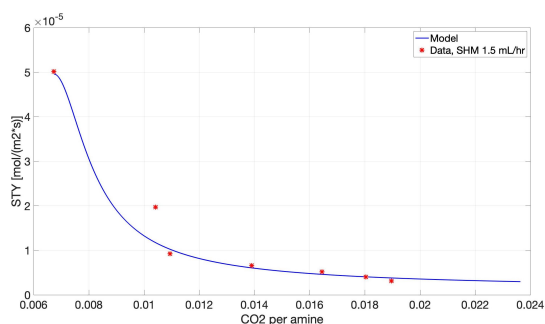


Figure 5.33: UMD mass transfer model validation: passive mixing experiment #7

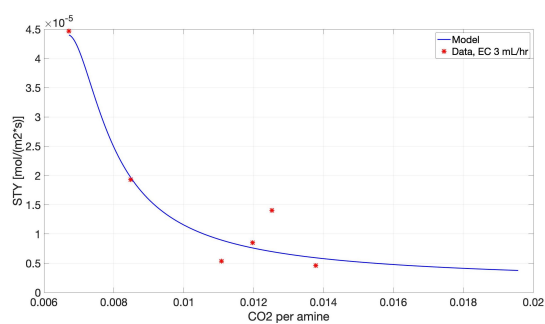


Figure 5.34: UMD mass transfer model validation: passive mixing experiment #4

The following conclusions can be traced from the depicted pictures:

- Comparison with experimental results has shown a good agreement between the predictions from the model and the data collected during the experimental investigation. This is considered to be a good result especially because **the model contains no fit of experimental data** and the predictions are made just by solving the governing equations of the proposed physical interpretation. That is, this model can **represent the experimental data with a satisfying degree of accuracy** and also, **it adds credibility to the proposed physical interpretation** (described in the next section).
- The model is coherent with experimental data **when the coefficient for diffusion of CO_2 in the heavily loaded top sorbent layer ("Ice-Sheet") is $10^{-15} m^2/s$** . This coefficient is smaller than the one estimated in previous works at ZEF [14], [38]. This divergence is to be expected when considering that previous calculations were made for diffusion through the whole sorbent bulk. That is, while in the model presented in this thesis, the diffusion coefficient is specific for CO_2 diffusion in the IS, the one found in previous studies was more an estimated coefficient for diffusion in a mixture of "Ice-Sheet" and pure sorbent.
- The model predicts an increase in the absorption performances when the sorbent flow rate on the absorption plates is increased. Or, equivalently, when the residence time of the sorbent on the absorption plates is decreased. This is in agreement with experimental results and it also means that **the model provides a useful tool in the engineering of the absorption column since it can be used to predict the resulting STY at a certain sorbent loading in function of the sorbent residence time on the absorption plates.**

5.3. Process' physical interpretation: the "Ice-Sheet" equivalence

This section is finally focused on describing the absorption of CO_2 molecules in the investigated process. Firstly, it is described with a step-by-step approach how the process works from a molecular level. At the end, conclusions and consequences of this theory are presented. **The theory is explained considering only diffusion in the liquid phase. It is assumed that diffusion in the gas phase happens instantaneously and that the time for reaction between CO_2 molecules and sorbent molecules is much smaller than the diffusion time.**

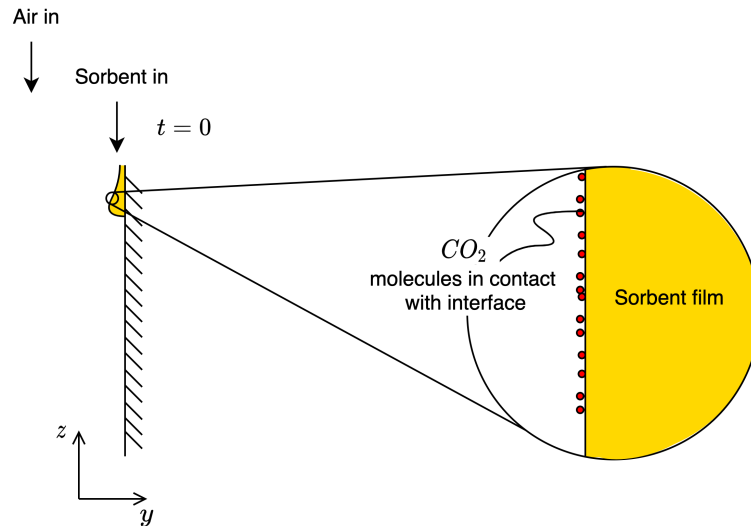


Figure 5.35: Absorption of CO_2 in a polyamine sorbent, step #1

Referring to figure 5.35, at time $t = 0$, the sorbent (in yellow) starts to flow on the absorption plate. The presence of a flow of air will bring CO_2 molecules in contact with the gas-liquid interface. Please note that only the liquid phase is considered here.

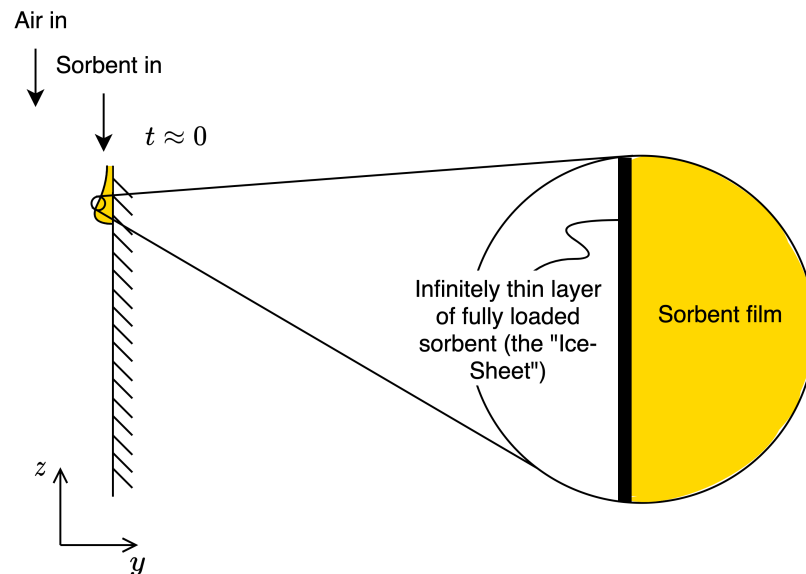


Figure 5.36: Absorption of CO_2 in a polyamine sorbent, step #2

If it is assumed that CO_2 molecules react extremely fast, at a time still close to zero, the first molecules in contact with the interface will react until saturation is not reached in proximity of the gas-liquid interface. That is, on the free surface of the sorbent flow, an infinitely thin, fully loaded sorbent layer will be formed (figure 5.36). From now on, we will refer to this layer as the "Ice-Sheet". Reason for that will be given later in this section.

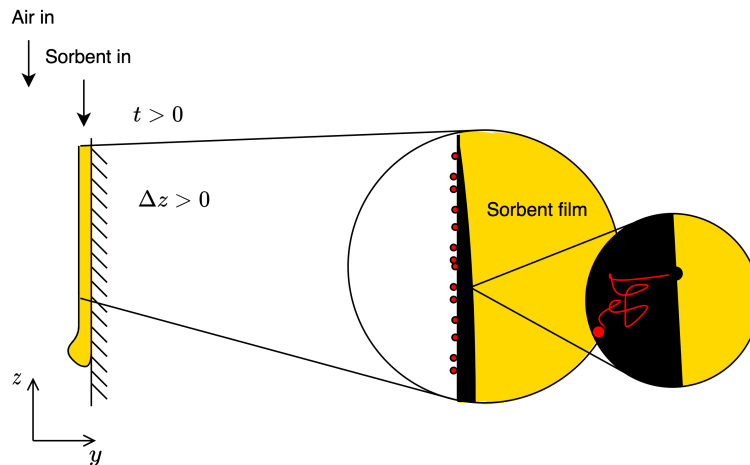


Figure 5.37: Absorption of CO_2 in a polyamine sorbent, step #3

Figures 5.35 and 5.36 are describing the absorption process when the elapsed time is very close to zero. Clearly, while the first "Ice-Sheet" is being formed, CO_2 gas molecules will keep diffusing toward the gas-liquid interface. As a consequence of that, **for a time different from zero, since the "Ice-Sheet" is now present at the interface, molecules cannot react instantaneously with the sorbent, but they have to diffuse through this layer of ice before being able to react** and, therefore, being absorbed. Figure 5.37 show that, if one considers a time interval bigger than zero and takes into account a distance on the plate different from the inlet region, it can be imagined how the thickness of the "Ice-Sheet" will vary moving downstream on the plate. In fact, as the sorbent proceeds on the plate, CO_2 molecules will have more time to diffuse through the layer, thus increasing its thickness. Clearly, this happens because ice sheet-free sorbent is coming from the inlet of the plate. The absorption process is diffusion limited because diffusion of CO_2 molecules in this saturated sorbent layer is extremely slow ($D = 10^{-15} \text{ m}^2/\text{s}$ according to the mass transfer model). Moreover, a slower sorbent will generate a thicker "Ice-Sheet", thus slowing the absorption process even more for longer plate flowing times. Assuming this theory holds, **figure 5.38 shows how a possible concentration profile looks like**. Please note that, for the air side, it is assumed the existence of a turbulent region ("bulk gas"). Clearly, depending on the magnitude of the air flow rate, it could also be that a laminar region only exists. Within the bulk (liquid film), before mixing happens (before breaking the ice), the concentration stays always at zero. In fact, as soon as the CO_2 molecules diffuse through the "IS", they react with fresh TEPA molecules and, instead of continuing to diffuse in the bulk, they become "IS" themselves, thus increasing the thickness of the layer.

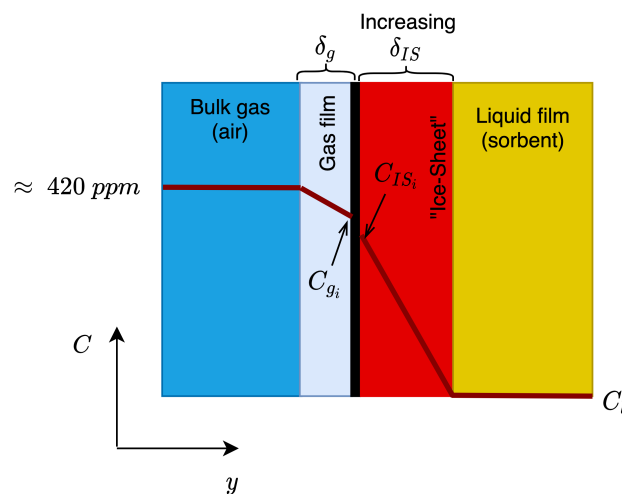


Figure 5.38: Concentration profile according to the "IS" theory

With a bit of imagination, **one can trace an analogy between mass diffusion in this absorption process and heat transfer in a frozen lake.** In fact, as soon as a layer of ice is formed on the surface of an iced lake, the **"Ice-Sheet"** will act as a natural insulator to heat transfer between the (still) liquid water of the lake and the atmosphere, thus preventing the entire lake to freeze down. Here, a very similar process is happening with a top surface layer preventing (mass) transfer between what is above and below the layer, thus slowing down the whole process. **As we have seen with the mixing experiments, a solution to this problem is to "break the ice" by actively mixing the sorbent stream.**

Literature's back-up In 2014, Wilfong et al. presented a study about absorption of CO_2 molecules on Tetraethylenepentamine (TEPA) films [104]. They describe how, for a film thickness higher than 20 μm , *"a thick, interconnected surface network of strongly adsorbed species"* is formed. And more, they describe how this network contains *"a high concentration of ammonium ions which slows down CO_2 gas diffusion and diminished access of the bulk amine groups"*. Moreover, they confirm that, in thick TEPA films, there is a *"low concentration of adsorbed CO_2 within the bulk due to diffusion limitations"*.

In the experimental investigation relevant to this thesis project, the film thickness was in the order of tens of μm , very similar to the film thicknesses investigated in that study. Therefore, **it does not look far from the truth to imagine that what is called the "Ice-Sheet", is nothing else than a layer of highly interconnected network of ammonium ions slowing down the diffusion process. Clearly, that is yet to be proven.**

Conclusions from the "Ice-Sheet" theory Main conclusions from the physical interpretation to the absorption process presented in this section are collected below:

- The "IS" theory is developed in the framework of **explaining the absorption process at a molecular level.** It is believed that this theory resembles reality and proofs of that are provided through the validation of the mass transfer model with experimental data and confirmations obtained from international research studies about CO_2 absorption using the same amine absorbent.
- With previous research, it clearly appeared how the CO_2 absorption was diffusion limited and that mixing would help solving this issue. However, it was not very clear/proven, what was happening layer-wise in the sorbent and in which way mixing would help solving this issue. **One of the main outcomes of this thesis is that the process is limited by CO_2 diffusion into the "IS". That is, a homogeneous layer made of heavily loaded, highly viscous TEPA that limits, thus "decides", the rate of CO_2 absorption.** For diffusion through that layer, via a mass transfer model, a diffusion coefficient of $D = 10^{-15} m^2/s$ is estimated.
- **To improve the process, it is now clear that it is needed to "break" this "Ice-Sheet" and make room for fresh amine sorbent on the top of the channel.** That will avoid the diffusion limitations coming from the layer.
- It must also be specified that, together with CO_2 diffusion in the "IS", also the whole layer is diffusing through the bulk TEPA. The mixing process should have the double task of braking the ice as much as possible in order to avoid limitations from slowly diffusing CO_2 and also of quickly homogenizing the fresh TEPA with the "IS". That is, dissolving it into the bulk of sorbent as much as possible in order to have TEPA with a very low concentration of CO_2 molecules on the free surface. In an ideal world, one could look at this problem as built up in layers. **Ideally, you would want to have 100% TEPA on the free surface always, thus, ideally, you would want to "collect" all the "Ice-Sheet" layers somewhere in the bulk of TEPA without mixing them with the fresh sorbent, thus maximizing the free "reaction spots" on the free surface.**
- Finally, When talking about absorption of CO_2 in TEPA, we are actually talking about diffusion of CO_2 in a very dense, very loaded sorbent layer, then reaction of diffused CO_2 molecules with free polyamine molecules and a free base in a two step reaction and, finally, diffusion of the reaction product into the polyamine bulk. In designing the absorption column it must be considered how all these phenomena could limit the process and how to reduce their influence.

6

Absorption column engineering

The common goal for all the different research questions and task addressed in this project is to engineer a new version of ZEF's absorber for CO_2 and H_2O capture. As specified in chapter 5, active mixing is selected as the mixing strategy for the column. That is, the column is designed similarly to the active mixing setup.

In this chapter, the design of the absorber is presented. Firstly, the design of the sorbent side of the column is described. That is done together with a sensitivity analysis on the main design parameters. After that, the air side design is presented and, finally, a cost analysis is used as a tool for selecting the main design parameters. The last section includes an overview of the column's conceptual design.

6.1. Sorbent side design

The main tool in the design of the column's requirements on the sorbent side is the UMD mass transfer model presented in chapter 5. After comparing the model results with the experimental results and because the model is backed up with information available in literature, **the model is considered to be a powerful tool for predicting the flux of CO_2 molecules in function of the sorbent residence time on the absorption plate and the CO_2 bulk concentration** in the case of active mixing configuration.

Sorbent side design: assumptions In designing this part of the absorber, the following assumptions are considered:

- The design is based on a **mass balance between the rate of CO_2 desorbed in the stripper unit and the rate of CO_2 captured in the absorber unit**. Those two are balanced over a daily operational period of 8 hours.
- During operation, the stripper will continuously remove rich sorbent and inject fresh one. It is assumed that this process does not influence the operating concentration of the absorber since the mass of CO_2 removed by the stripper is always balanced with the mass of CO_2 coming from the absorber. For this assumption to be true, it must be assumed that **mixing of the fresh sorbent with the loaded sorbent is a uniform and quick process**.
- The mass is balanced in a steady state operation at a certain operational sorbent bulk loading. That is, **the transition of the absorber from pure sorbent to sorbent loaded at the operational concentration is not considered in this analysis**.
- When the stripper removes a certain mass flow of loaded sorbent, together with CO_2 , it will also remove a certain mass flow of H_2O . It is assumed that the absorber is able to balance the removal of H_2O by capturing water at a certain rate. Due to a lack of mass transfer model predicting the flux of H_2O , this assumption is verified by calculating how much flux of H_2O the experimental setup was producing when close to H_2O saturation. It is observed that the rate of H_2O capture is more than 3 times higher than the rate of CO_2 captured at the operational concentration. More

than enough to satisfy the design requirements.

Therefore, **while the CO_2 capture rate is predicted via the mass transfer model, the H_2O capture rate is taken from the experiments.**

- The sizing of the absorption column is done assuming a constant absolute Space-Time Yield (flux for CO_2 and H_2O , equation 6.1) always in the column. **That is, the performance of the absorber is constant across all of its length.** This performance is calculated with a mass transfer model which assumes that the process is limited by the liquid phase. More specifically, that the rate of diffusion of CO_2 in the liquid phase (in particular, in the "Ice-Sheet"), is the slowest in the entire process. This is assumed to hold even when air concentration decreases toward the end of the column.

This assumption can be (partially) justified considering that the diffusion coefficient for the air side ($D_{air} = 1.6 \cdot 10^{-6}$) is 9 orders of magnitude higher than the predicted diffusion coefficient for the liquid side ($D_{Ice-Sheet} \approx 10^{-15}$). Therefore, it is reasonable to expect a huge difference in CO_2 diffusion speed, between the liquid Ice-Sheet and the diffusion boundary layer in proximity of the gas-liquid interface.

It must be specified however, that the diffusion problem at the air side is not investigated in this thesis. A mass transfer model including transport of CO_2 in the air side as well as the liquid side, would solve/verify this assumption.

- The viscosity of the sorbent at the operational concentration is taken from table 2.1.

Sorbent side design: main algorithm The design of the sorbent side of the absorption column is done in Matlab by defining a certain algorithm. **This algorithm relies on inputs coming from three, very distinct, sources:**

1. Parameters selected by the user (for design optimization)
2. Parameters coming from ZEF's requirements for the absorption column
3. Parameters calculated with the mass transfer model

The link between the parameters coming from the sources above defines the algorithm used in the design of the sorbent side. That is shown in figure 6.1.

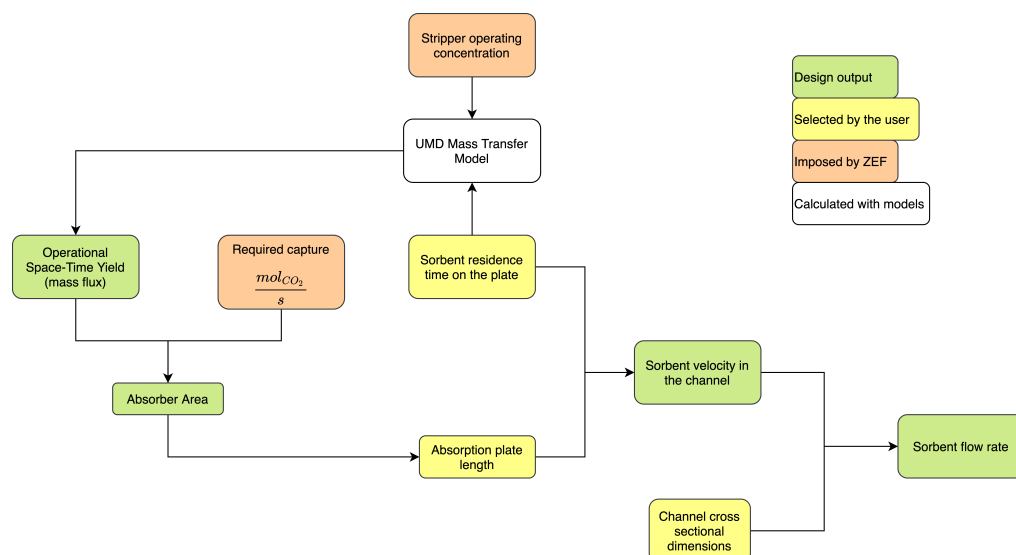


Figure 6.1: Main algorithm in the design of the sorbent side of the absorption column

As described above, it can be seen how the CO_2 Space-Time Yield is defined with the mass transfer model as a function of the stripper operating concentration (i.e. the operational concentration of the

absorber) and the sorbent residence time on the plate (i.e. the time required by the sorbent to flow from the inlet to the outlet of the plate). As a consequence, **the absorber area will be a function of the operational concentration and the sorbent residence time**. The influence of those and other design parameters is described in a sensitivity analysis presented in next section.

Sorbent side design: Space-Time Yield calculation As specified before, the absorber is designed at a certain specific operating concentration. For this reason, the considered equation for the calculation of the Space-Time Yield is different from equation 5.2. In fact, that equation calculates a cumulative STY summing up all the captured moles of CO_2 and considered the total elapsed time. **For the absorber design, the specific STY at the operating concentration (absolute STY) is rather used:**

$$STY_{absolute} = \frac{moles_{CO_2}(C_{bulk})}{A \cdot t_{plate}} \quad (6.1)$$

It can be seen how this equation **calculates the STY considering the moles of CO_2 captured on a single passage on the plate at a certain rich loading concentration**. More information about how the absolute and cumulative STY evolves with bulk concentration can be found in appendix D.

6.1.1. Sensitivity analysis on sorbent side design

Figure 6.1 shows that multiple parameters can be varied in the conceptual design of the absorption column. Observing the influence of each parameter is a useful way to understand the design methodology better and, also, to check the various algorithms used in the design.

Area function of rich loading and sorbent residence time on the plate The surface area of the absorber is calculated in the following way:

$$A = \frac{CO_2 \text{ capture rate}}{STY_{absolute}} \quad (6.2)$$

Where the source of the various parameters follows the schematic presented in figure 6.1. As seen before from the experimental and model results, the Space-Time Yield is a function of the CO_2 concentration in the sorbent. Therefore, also the area will be a function of that. Figure 6.2 shows this dependence and, also, how that is influenced by the sorbent residence time on the plate.

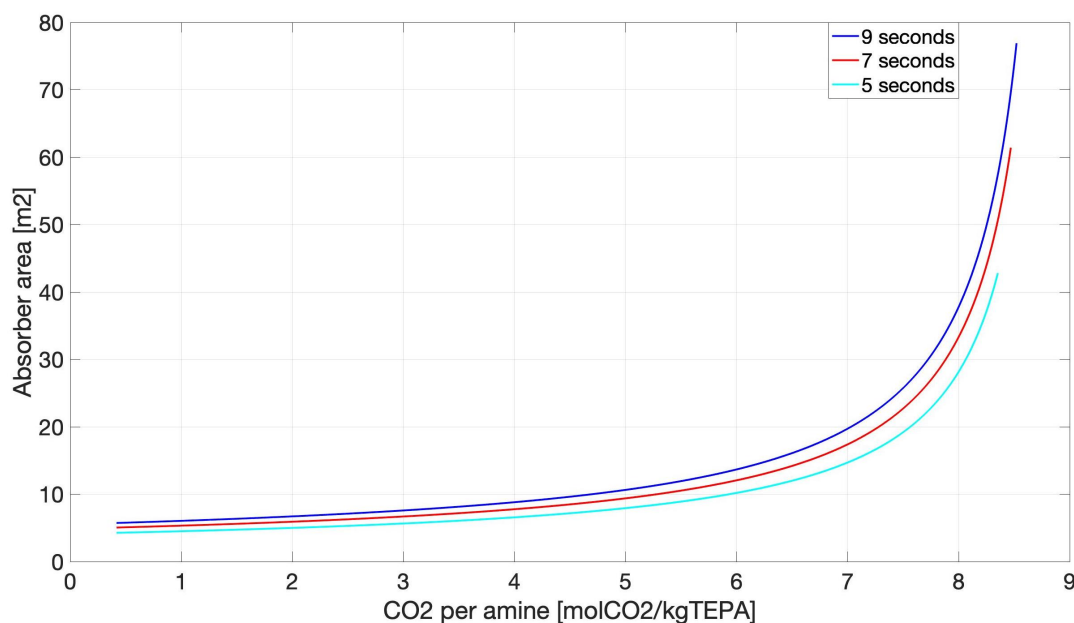


Figure 6.2: Absorber area in function of the operational rich loading and sorbent residence time on the plate for a certain CO_2 capture rate

It can be seen how **the absorber area increases together with the CO_2 concentration in the bulk**. In particular, it approaches an infinite value when the concentration is about 9 moles of CO_2 per kilogram of TEPA. This is in line with the fact that **diffusion in the liquid phase depends on a difference in concentration between the "Ice-Sheet" and the sorbent bulk**. The CO_2 concentration in the ice layer is nothing else than the saturation concentration for TEPA. That was found to be about 9 moles of CO_2 per kilogram of TEPA in previous experiments at ZEF. When the operational concentration of the absorber ($C_{CO_2,bulk}$) goes to that value, the driving force goes to zero. Therefore, for that operational concentration, the STY has zero value and, because of equation 6.2, the area goes to infinity. Moreover, the curves are logarithmically approaching infinity because the absorption performances are predicted via the mass transfer model with equation 4.37. That is, this trend is according to the developed model and, in particular, the developed "Ice-Sheet" theory.

Regarding the influence of the sorbent residence time on the plate, **it is predicted an increase in the area requirements when the residence time increases**. This is in accordance with the observed experimental results where a higher sorbent mass flow rate, thus a lower residence time, yielded better performances in terms of STY. Regarding the developed theory, this increase in area is explained with an increase in the Ice Layer thickness corresponding to an increase in the sorbent residence time. This will limit more the diffusion in the liquid side, thus increasing the absorber area.

Area function of CO_2 capture requirements and sorbent residence time on the plate The various features of the absorber will be presented later, for now it is enough to consider that it is designed to operate at a concentration of 5 moles per kilogram of TEPA and to capture a total of more than 825 grams of CO_2 every 8 hours of operation. Figure 6.3 shows how the area of the absorber changes in function of the required capture of CO_2 over 8 hours at an operational concentration of 5 moles per kilogram of TEPA.

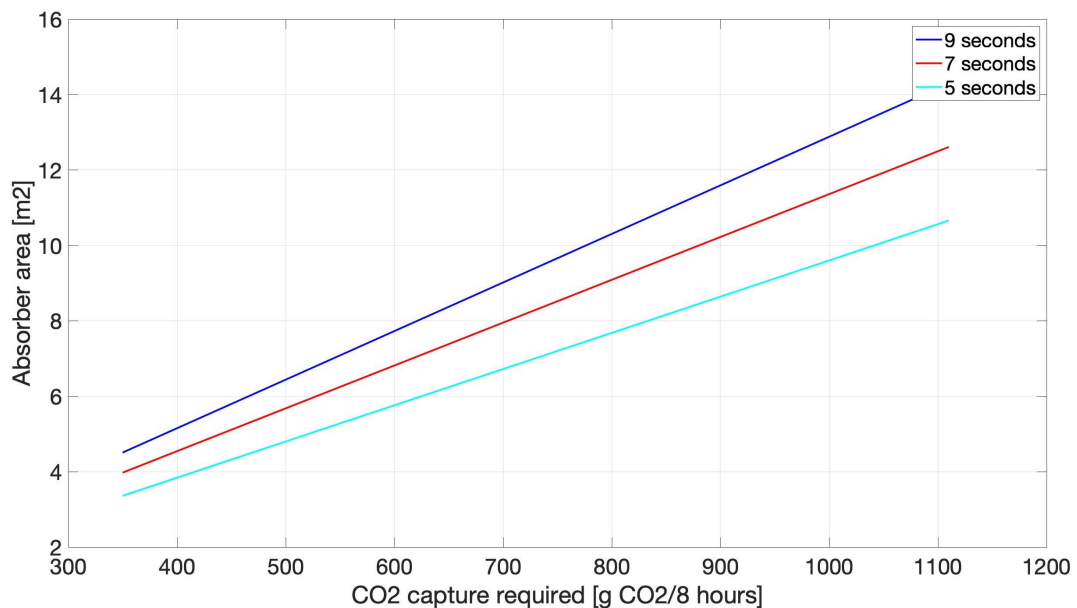


Figure 6.3: Absorber area in function of the required CO_2 capture and sorbent residence time on the plate for a rich loading of 5 moles of CO_2 per kilogram of TEPA

As expected, since the absorber area and the required CO_2 capture are directly proportional as shown in equation 6.2, **a linear increase of the required area is predicted when increasing the carbon captured amount**.

In the engineering of the sorbent side for the absorption column, the operational loading and the sorbent residence time on the plate are the main design parameters. The influence of secondary design parameters like those related to the geometry of the absorption plate and the channels is collected in appendix D.

6.2. Air side design

In parallel to the design of the absorber's sorbent side, the air side is engineered as well. **The goal of this design is to find the necessary air inlet flow rate to provide for the absorption requirements.**

The design of the sorbent side estimates the rate of CO_2 and H_2O mass capture, since the transferred mass is coming from the air side of the absorber, the design is based on a simple mass balance between the mass of air entering the absorber, and the mass transferred from the air side to the liquid side. Once again, it is assumed that the absorption performance of the absorber does not change over the length of the column. Therefore, the rate of mass transfer is assumed to be always constant and not affected by the decrease in the CO_2 and H_2O concentrations.

Air side design: main algorithm Once again, the parameters used in this design can come from three different sources. Figure 6.4 shows the main algorithm used in this design together with the source of the various parameters.

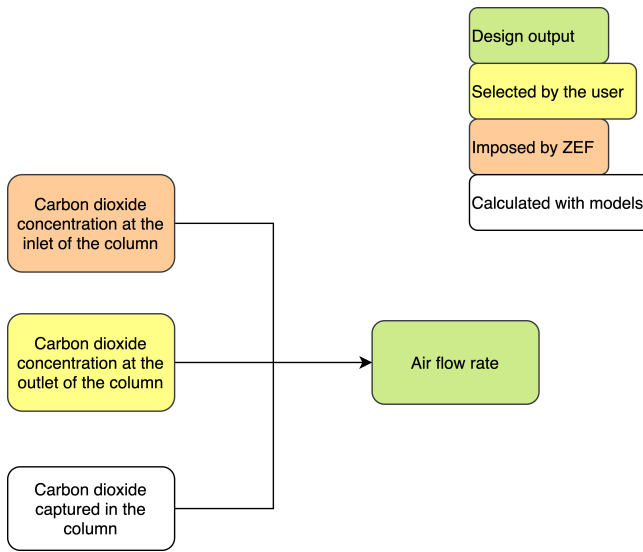


Figure 6.4: Main algorithm in the air side design of the absorption column

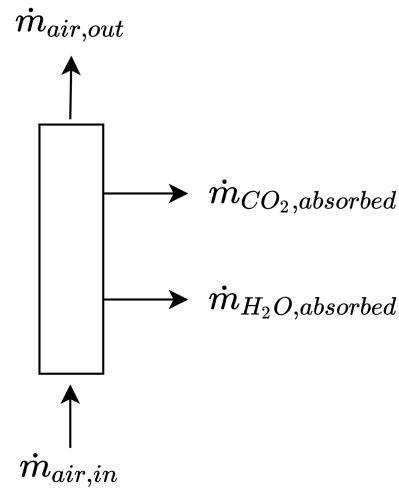


Figure 6.5: Mass balance for the air side: control volume

The governing equations for the mass balance are written for the control volume shown in figure 6.5:

$$\dot{m}_{air,out} = \dot{m}_{air,in} - \dot{m}_{CO_2,absorbed} - \dot{m}_{H_2O,absorbed} \quad (6.3)$$

$$\dot{m}_{CO_2,in} = \dot{m}_{CO_2,out} + \dot{m}_{CO_2,absorbed} \quad (6.4)$$

$$\dot{m}_{CO_2,out} = \dot{m}_{air,out} \cdot C_{CO_2,air,out} \quad (6.5)$$

$$\dot{m}_{CO_2,in} = \dot{m}_{air,in} \cdot C_{CO_2,air,in} \quad (6.6)$$

The equations above constitutes a system of four equations in four unknowns when including the following known parameters:

$$\dot{m}_{CO_2,absorbed} = STY_{CO_2} \cdot A \cdot MW_{CO_2} \quad (6.7)$$

$$\dot{m}_{H_2O,absorbed} = STY_{H_2O} \cdot A \cdot MW_{H_2O} \quad (6.8)$$

$$C_{CO_2,air,in} = 412 \text{ ppm} \quad (6.9)$$

$$C_{CO_2,air,out} = \text{user imposed} \quad (6.10)$$

Solving those equations, one obtains the mass balance for the air side in the case of CO_2 transfer. Similar equations can be written for the case of H_2O as well. Those are collected in appendix D.3.

From the mass balance, it is clear how the air inlet flow rate strongly depends on the chosen CO_2 outlet concentration.

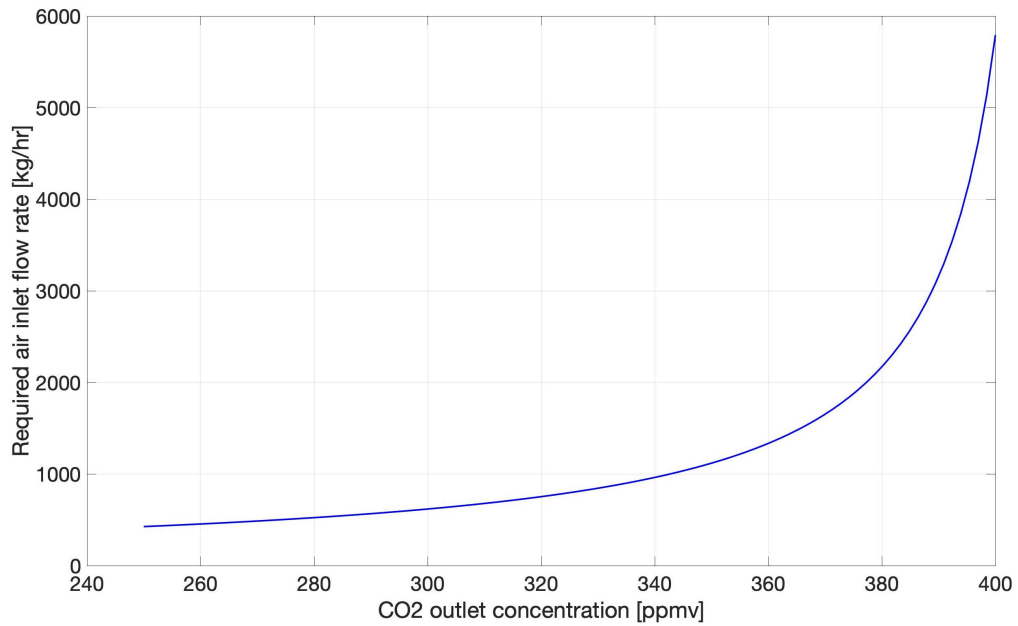


Figure 6.6: Required air flow rate in function of designed CO_2 outlet concentration

Figure 6.6 shows that, when the air outlet concentration is imposed to be closer and closer to the air inlet concentration (412 $ppmv$), the required inlet flow rate increases significantly. **The optimal value for the CO_2 outlet concentration is the minimum value that does not limit the absorption process in the gas phase more than it is already limited by the liquid phase.** That is, choosing an optimum value is related to the discussion in section 6.1.

In this case, the outlet concentration is imposed to be 350 $ppmv$. The evolution of the CO_2 concentration over the column length is shown in figure 6.7.

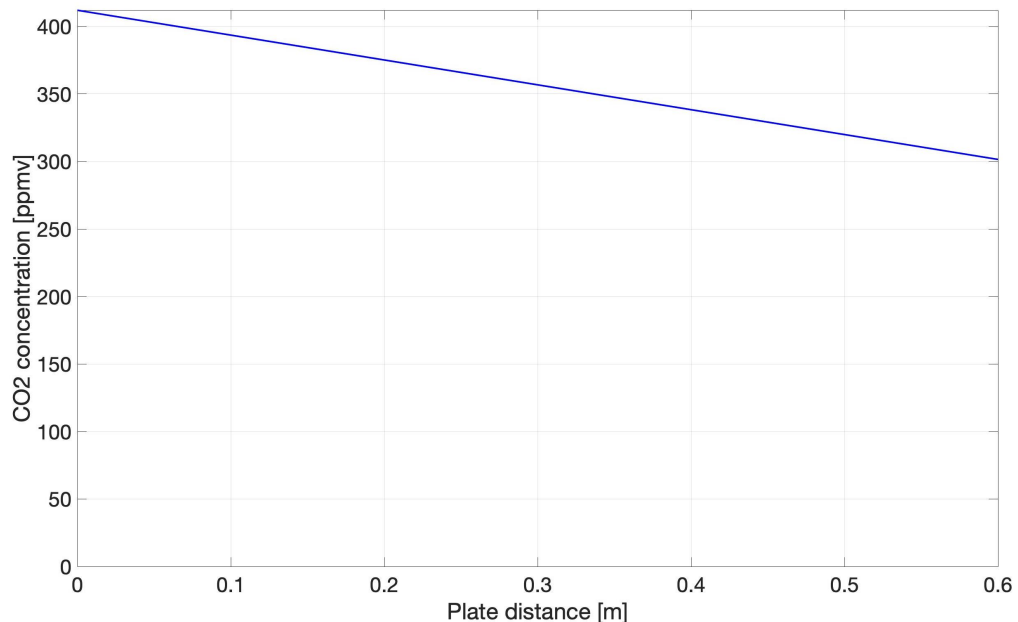


Figure 6.7: CO_2 concentration in air over the column length

The predicted trend is linear because the Space-Time Yield is considered to be constant over all the column length.

6.3. Cost analysis

This chapter underlines how the size of the absorption column depends on multiple parameters. It is also observed how, with this particular design, the highest influence is coming from the selected sorbent residence time on the plate. In fact, according to the mass transfer model, that will directly influence the absorber area requirements and the sorbent flow rate requirements. In order to select an optimum value for the design, a cost analysis is built. The cost analysis includes **parts of both the operational and capital costs**. Table 6.1 collects the considered inputs to the cost analysis.

Parameter	Value
Payback period [years]	20
Area cost [€/m ²]	10
Energy cost [€cents/kWh]	2

Table 6.1: Inputs to the cost analysis

Using the parameters in table 6.1, it is possible to give an estimate for the material costs coming from the size of the absorber (defined in function of the absorber area) and energy costs coming from the pump and the fan used for the sorbent and air flow rate. Estimating the pump and fan energy consumption requires to calculate the pressure drop in the pipes where the sorbent is flown and the air pressure drop across the column. The pressure drop in the sorbent and air side is calculated with the following equation:

$$P = \rho gh + \frac{128L}{\pi} \mu \frac{\dot{Q}}{D^4} \quad (6.11)$$

Where:

- P is the pressure drop of either the sorbent or air in [pa]
- ρ is the sorbent or air density in $\left[\frac{kg}{m^3}\right]$
- g is the acceleration of gravity in $\left[\frac{m}{s^2}\right]$
- h is the absorber height in [m]
- L is an estimate for the total length of the pipes for $P = P_{sorbent}$, and is the plate length for $P = P_{air}$.
- μ is the dynamic viscosity of either the sorbent or air in [pa s]
- \dot{Q} is the sorbent or air volumetric flow rate in $\left[\frac{m^3}{s}\right]$
- D is the equivalent diameter in [m]

Equation 6.11 is a sum of head pressure losses (first term, right end side) and friction losses due to laminar flow in the duct (described by the Darcy-Weisbach equation [105]). Being a gas, the head pressure losses in the case of air can be neglected. Moreover, the air flow will be in a square duct. Therefore, while D for the sorbent is simply the internal diameter of the pipes, for the air flow it is necessary to calculate an **equivalent diameter** to use in equation 6.11 [106]:

$$D_e = 1.3 \frac{(ab)^{0.625}}{(a+b)^{0.25}} \quad (6.12)$$

Where a and b are the dimensions of the square section.

Moreover, for the air flow, it is interesting to find out the Reynolds number. The hydraulic diameter D_h is used when dealing with flow in square ducts:

$$D_h = \frac{4A}{P} \quad (6.13)$$

$$Re_{air} = \frac{uD_h}{\nu} = 1057 \quad (6.14)$$

That falls in the laminar regime.

It is found that the most relevant pressure drop, thus the most relevant source of energy cost comes from the pressure drop in the liquid phase. Therefore, it is chosen to neglect from the analysis costs coming from the use of the fan. It must be considered that this assumption might fall as soon as a more accurate way for estimating the pressure drop in the air side will predict a different, higher result for the pressure drop. This is very likely to be the case since this pressure drop estimation is only considering pressure losses due to air flowing in between two consecutive absorption plates. It is realistic to expect pressure losses also due to the expansion of air (since the fan section is smaller than the column section) and losses due to the presence of flow distributors in the column.

At the designed CO_2 capture rate, knowing a required payback time, it is possible to estimate the cost of capturing a single tons of CO_2 for the designed absorber. The cost is obtained by simply multiplying the calculated pressure drop with the required flow rate (air or sorbent). **Since this design excludes components selection, the operational efficiency of the pump and the fan are not taken into account.** Figure 6.8 shows the two main contributors to the cost of the absorber (pump energy and absorber's area) as function of the sorbent residence time on the plate (plate flowing time). The costs are obtained for a system which operates at the designed conditions of 5 moles of CO_2 per kilogram of TEPA and 825 grams of CO_2 captured every 8 hours of operation.

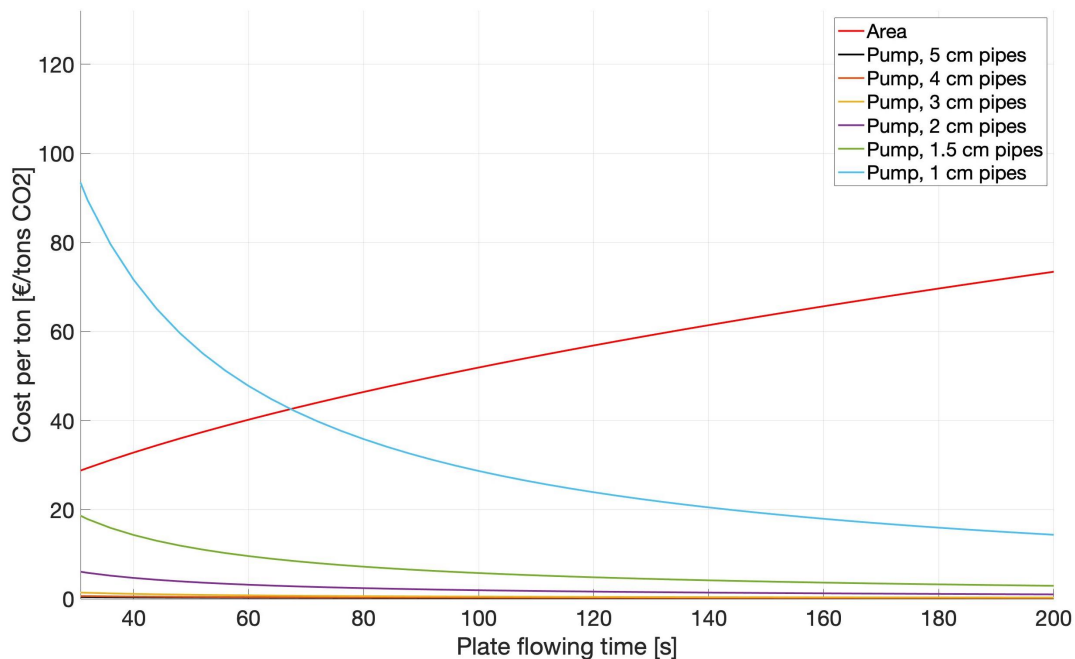


Figure 6.8: Area and pump energy cost in function of sorbent plate residence time and pipe's internal diameter

The following conclusions can be traced from figure 6.8:

- As seen before, **the area of the absorber depends on the sorbent residence time on the plate (or sorbent flowing time)**. As a consequence, also the area cost will depend on that. In particular, the higher the sorbent residence time on the plate, the higher is the area cost. That is in agreement with a reduction in the STY when the sorbent residence time on the plate is increased.
- On the other side, **the cost of the energy of the pump is decreasing as the sorbent residence time on the plate increases**. This happens because a slower flowing sorbent (higher plate residence time) also means a lower mass flow rate generated by the pump. That will decrease the pressure drop in the pipes and, in turn, the energy cost of the pump.

- Figure 6.8 shows the cost of the pump also in function of the pipe's diameter. In fact, equation 6.11 describes a power 4 relation between the pressure drop in the pipe and the pipe's diameter. **That is, the choice of the pipe's diameter has a massive influence on the overall energy consumption of the pump.**

Total cost and parameter selection The total cost of the absorber can be found by summing the cost of the surface area with the cost for the pump's energy. The result is shown in figure 6.9

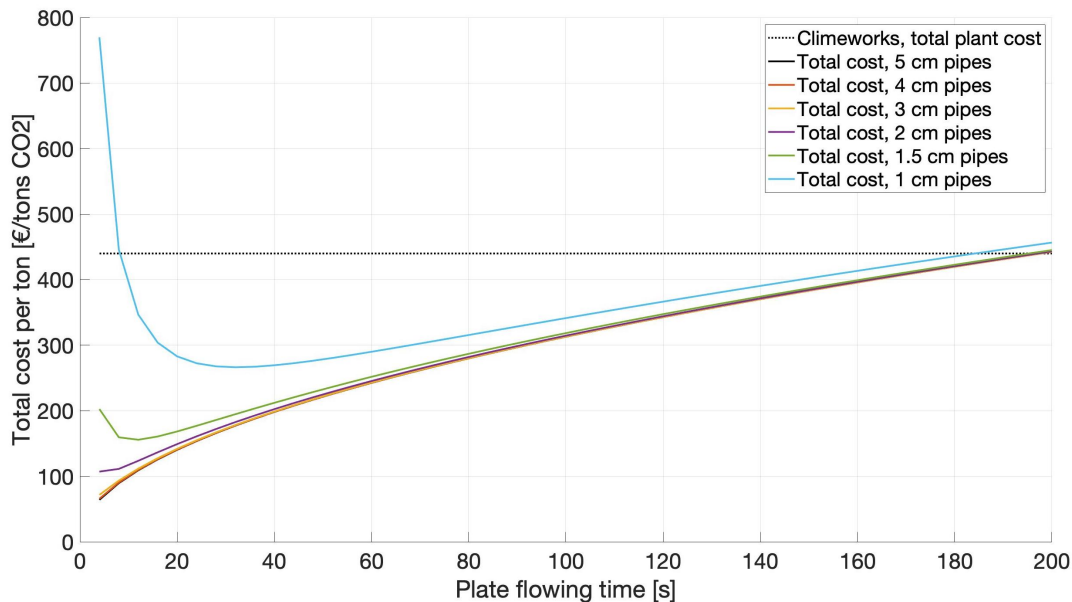


Figure 6.9: Total cost of the absorber

1 cm is considered to be a reasonable value for the internal diameter of the pipes since a value bigger than that would add significant material costs. It can be seen how the light blue curve in figure 6.9 presents a minimum at around 32 seconds for the sorbent residence time on the plate. **Targeting cost minimization, this value is selected for the conceptual design of the absorber.**

It is also interesting to compare the cost of the designed system with the cost of an industrial-scale DAC system. Already mentioned in section 2.2, the cost of the Climeworks system is estimated as 440 € per ton of captured CO_2 [107]. Clearly, this comparison is just a qualitative one because the cost estimated for the Climeworks plant takes into account the whole DAC system, while the analysis presented in this thesis only considers the cost of the absorber. However, it is still an interesting exercise to note that, for being the cost of the absorption column only, **it is predicted a very high cost**. That is believed to be the case because this design is done using pure TEPA as absorbent and, also, designing the absorber to operate at a very high rich loading. Those are far from being optimal operating conditions.

6.4. Absorber overview

In this section, a summary of the main features of the absorption column are presented via a collection of cartoons. The design parameters are selected following the sensitivity and cost analysis described earlier in this chapter.

Figure 6.10 shows an overview of the absorption column:

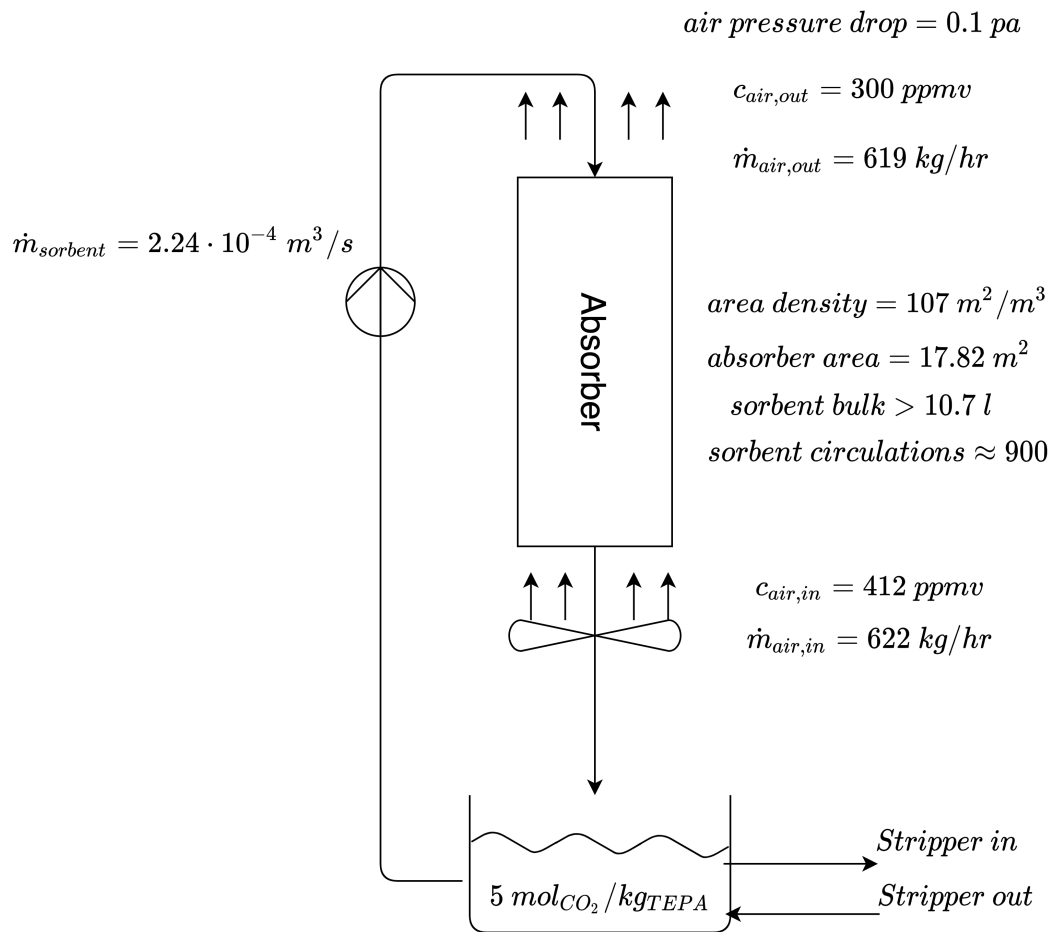


Figure 6.10: Summary of the main features of the absorption column

It can be seen that the overall layout of the column is made with active mixing in mind. The amount of sorbent circulations is computed over a period of 8 hours. The air is flowing counter currently to the sorbent and the stripper is sucking rich sorbent from a container at the bottom of the column. An exploded view of the absorber is shown in Figure 6.11:

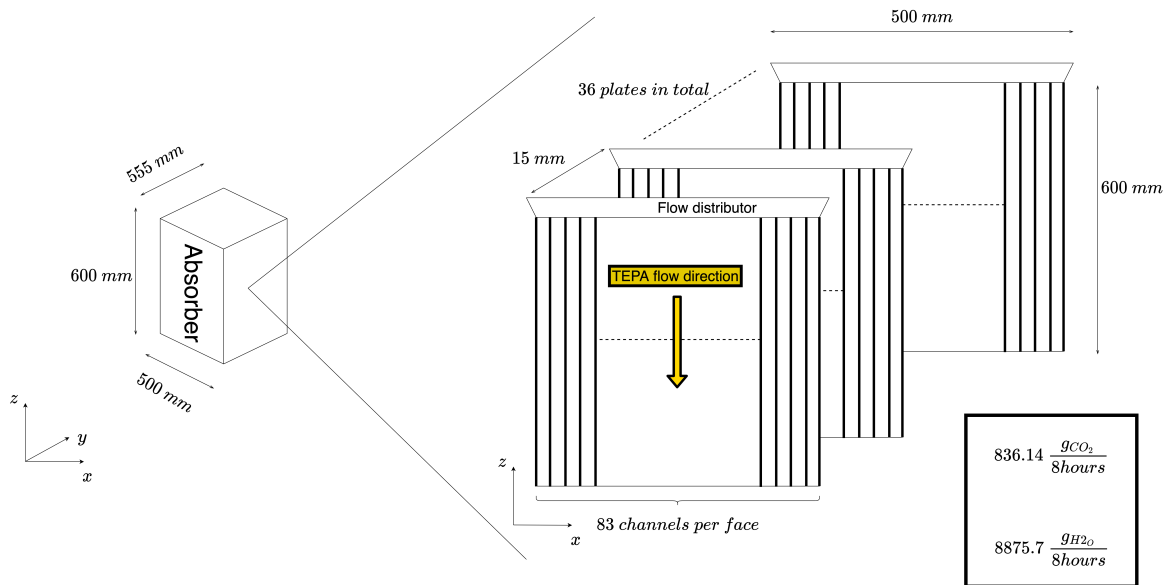


Figure 6.11: Exploded view of the absorber

This image underlines how the plates are distributed in parallel within the absorber and gives some information about the overall amount of captured CO_2 and H_2O . Looking at the absorber operating concentration in figure 6.10 and at the total amount of captured CO_2 and H_2O in figure 6.11, it can be concluded that **the proposed conceptual design satisfies the requirements proposed in chapter 1.**

7

Conclusions & Recommendations

In this chapter, the main conclusions of this research project are collected. Those conclusions are taken directly from chapter 5 and 6 and they are organized here with respect to the relevant research questions and goals.

Finally, recommendations for future research are included.

7.1. Conclusions

The main conclusions are taken from results of the performed experiments, models and design. Refer to chapter 1 for the relevant research goal and objectives, and to chapter 5 and 6 for a detailed explanation of the reported conclusions.

Conclusions from the passive mixing experiments:

1. An experimental sensitivity analysis on the Empty Channel (EC) geometry, underlines how **absorption of CO_2 in this novel absorption process is limited by slow diffusion of CO_2 molecules in the liquid phase**. In particular, it is shown how only the sorbent layers near the liquid-gas interface are contributing to effectively capture CO_2 molecules. In fact, slow diffusion toward the sorbent bulk prevents distant sorbent layers from contributing to the absorption process. That is backed up by experimental results in section 5.1.1 and agrees with previous research at ZEF [14].
2. **Experimental results on the passive mixing channels, show no change in absorption performance, with respect to a base case experiment (Empty Channel)**. In fact, it is observed that the Empty Channel geometry performs equally to the designed passive mixing geometries. That is explained in section 5.1.1.
 - In particular, results from the **Direct Numerical Simulation** model shown in section 5.2.1, **can be used to estimate the magnitude of the circulation velocity generated by the designed passive mixing channels. It is concluded that mixing is not generated because the circulation velocity is extremely small for the investigated experimental conditions. Moreover, due to a stokes flow behavior, circulation can not be used to induce chaotic mixing between different sorbent layers**. For the passive mixing experiments, for channels where mixing grooves are present on the floor, the Direct Numerical Simulation model is a tool for the describing the fluid dynamics of the investigated process.

It is observed a divergence of reported results for mixing induced with the Bridges (BR) geometry. In fact, work from [14], shows that mixing can be induced using that geometry, while in this thesis that is not observed to be the case. It is believed that the divergence can be explained looking at different experimental methodologies and/or at different bridges design. However, as of today, it was not possible to develop a satisfactory explanation for that.

3. Either way, results from the passive mixing experiments can be used to partially answer the following **research question**: *"Is it possible to circulate particles from the top surface of the channel into the bulk of the flow?"* **Answer**: *"Experiments suggest that no circulation is being generated because of the use of passive mixing elements in the channel. In particular, even if the DNS model predicts that extremely slow circulation might be induced, that is completely irrelevant in the context of improving the investigated absorption process because the circulation velocity is extremely small."* This also implies that **passive mixing is not suggested for the design of the absorption column.**

Conclusions from the active mixing experiments:

4. Designed to reduce limitations coming from slow CO_2 diffusion in the liquid phase, **results on the active mixing experiments** showed much more promising results than the passive mixing experiments. It is concluded that, for the investigated experimental conditions, **at very low relative CO_2 loading, mass transfer in the air side can actually be slower than diffusion in the liquid phase.** That is believed to be a very interesting result since, so far, it was possible to observe mass transfer limitations coming from the liquid phase only. This conclusion is based on experiments performed with different air flow rate and reasons for the conclusion are explained in section 5.1.2.
5. Following results from active mixing, experiment #3, it can be concluded that **a higher sorbent flow rate gives a higher cumulative Space-Time Yield** with respect to the same experiment using a lower sorbent flow rate, **at the same relative CO_2 and H_2O loading.** This conclusion is relevant in the framework of designing an absorber for the investigated process. In fact, **it can be concluded that the flowing velocity of the sorbent stream on the absorption plate, has an effect on the reported cumulative STY for a certain relative bulk concentration.** In particular, the higher is the flowing velocity, the higher is the reported cumulative STY. This conclusion is backed up also by results coming from the developed mass transfer model when different sorbent flowing speed are modelled.
6. Following the active mixing experimental results, it is possible, once again, to give an answer to the **research question**: *"Is it possible to circulates particles from the top surface of the channel into the bulk of the flow?"* **Answer**: *yes, with the engineered active mixing experimental setup, it is possible to actively mix the top surface of the sorbent stream with the bulk of it.* Moreover, now it is also possible to answer a **research subquestion**: *"are absorption performances improved because of that?"* **Answer**: *"yes, comparison between single channel flow experiments and active mixing experiments, show that actively mixing the sorbent increases the reported Space-Time Yield at the same relative CO_2 loading. Thus, absorption performances are improved because of that."*
7. For that experimental results, it is also worth noting a divergence in behavior between CO_2 and H_2O . In fact, figure 5.21 shows that the reported STY values for water capture are the same for both active and passive mixing experiments. It can be concluded that, **while active mixing is effective in improving CO_2 capture rate, the same can not be said about H_2O .** It is believed that is the result of a **significant physical difference in the way those two gas are absorbed.** In fact, CO_2 is chemically absorbed, while H_2O is physically absorbed. That is, H_2O can diffuse into the amine bulk quite quickly, while CO_2 is only diffusing very slowly in the (chemically formed) "Ice-Sheet" on the top surface of the sorbent stream. That is, "breaking the ice" works for CO_2 absorption, but not for H_2O .
8. Conclusions about the passive mixing experiments show that the **research goal** of *"inducing mixing in the absorption process"* is reached. Moreover, that justifies the use of active mixing in the design of the absorber.

Understanding the reactive absorption of CO_2 :

9. Following the interpretation of the experimental results, it was possible to develop an understanding of mass transfer in reactive CO_2 absorption. That converged in the **definition of a theory called the "Ice-Sheet" equivalence**. This theory, described in greater details in section 5.3, describes how the firstly absorbed CO_2 molecules will form a heavily loaded, highly viscous layer of sorbent, in proximity of the gas-liquid interface. This layer will slow down further absorption because the CO_2 molecules coming from the air side will have to diffuse through that layer before being absorbed. According to the theory, a concentration profile for this process can be drawn (figure 5.38).
10. **Validation of the theory is done in a dual way by looking at confirmations from literature and by building a theory-based mass transfer model to be compared with the experimental results.**
- A recent study from Wilfong et al. [104], concludes that, for absorption of CO_2 in TEPA films, due to diffusion limitations, a low concentration of CO_2 in the bulk is observed. Moreover, it is explained how the diffusion limitations are due to a highly interconnected network of ammonium ions generated on the top surface of the sorbent stream. **It can be concluded that this paper adds credibility to the proposed theory. In fact, even if the presence of ammonium ions in the investigated process is not proven (and not investigated), the way the diffusion limitations are described to happen is recognized to be very similar to the formation of the "Ice-Sheet" described by the theory.**
 - Regarding **the mass transfer model**, that is nothing else than the mathematical formulation of the "Ice-Sheet" theory in the form of unimolecular diffusion of CO_2 in the "Ice-Sheet". Section 5.2.2 is believed to **show very good correlation between the model predictions and the experimental results for both active and passive mixing experiments.**

From the above described results, it is possible to give an answer to the following **research question**: *"how is diffusion limitation happening for the investigated process?"* **Answer**: *"diffusion limitation on the liquid phase is happening due to the formation of a fully loaded sorbent layer in proximity of the gas-liquid interface. This layer, also referred to as the "Ice-Sheet", significantly slows down CO_2 diffusion, thus jeopardizing CO_2 absorption. The validity of the theory is proven via the validation of a theory-based mass transfer model and looking at confirmations from recent literature."*

11. After validating the mass transfer model, **it can be concluded that an estimated value for the diffusion coefficient of CO_2 into the "Ice-Sheet" is on the order of $10^{-15} m^2/s$.**

Conclusions on the absorber design:

12. The main research goal of this thesis project is to propose a conceptual design for an iteration of ZEF absorber, which satisfies requirements described in table 1.1. Looking at results presented in section 6.4, it can be concluded that **the presented design satisfies the requirements** described in table 1.1. Moreover, from the engineering process, the following conclusions can be traced:
- **The area of the absorber goes to infinity when the operating concentration (rich loading) is 9 moles per kilogram of TEPA.** An extensive explanation of this behavior is reported in section 6.1.1.
 - The required absorber area increases linearly with the CO_2 capture rate.
 - The absorber is designed on a cost reduction basis. **The biggest contributions in the cost of the absorber** are believed to **come from the energy expenses for the pump used to flow the sorbent and from the material costs of the absorption plates' area**. It is understood, that this conclusion may not be true anymore, when a proper way of calculating pressure drops on the air side is defined.
 - **It is understood that the predicted cost of the absorber is very high.** It is believed that the cause lies in the use of pure TEPA as sorbent and in the very high rich loading

concentration. In fact, pure TEPA brings the limitations connected to the formation of the "Ice-Sheet", while the high operational loading increases the viscosity of the sorbent significantly, thus making the operation of the absorber far from an optimum one since the absorber area significantly increases with an increase in the operating concentration.

7.2. Recommendations

This section collects a series of suggestions for continuing the research targeted by this thesis project. **All the experiments, models and theories presented in previous chapters, converged into the definition of a theoretical framework for the absorption of CO_2 in continuously flowing TEPA.** Also referred to as the "Ice-Sheet" theory, **it underlines how the absorption process is limited by the formation of a heavily loaded layer of sorbent on the top surface of the free-flowing TEPA stream.** Therefore, a series of recommendations for solving that problem in future iterations of the absorber are collected. Moreover, since this investigation focused on multiple aspects of the process, it is recognized that some of them could be investigated and described in a more detailed way. Those type of suggestions, relative to this thesis' specific investigation, are included in the second part of this section.

7.2.1. Recommendations for future research

1. **Change the sorbent type.** In this process, the use of pure TEPA is connected with CO_2 diffusion limitation in the liquid phase generated by the formation of the so-called "Ice-Sheet". The result is a very high absorber cost. **Since this thesis proves that the formation of the "Ice-Sheet" happens in the case of pure TEPA sorbent, it is suggested to use a different sorbent type.** For example, reducing the viscosity of the sorbent might be helpful since, according to the Stokes-Einstein diffusion equation, a lower viscosity means a higher diffusion coefficient. However, at this point, it is not very clear how a lower sorbent viscosity would affect diffusion in the "Ice-Sheet" (which is what is really limiting the process). Research should focus on that as well. Another interesting investigation might target validation of results from [104]. In fact, even if not proven yet, it might be that the "Ice-Sheet" is formed by the same type of ammonium ions on the top surface of the sorbent film. If that is proven to be the case, one could try to use a sorbent which does not form those kind of interactions when absorbing CO_2 . **In conclusion, while it is not clear which type of sorbent could remove diffusion limitations in the liquid side, it is quite clear that pure TEPA is far from being the right sorbent for this process because of the "Ice-Sheet" formation.**
2. **Decrease the film thickness** In [104] it is specified that " CO_2 adsorbed onto the $4 \mu m$ film as ammonium carbamate ion pairs and zwitterions, rapidly diffused into the bulk". On the other side, "*increasing the film thickness to $20 \mu m$ resulted in a thick, interconnected surface network of strongly adsorbed species*". Once again, the film thickness in the considered experiments was observed to be around $10 \mu m$. **IF future research succeeds in proving that the "Ice-Sheet" is actually formed by a network of ammonium ions, it would then be extremely interesting to design an absorption geometry able to generate a very thin film.** In that framework, a flowing channel does not look promising. For instance, TEPA flowing onto a very thin string of some plastic material could be a better idea. The surface tension effects would keep the sorbent together and a very thin film, concentric to the string, could be obtained. Clearly, obtaining a very thin film for the very viscous pure TEPA might be extremely difficult and unpractical to achieve.
3. **Map the effects of relative humidity and temperature.** In previous chapter, it was underlined how a variation in ambient relative humidity can have an influence in the absorption rate of H_2O . However, a correlation between the ambient relative humidity and the absorption of CO_2 is still missing. In section 2.3, it was reviewed how absorption differs for wet and dry amines. That aspect of the process still needs to be investigated. Moreover, since ZEF plans to install microplants in different regions of the world, it makes sense to **understand, together with the effects of ambient humidity, also the effects of ambient temperature.** For example, a setup similar to the one used for active mixing experiments could be used inside a climate chamber. That way, the experiments performed following table 3.5 could be repeated in a controlled environment.

7.2.2. Recommendations for improving this research project

Regarding improvements of the investigation described in this report, some suggestions are collected below:

1. **Explore process' limitations in a more detailed way.** Despite the promising performances, due to time constraints, only three experiments were performed with the active mixing experimental setup. Therefore, it is suggested to add at least two experiments to the experimental plan defined in table 3.5. Firstly, it is suggested to perform an experiment with a high air flow rate, then another one with a low sorbent mass flow rate. Table 7.1 collects the experimental parameters for the two proposed experiments.

Experiment number	Pump voltage (affects sorbent flow rate) [V]	Fan voltage (affects air flow rate) [V]	Sorbent initial conditions	Plate inclination	Plate length [mm]	Number of plates	Sorbent initial mass [g]
4	7	10	Pure TEPA	vertical	50	2	140
5	4	7	Pure TEPA	vertical	50	2	140

Table 7.1: Active mixing, additional experiments

These two extra experiments are proposed to **have at least three experiments targeting limitations in the air and three targeting limitations in the liquid side of the process.** That should help in defining the boundaries for the two limitations.

2. **Combine passive and active mixing.** The active mixing experiments showed that the process can be improved by "breaking the ice" on the top surface of the flowing TEPA stream. That process could be improved by combining active and passive mixing with a smart, more complex design of the flowing plates. For instance, Staggered Herringbones or other mixing patterns could be included on the plate (figure 7.1). In fact, since active mixing works with fast flowing sorbent, passive mixing performances should be improved as well.

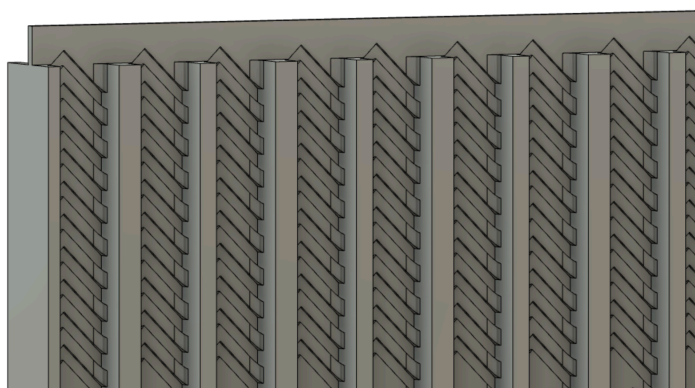
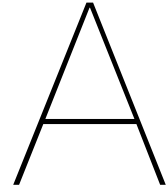


Figure 7.1: Example of plate design for combining active and passive mixing

3. **Build a comprehensive mass transfer model which models the gas phase as well.** The main features of the model should include:

- Connected to the extra proposed experiments, once the boundaries for gas and liquid phase limitations are known, **it should be possible to couple the UMD mass transfer model presented in chapter 4 with a model describing diffusion in the gas phase.** That should significantly increase the ability of making predictions about the absorption process. Moreover, diffusion in the gas phase should be easier to model since no chemical reaction is involved and coefficients for diffusion of CO_2 and H_2O in air are well known.
- The model should be able to predict which phase is limiting the process and adjust the absorption rate accordingly. For instance, depletion of CO_2 in the air side can shift the limit from the liquid to the gas phase.

- Ideally, reaction kinetics of CO_2 with TEPA should be included in the model.
 - Diffusion of H_2O in the gas phase and, later, in the bulk of sorbent could be easily included since no reaction is involved with that gas. **Including water absorption rate is important since the presence of water influences the relative concentrations in the bulk, thus the driving force for diffusion.**
4. **Understand is stirring is really necessary.** In the active mixing experiments, a magnetic stirrer is used to "break the ice" by mixing the loaded sorbent inside a container. However, it is not clear yet if active stirring is necessary or not. In fact, pumping the sorbent from the container to the inlet of the channel might be sufficient for mixing of the bulk. **That can be easily investigated by repeating one of the experiment without the use of the stirrer.** This investigation is relevant in the framework of reducing the absorber cost by reducing energy consumption.



Detailed experimental methodology

A.1. Passive mixing experiments

The experimental methodology used to collect samples for the passive mixing experiments is the following one:

1. In this thesis, a typical experiment is started by selecting the experimental parameters. These are the following ones:
 - Plate (or channel) inclination
 - Channel type
 - Channel length (or number of modules)
 - Sorbent initial conditions
 - Sorbent flow rate
 - Fan operating voltage
2. Once all the parameters are selected, the modules are assembled using clips and O-Rings. In order to check for eventual leakages, laboratory blue paper is taped at the connection points. That kind of paper has high absorbing characteristics, therefore a leakage, if present, will become evident.
3. After that, the syringe pump is prepared by setting the correct volumetric flow rate and by plugging the rubber hose at the end of the syringe nozzle.
4. At this point, environmental relative humidity and temperature are measured.
5. The experiment can now start: the syringe pump and the fan are activated. Air flow must be present over all the length of the assembled plastic modules in order to avoid any air depletion.
6. For future data analysis, the residence time of the sorbent on the plastic modules needs to be measured. For that, a simple stopwatch is used to note down the time taken by the first droplet to reach the end of each module.
7. When the first injected sorbent reaches the end of the last module, the total residence time is known. At that point, at least 50% of the overall residence time is waited before the sample collection can start in order for the experiment to reach steady state conditions.
8. The samples collection can now start from the end of the last module. At least 0.1 *mL* of sorbent are collected.
9. The last module is disconnected and the remaining modules are slid down toward the fan.

10. This procedure is repeated until the sorbent from the end of the first module is collected. Please note that, in the collection, the sorbent is taken only from the end of each module. This means that collection happens at single distances from the beginning of the assembled modules.
11. When the samples from each module are collected, all the modules are properly clean to make sure no sorbent residue is present when a new experiment is started.

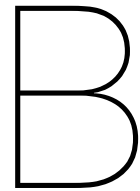
When cleaning the modules, it was noted that TEPA can penetrate into PLA and soak wet the plastic material. That happens especially when the 3D printer leaves some clearance in the printed parts. For that reason, the modules are periodically substituted.

A.2. Active mixing experiments

The methodology of the active mixing experimental investigation is described here. Similarly to the passive mixing experiments, the goal is to give the researcher a structured way for performing the experiments and collecting the relevant results.

1. Once again, the first step is the selection of the relevant experimental parameters. These are:
 - Sorbent flow rate. Please note that this parameter is imposed indirectly by actually imposing the pump power. That is, the sorbent flow rate is a consequence of operating the pump at a certain power (voltage). That is, the real imposed parameter is the pump power while the sorbent flow rate is measured during the experiment.
 - Fan operating voltage
 - Sorbent initial conditions
 - Sorbent initial mass
 - Plate inclination
 - Number of plates
 - Plate length
2. Ambient relative humidity and temperature are measured similarly as in the passive mixing experiments
3. The sorbent is placed in the container and part of it is injected into the hose connected to the low pressure side of the pump with the use of a syringe. This way the pump can be primed before being powered.
4. The fan, pump and stirrer are turned on and the experiment can begin
5. The sorbent is collected at the outlet of the flow collector at specific time intervals. This is done because, at the beginning of the experiment, the sorbent is fresh and a lot of gases are captured. Therefore, it is requested to have a higher resolution of data at the beginning of the experiment compared toward the end of it. More or less, that is how collection happens:
 - Collect a sample every 10 minutes for the first hour of experiment.
 - Collect a sample every 30 minutes after the first hour of experiment, until the end of the first day of experiment.
 - Collect a sample every 90 minutes after the first day of experiment, until the experiment is over.
6. Once every couple of hours the mass flow rate (and also the volumetric flow rate) is measured in the following way:
 - Fill a 10 mL plastic container by placing it below the stream of sorbent exiting the collector.
 - While that happens, with a stop watch, measure the time it takes to fill the container.
 - Weight the full container and subtract the weight of the container to the result.

- Knowing the mass of the sorbent and the time it takes for that to flow, the sorbent mass flow rate can be calculated.
 - Put the collected sorbent back into the container.
7. These experiments are predicted to last around a full week. That means the methodology should account for interrupting the experiment overnight and starting it again the next morning. For that to happen, at the end of the day, all the equipment is switched off and the container with all the sorbent is sealed with a plastic glove to prevent absorption overnight. The next morning, the experiment is started again from point #2 of the methodology.
 8. The experiment is interrupted when the viscosity of the sorbent is so high that the magnetic stirrer does not work anymore.
 9. Finally, the setup is cleaned by running water into it for at least 30 minutes.



Autodesk CFD model

Before the development of the DNS fluid dynamics model, a quick CFD simulation in Autodesk CFD was performed on the passive mixing experiments. The goal of this simulation was simply to give a **qualitative, but not quantitative** evaluation of mixing performance of the selected channels. Being a very preliminary simulation, the idea was to include multiple channel geometries apart from the ones selected for the experiments (EC, SHM, BR). Eventually, this simulation turned out to be a useful tool in evaluating the qualitative flow behaviour for different channels, especially because of the possibility of performing simulations in a three-dimensional environment. That gave the possibility of, for instance, discarding some channels geometry from the passive mixing experiments. However, results are not considered to be reliable enough (quantitatively) to include them in the report mostly due to the lack of in-depth knowledge of the software from the author of this report. That is why this part of the research is presented in the appendix.

B.1. General overview of the simulation

The channels' geometries investigated in this simulation are the following ones:

- Staggered Herringbone Mixer (SHM), figure [B.1](#)
- Oblique Ridges (OR), figure [B.2](#)
- Sinusoidal Channel (SC), figure [B.3](#)
- Obstructed Channel (OC), figure [B.4](#)
- Kenics Mixer (KM), figure [B.5](#)

The top view of the channels geometries for this simulation is the following one:

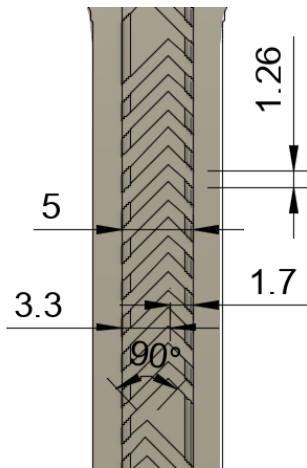


Figure B.1: Staggered Herringbone Mixer

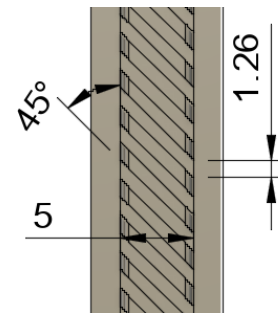


Figure B.2: Oblique Ridges

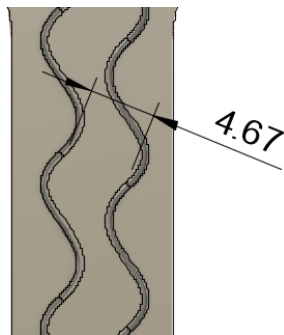


Figure B.3: Sinusoidal Channel

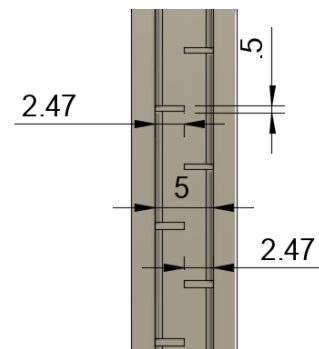


Figure B.4: Obstructed Channel

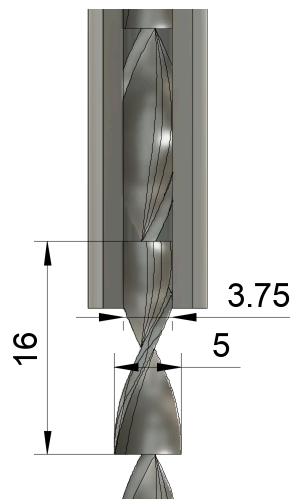


Figure B.5: Kenics Mixer

For performing the CFD simulation, the liquid phase only is considered. That is, the control volume for the simulation is the "negative" of the one shown in the pictures above. The imposed boundary conditions are the following ones:

- **Inlet:** Velocity boundary condition
- **Walls:** No slip boundary conditions

- **Free surfaces (top and outlet):** Zero pressure (gage) boundary condition

And table B.1 shows some more information about the simulation's settings.

Fluid Properties	20°C Pure TEPA
Inlet Flow Rate $\left[\frac{m}{s}\right]$	$4.3e^{-4}$
Gravity Direction (wrt flow direction)	45°
Mesh Resolution (# of elements)	>300k
Maximum residual magnitude	$< 10^{-5}$

Table B.1: CFD simulation general info

B.2. Results of the simulation

Results for this simulation are shown with respect to the streamlines predicted by the software and the vorticity in the direction of interest. Regarding the latter, the idea is to find a parameter which could give an idea about the tendency of the flow of generating surface renewals. In this framework, vorticity is a measure of the tendency of the flow particles to rotate. Therefore, in this case it is of interest to quantify vorticity toward the top free surface of the domain. The vorticity equation is the following one, where u is the velocity field:

$$(\nabla \times \mathbf{u}) \cdot \hat{y} \quad (\text{B.1})$$

SHM results Figure B.6 and B.7 show the results for the Saggered Herringbone Mixer simulation:

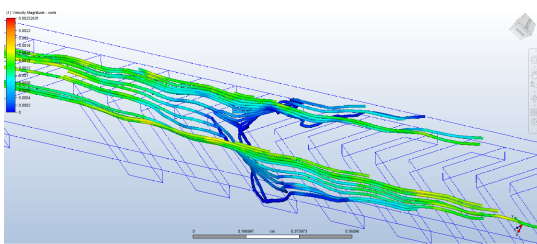


Figure B.6: SHM, traces

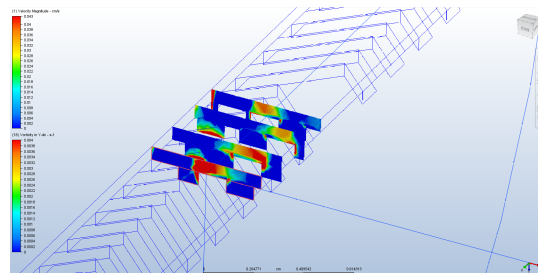


Figure B.7: SHM, vorticity

Results show that surface renewals are generated with this geometry. In fact, figure B.6, depicts stream lines moving from a region of higher speed (top of the channel) to a region of low speed (bottom of the channel, inside the grooves), then again to a region of high speed. That is, it looks like circulation toward the free surface of the channel is possible. This result is coherent with the vorticity plot (figure B.7) showing that particles rotate upward and are moved toward the lateral wall of the channel in doing so.

B.2.1. OR results

Results for the Oblique Ridges geometry is shown below:

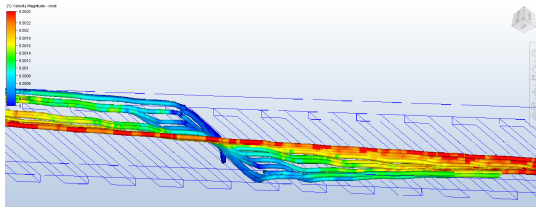


Figure B.8: OR, traces

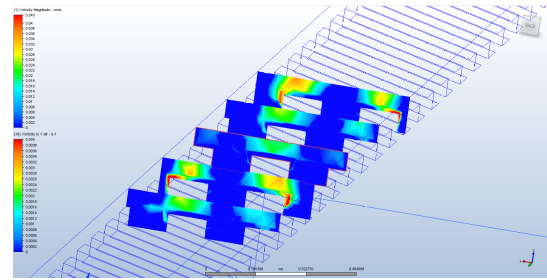


Figure B.9: OR, vorticity

The oblique ridges geometry is showing surface renewals as well. In this case, since the shape of the ridges is not an herringbone, there is a single circulation across the width of the channel. However, compared to figure B.6, it looks like the velocity of circulation is higher. That could be explained by a lower pressure drop across the channel length. In the vorticity plot, figure B.9, it can be observed how the vorticity intensity follows the shape of the ridges toward the lateral wall of the channel. It seems like that vorticity intensity is lower as compared to the SHM case.

B.2.2. SC results

Sinusoidal Channel results are shown below:

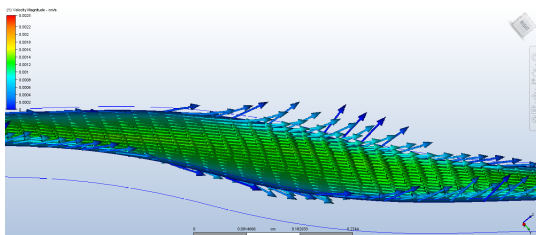


Figure B.10: SC, velocity vector

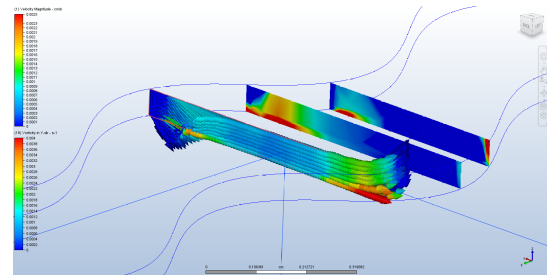


Figure B.11: SC, vorticity

Figure B.10 shows the velocity vectors for the SC channel geometry. As it can be seen, in the middle of the channel, the flow is simply laminarly flowing and no velocity vectors are pointing toward the free surface of the flow. That seems to happen in proximity of the channel wall, but it is a thought of the author that this effect is only present since the CFD software is solving the mass balance equation. The same can be said about figure B.11: it looks like some vorticity is present in proximity of the wall, but only because of mass conservation of an incompressible flow field.

This result was predicted in section 2.5 since the Reynolds number of this simulation is orders of magnitude smaller than the one of the results described in literature.

B.2.3. OC results

Results for the Obstructed Channel geometry are shown in B.12 and B.13.

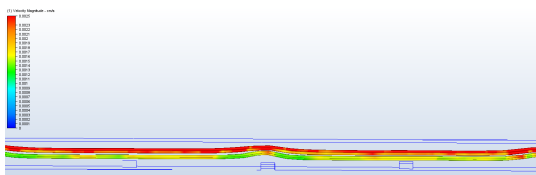


Figure B.12: OC, traces

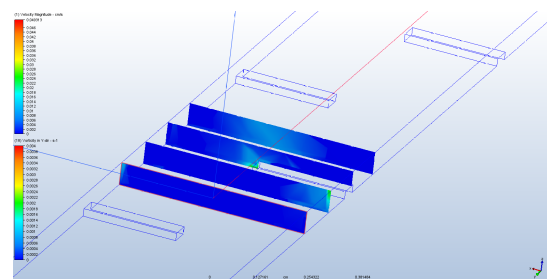


Figure B.13: OC, vorticity

This simulation only shows once again how the flow of interest has a Stokes flow behavior. In fact, figure B.12, shows how the streamlines are simply going over the obstructions and then down again to proceed toward the end of the channel. This "slime" type of behavior is typical of a Stokes flow. It comes with no surprise that very little to none vorticity is observed in figure B.13.

B.2.4. KM results

Regarding the Kenics Mixer:

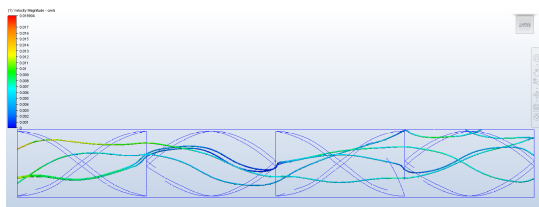


Figure B.14: KM, traces

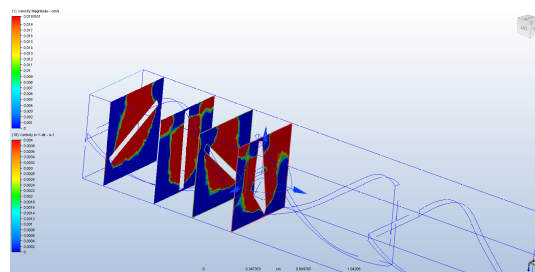
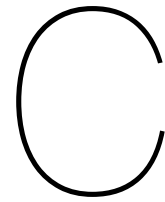


Figure B.15: KM, vorticity

The streamlines depicted in figure B.14, are showing how the traced particles follow the geometry of the mixer, therefore, picture B.15 shows high vorticity in proximity of the external passive mixing element. Clearly, this is an ideal situation where the external mixer has perfect clearance with respect to the channel walls and, therefore, the fluid is perfectly following the mixer geometry. Different 3D printed prototypes showed major difficulties in 3D printing a channel with the same characteristics of the simulated one. Moreover, in this simulation, the channel is entirely full with liquid, while in reality, that will not happen since an open surface is necessary for contacting the amine flow with the stream of air. That will massively influence the mixer ability of displacing the fluid in the required way.



DNS model validation

An analytical solution for stokes flow in an open channel can be obtained by directly solving the NS momentum equations in the z and y direction (referring to the nomenclature in chapter 4 and figure C.1).

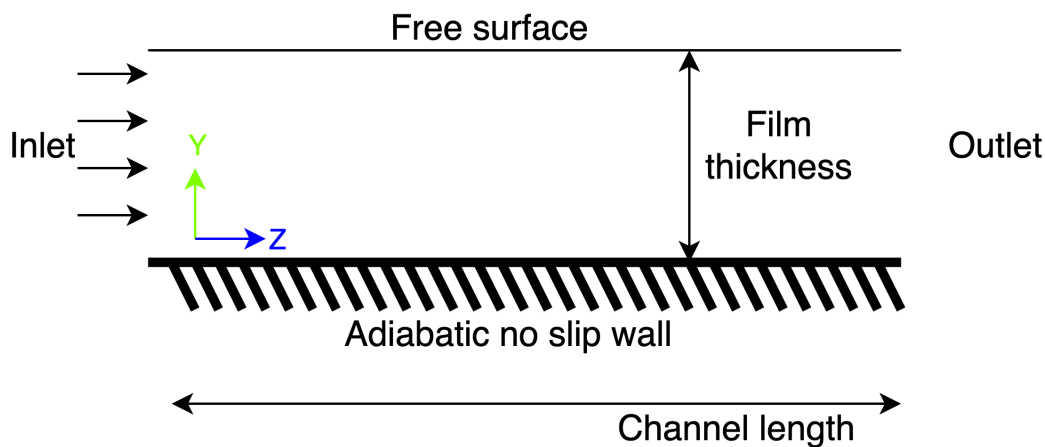


Figure C.1: Open channel flow problem illustration

The two governing equations are:

$$\mu \frac{\partial^2 w}{\partial y^2} = \frac{\partial P}{\partial z} + g \cos \alpha \quad (\text{C.1})$$

$$\frac{\partial P}{\partial y} + g \sin \alpha = 0 \quad (\text{C.2})$$

Referring to equation C.2, since the flow is fully developed, $v = 0$ always. Therefore, we can immediately say that P is not a function of y and proceed with the integration of the z momentum equation (equation C.1) in the y direction:

$$\int_0^y \mu \frac{\partial^2 w}{\partial y^2} dy = \int_0^y \frac{\partial P}{\partial z} + g \cos \alpha dy \quad (\text{C.3})$$

That equals:

$$\mu \frac{\partial w}{\partial y} - \tau_{wall} = \frac{\partial P}{\partial z} y + g y \cos \alpha \quad (\text{C.4})$$

Where τ_{wall} is the shear stress at $y = 0$:

$$\tau_{wall} = \mu \frac{\partial w}{\partial y} \Big|_0 \quad (\text{C.5})$$

Let's now compute an expression for $\frac{\partial P}{\partial z}$ looking at $y = \text{film thickness} = h$. Due to the free surface, we know that the shear stress is zero at that location, therefore we can write:

$$\tau = \mu \frac{\partial w}{\partial y} \Big|_h = 0 \quad (\text{C.6})$$

Please note that $\tau \neq \tau_{wall}$. Evaluating equation C.4 at $y = h$ one can write:

$$0 - \tau_{wall} = \frac{\partial P}{\partial z} h + gh \cos \alpha \quad (\text{C.7})$$

or, equivalently,

$$\frac{\partial P}{\partial z} = -\frac{\tau_{wall}}{h} - g \cos \alpha \quad (\text{C.8})$$

Substituting this result into equation C.4, one obtains:

$$\mu \frac{\partial w}{\partial y} = \tau_{wall} \left(1 - \frac{y}{h}\right) \quad (\text{C.9})$$

Integrating once again in the y direction:

$$w(y) = \frac{\tau_{wall}}{\mu} y - \frac{y^2}{2h} \frac{\tau_{wall}}{\mu} \quad (\text{C.10})$$

or:

$$w(y) = y \frac{\tau_{wall}}{\mu} \left(1 - \frac{y}{2h}\right) \quad (\text{C.11})$$

Moreover, τ_{wall} can be computed from the DNS solver with the following expression computed in proximity of the wall:

$$\tau_{wall} = \frac{w(i) - w(i-1)}{\Delta y} \quad (\text{C.12})$$

Equation C.11 gives the analytical solution for the problem. The calculated velocity profile can be compared with the predicted one shown in figure 5.26 to obtain a plot of the residuals. Results are shown in figure C.2 in function of the film height.

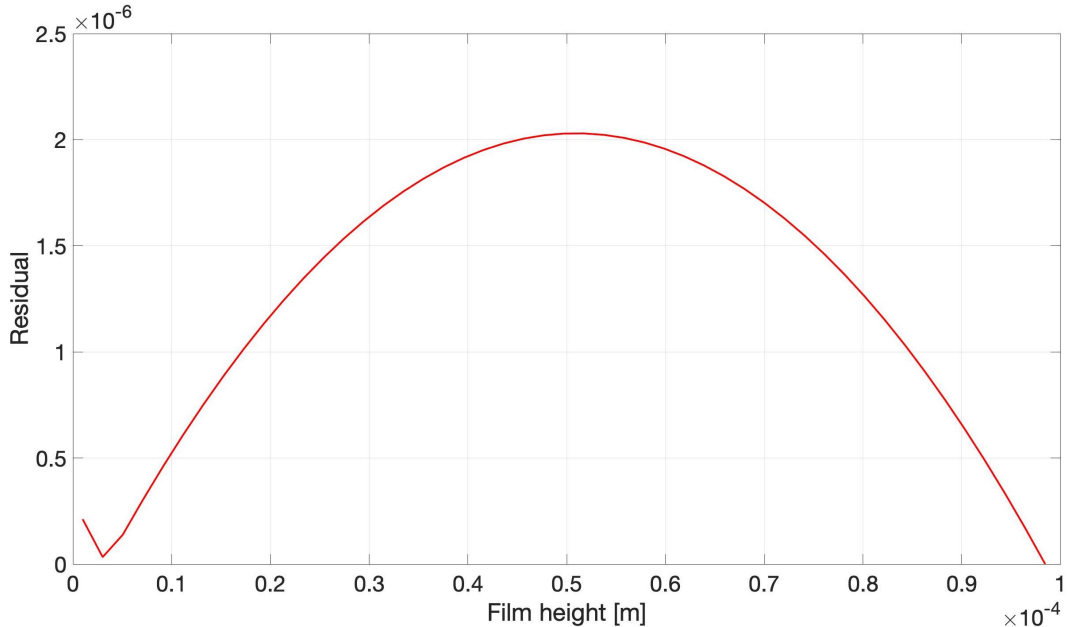
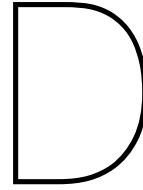


Figure C.2: Residuals for the open channel flow

The magnitude of the residuals are on the order of 10^{-6} , two order of magnitudes lower than the velocity magnitude. That is believed to add credibility to the developed model.



Detailed absorber design

D.1. Detailed sensitivity analysis

Apart from the operational loading and the sorbent residence time on the plate, other design parameters have an influence on the absorber design. Those are listed below:

- **Plate width:** this parameter influences the width of the absorption plate. Given a certain channel dimensions, that will also influence the number of channels in the single plate, thus the amount of plates necessary in the absorber. That has influence on parameters like the cost of the absorber and the sorbent flow rate.
- **Channel depth:** this parameter directly affects the cross sectional dimension of the absorption channels. In particular, a lower cross section means a higher sorbent average speed. As a consequence, the smaller is this parameter, the lower is the sorbent residence time on the plate and, therefore, the absorber area. Clearly, this parameter cannot be reduced too much due to the risk of overflowing the sorbent outside of the various channels.
- **Channel length:** this parameter has a direct influence on the total absorption area of the single absorption plate. This also means that the longer are the absorption channels, the higher the length of the column, but, also, the lower the amount of total required absorption plates.
- **Clearance between the plates:** this parameter influences the spacing between the different absorption plates forming the absorber. The higher is the spacing, the lower the pressure drop on the air side. Moreover, a higher spacing also means an overall larger column.

D.2. Cumulative vs. absolute STY

The Space-Time Yield can be calculated in multiple ways from both the experimental data and the mass transfer model. Two main definitions for the STY can be considered to be when either averaging the STY over all the operational concentrations (cumulative STY) or just calculating the STY at a single operational concentration. The two different equations follows:

$$STY_{cumulative} = \frac{\sum_{t=0}^{t_{end}} moles_{CO_2}(t)}{A \cdot t_{end}} \quad (D.1)$$

$$STY_{absolute} = \frac{moles_{CO_2}(C_{bulk})}{A \cdot t_{plate}} \quad (D.2)$$

Since the absorber is designed to operate in steady state conditions (at the operational rich loading), the absolute STY (equation D.2) is used in the design.

D.2.1. Cumulative vs. absolute STY: influence of rich loading

It is considered to be interesting to understand how both the cumulative and absolute STY change in function of the operational loading:

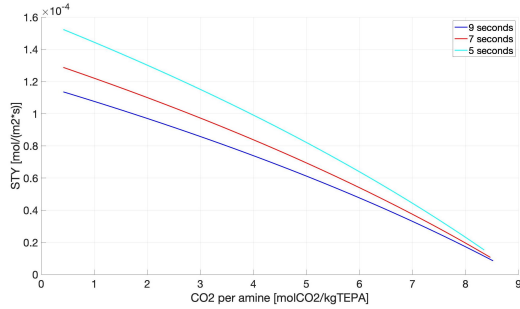


Figure D.1: Absolute STY in function of the operational loading and the sorbent's plate residence time

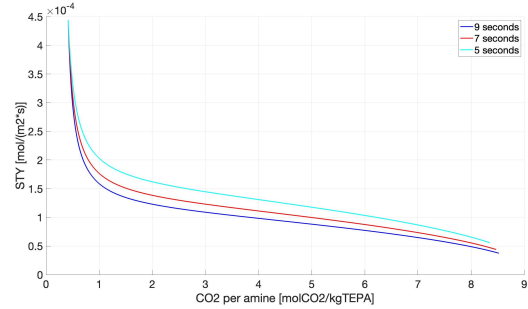


Figure D.2: Cumulative STY in function of the operational loading and the sorbent's plate residence time

D.3. Air side design: governing equations for H_2O mass balance

In designing the air side of the absorber, the following equations hold in the mass balance for H_2O . The water inlet concentration is estimated assuming an average relative humidity [105].

$$\dot{m}_{H_2O,in} = \dot{m}_{air,in} \cdot C_{H_2O,air,in} \quad (D.3)$$

$$\dot{m}_{H_2O,out} = \dot{m}_{H_2O,in} - \dot{m}_{H_2O,absorbed} \quad (D.4)$$

$$C_{H_2O,air,out} = \frac{\dot{m}_{H_2O,out}}{\dot{m}_{air,out}} \quad (D.5)$$

D.4. Extra images for the conceptual absorber design

Images showing more details of the conceptual design of the absorber are shown below:

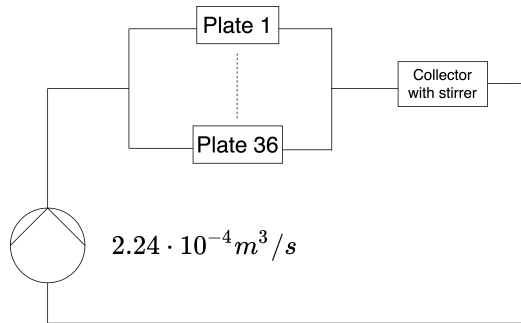


Figure D.3: Absorber design: circuit for the pump

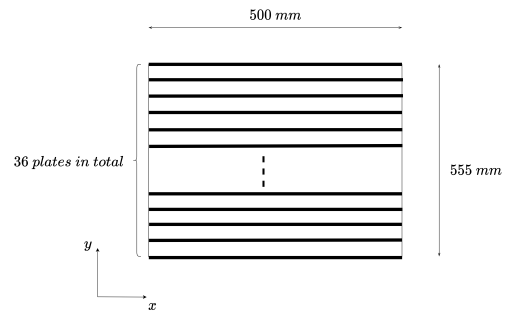


Figure D.4: Absorber design: top view

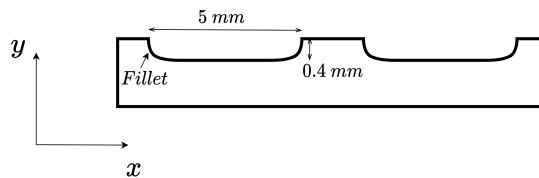
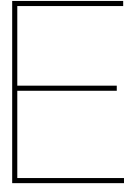


Figure D.5: Absorber design: channel view



Extra plots

E.1. Active Mixing: absolute Space-Time Yield

In chapter 5, results are shown for a cumulative STY (equation 5.2). Figures E.1 and E.2 show the experimental results computed with equation D.2, the absolute STY.

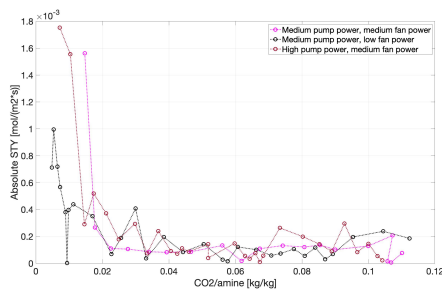


Figure E.1: Active Mixing: absolute STY in function of CO_2 per amine loading

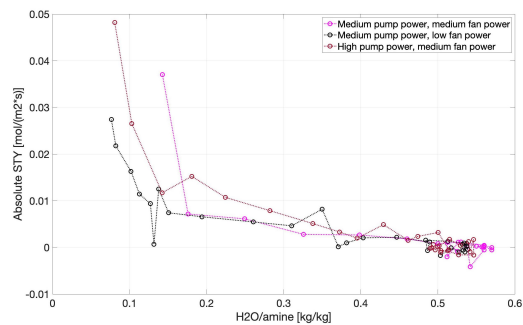


Figure E.2: Active Mixing: absolute STY in function of H_2O per amine loading

E.2. Active Mixing: other plots

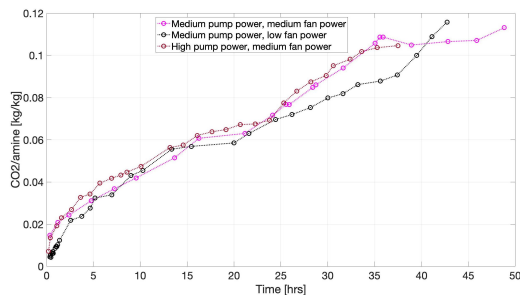


Figure E.3: Active Mixing: CO_2 per amine loading vs. time

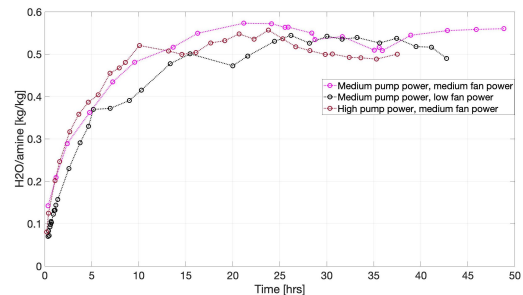


Figure E.4: Active Mixing: H_2O per amine loading vs. time

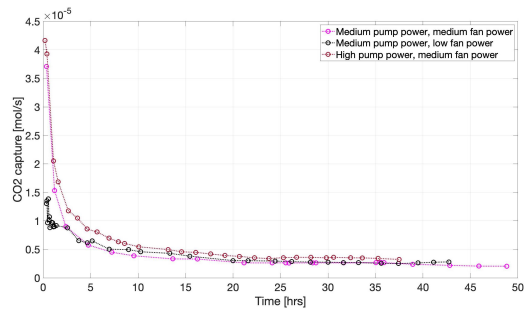


Figure E.5: Active Mixing: CO_2 capture rate vs. time

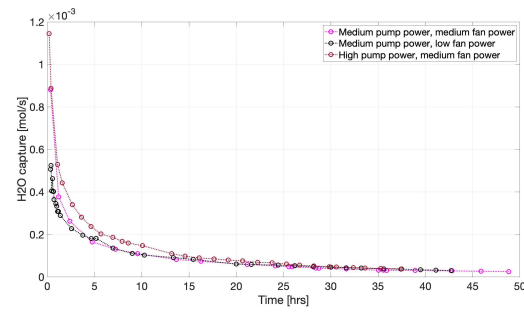


Figure E.6: Active Mixing: H_2O capture rate vs. time

E.3. Passive Mixing: absolute Space-Time Yield

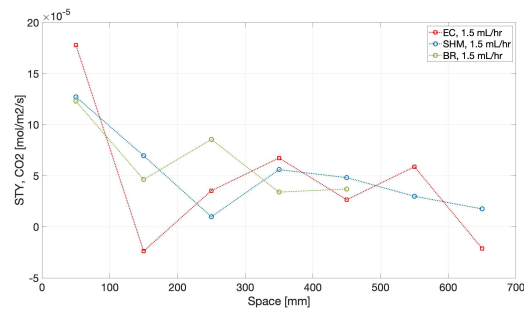


Figure E.7: Passive Mixing, 1.5 mL/hr: CO_2 absolute STY in function of space

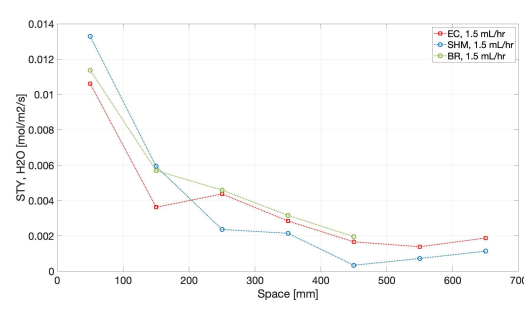


Figure E.8: Passive Mixing, 1.5 mL/hr: H_2O absolute STY in function of space

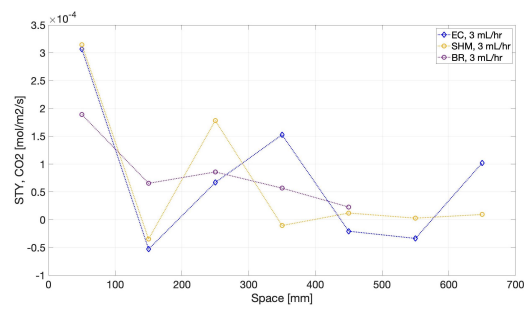


Figure E.9: Passive Mixing, 3 mL/hr: CO_2 absolute STY in function of space

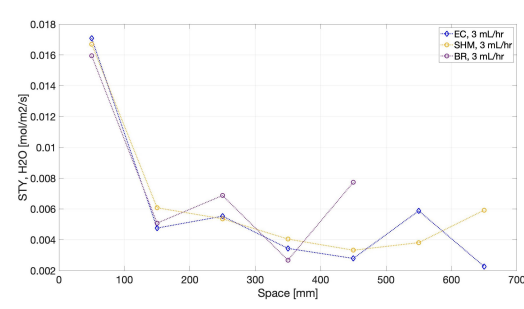


Figure E.10: Passive Mixing, 3 mL/hr: H_2O absolute STY in function of space

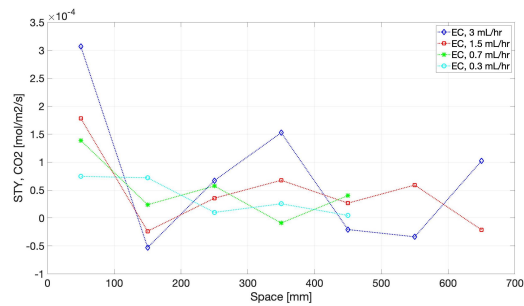


Figure E.11: Passive Mixing, sensitivity analysis: CO_2 absolute STY in function of space

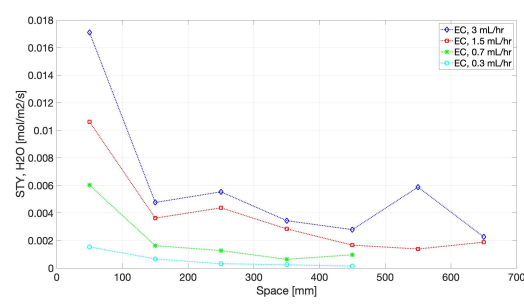


Figure E.12: Passive Mixing, sensitivity analysis: H_2O absolute STY in function of space

Bibliography

- [1] British petroleum company. Bp statistical review of world energy. Report, 2018.
- [2] 2020. URL https://data.giss.nasa.gov/gistemp/maps/index_v4.html.
- [3] World Energy Council. Energy efficiency technologies: Overview report. Report, World Energy Council, 2013.
- [4] Mai Bui, Claire S. Adjiman, André Bardow, Edward J. Anthony, Andy Boston, Solomon Brown, Paul S. Fennell, Sabine Fuss, Amparo Galindo, Leigh A. Hackett, Jason P. Hallett, Howard J. Herzog, George Jackson, Jasmin Kemper, Samuel Krevor, Geoffrey C. Maitland, Michael Matuszewski, Ian S. Metcalfe, Camille Petit, Graeme Puxty, Jeffrey Reimer, David M. Reiner, Edward S. Rubin, Stuart A. Scott, Nilay Shah, Berend Smit, J. P. Martin Trusler, Paul Webley, Jennifer Wilcox, and Niall Mac Dowell. Carbon capture and storage (ccs): the way forward. *Energy & Environmental Science*, 11(5):1062–1176, 2018. ISSN 1754-5692. doi: 10.1039/C7EE02342A. URL <http://dx.doi.org/10.1039/C7EE02342A>.
- [5] 2020. URL <https://zeroemissionfuels.com/>.
- [6] D. Keith Roper J. D. Seader, Ernest J. Henley. *Separation Process Principles. Chemical and Biochemical Operations*. John Wiley & sons inc., third edition, 2011.
- [7] W. K. Lewis and W. G. Whitman. Principles of gas absorption. *Industrial & Engineering Chemistry*, 16(12):1215–1220, 1924. ISSN 0019-7866. doi: 10.1021/ie50180a002. URL <https://doi.org/10.1021/ie50180a002>.
- [8] P. Chiesa and S. Consonni. Shift reactors and physical absorption for low-co2 emission igccs. *Journal of Engineering for Gas Turbines and Power*, 121(2):295–305, 1999. ISSN 0742-4795. doi: 10.1115/1.2817120. URL <https://doi.org/10.1115/1.2817120>.
- [9] David W. Keith, Geoffrey Holmes, David St. Angelo, and Kenton Heidel. A process for capturing co2 from the atmosphere. *Joule*, 2(8):1573–1594, 2018. ISSN 2542-4351. doi: <https://doi.org/10.1016/j.joule.2018.05.006>. URL <http://www.sciencedirect.com/science/article/pii/S2542435118302253>.
- [10] Mahdi Fasihi, Olga Efimova, and Christian Breyer. Techno-economic assessment of co2 direct air capture plants. *Journal of Cleaner Production*, 224:957–980, 2019. ISSN 0959-6526. doi: <https://doi.org/10.1016/j.jclepro.2019.03.086>. URL <http://www.sciencedirect.com/science/article/pii/S0959652619307772>.
- [11] O. Azzalini. Designing a carbon dioxide adsorption unit for producing sustainable synthetic fuels. Report, TU Delft, 2018.
- [12] R. W. van den Berg. Designing a direct air capture unit for methanol synthesis. Report, TU Delft, 2018.
- [13] Mrigank Sinha. Experimental study of absorption and desorption in a continuous direct air capture system to build a concept model. Report, TU Delft, 2019.
- [14] Mrigank Sinha. Direct air capture: Characterization and design of a novel absorption process. Report, TU Delft, 2019.
- [15] Mayurkumar Patil and Prakash Vaidya. New amp/polyamine blends for improved co2 capture: study of kinetic and equilibrium features. *The Canadian Journal of Chemical Engineering*, 98, 2019. doi: 10.1002/cjce.23647.

- [16] Sunghyun Park, Keunsu Choi, Hyun Jung Yu, Young-June Won, Chaehoon Kim, Minkee Choi, So-Hye Cho, Jung-Hyun Lee, Seung Yong Lee, and Jong Suk Lee. Thermal stability enhanced tetraethylenepentamine/silica adsorbents for high performance co₂ capture. *Industrial & Engineering Chemistry Research*, 57(13):4632–4639, 2018. ISSN 0888-5885. doi: 10.1021/acs.iecr.7b04912. URL <https://doi.org/10.1021/acs.iecr.7b04912>.
- [17] David S. Mebane, Joel D. Kress, Curtis B. Storlie, Daniel J. Fauth, McMahan L. Gray, and Kuijun Li. Transport, zwitterions, and the role of water for co₂ adsorption in mesoporous silica-supported amine sorbents. *The Journal of Physical Chemistry C*, 117(50):26617–26627, 2013. ISSN 1932-7447. doi: 10.1021/jp4076417. URL <https://doi.org/10.1021/jp4076417>.
- [18] Ian Glasgow and Nadine Aubry. Enhancement of microfluidic mixing using time pulsing. *Lab on a chip*, 3:114–20, 2003.
- [19] Goksen G. Yaralioglu, Ira O. Wygant, Theodore C. Marentis, and Butrus T. Khuri-Yakub. Ultrasonic mixing in microfluidic channels using integrated transducers. *Analytical Chemistry*, 76(13):3694–3698, 2004. ISSN 0003-2700. doi: 10.1021/ac035220k. URL <https://doi.org/10.1021/ac035220k>.
- [20] Abraham Stroock, Stephan Dertinger, Armand Ajdari, Igor Mezic, Howard Stone, and George Whitesides. Chaotic mixer for microchannels. *Science (New York, N.Y.)*, 295:647–51, 2002. doi: 10.1126/science.1066238.
- [21] Mohsen Parsa and Faramarz Hormozi. Experimental and cfd modeling of fluid mixing in sinusoidal microchannels with different phase shift between side walls. *Journal of Micromechanics and Microengineering*, 24, 2014. doi: 10.1088/0960-1317/24/6/065018.
- [22] Th Avalosse and M. J. Crochet. Finite-element simulation of mixing: 2. three-dimensional flow through a kenics mixer. *AIChE Journal*, 43(3):588–597, 1997. ISSN 0001-1541. doi: 10.1002/aic.690430304. URL <https://doi.org/10.1002/aic.690430304>.
- [23] 2015. URL <https://www.agilent.com/en/product/molecular-spectroscopy/ftir-spectroscopy/ftir-benchtop-systems/cary-630-ftir-spectrometer>.
- [24] A. Christensen, J. Olhoff. Lessons from a decade of emissions gap assessments. Report, 2019.
- [25] R.K. Pachauri and L.A. Meyer. Climate change 2014: Synthesis report. contribution of working groups i, ii and iii to the fifth assessment report of the intergovernmental panel on climate change. Report, IPCC, 2014.
- [26] M.R Allen, O.P. Dube, W. Solecki, F. Aragón-Durand, W. Cramer, S. Humphreys, M. Kainuma, J. Kala, N. Mahowald, Y. Mulugetta, R. Perez, M.Wairiu, and K. Zickfeld. Global warming of 1.5°C. an ipcc special report on the impacts of global warming of 1.5°C above pre-industrial levels and related global greenhouse gas emission pathways, in the context of strengthening the global response to the threat of climate change, sustainable development, and efforts to eradicate poverty. Report, 2018.
- [27] O Hoegh-Guldberg, M. Taylor D. Jacob, M. Bindi, S. Brown, I. Camilloni, A. Diedhiou, R. Djalante, K.L. Ebi, F. Engelbrecht, J.Guiot, Y. Hijioka, S. Mehrotra, A. Payne, S.I. Seneviratne, A. Thomas, R. Warren, and G. Zhou. Impacts of 1.5°C global warming on natural and human systems. Report, 2018.
- [28] United Nations Industrial Development Organization. Industrial development report 2016. the role of technology and innovation in inclusive and sustainable industrial development. Report, 2016.
- [29] Electric Power Research Institute (EPRI). Energy efficiency demonstration report. Report, 2012.
- [30] Kun He and Li Wang. A review of energy use and energy-efficient technologies for the iron and steel industry. *Renewable and Sustainable Energy Reviews*, 70:1022–1039, 2017. ISSN 1364-0321. doi: <https://doi.org/10.1016/j.rser.2016.12.007>. URL <http://www.sciencedirect.com/science/article/pii/S1364032116310620>.

- [31] A. Giampieri, J. Ling-Chin, Z. Ma, A. Smallbone, and A. P. Roskilly. A review of the current automotive manufacturing practice from an energy perspective. *Applied Energy*, 261:114074, 2020. ISSN 0306-2619. doi: <https://doi.org/10.1016/j.apenergy.2019.114074>. URL <http://www.sciencedirect.com/science/article/pii/S0306261919317611>.
- [32] Dennis Y. C. Leung, Giorgio Caramanna, and M. Mercedes Maroto-Valer. An overview of current status of carbon dioxide capture and storage technologies. *Renewable and Sustainable Energy Reviews*, 39:426–443, 2014. ISSN 1364-0321. doi: <https://doi.org/10.1016/j.rser.2014.07.093>. URL <http://www.sciencedirect.com/science/article/pii/S1364032114005450>.
- [33] 2017. URL <https://www.energy.gov/fe/petra-nova-wa-parish-project>.
- [34] Dennis Y. C. Leung, Giorgio Caramanna, and M. Mercedes Maroto-Valer. An overview of current status of carbon dioxide capture and storage technologies. *Renewable and Sustainable Energy Reviews*, 39:426–443, 2014. ISSN 1364-0321. doi: <https://doi.org/10.1016/j.rser.2014.07.093>. URL <http://www.sciencedirect.com/science/article/pii/S1364032114005450>.
- [35] 2017. URL <https://www.globalccsinstitute.com/projects/co2-utilisation-projects>.
- [36] 2020. URL http://www.globalccsinstitute.com/sites/www.globalccsinstitute.com/files/content/page/122975/files/Saga%20City%20Waste%20Incineration%20Plant_0.pdf.
- [37] 2010. URL <https://projecten.topsectorenergie.nl/projecten/development-of-an-air-to-methanol-micro-plant-00031804>.
- [38] N. S. Barthe. Absorption of co2 from the air using polyamines: Experiments, modelling and design. Report, TU Delft, 2019.
- [39] Najmus Saquib Sifat and Yousef Haseli. A critical review of co2 capture technologies and prospects for clean power generation. *Energies*, 12:4143, 2019. doi: 10.3390/en12214143.
- [40] Dennis Y. C. Leung, Giorgio Caramanna, and M. Mercedes Maroto-Valer. An overview of current status of carbon dioxide capture and storage technologies. *Renewable and Sustainable Energy Reviews*, 39:426–443, 2014. ISSN 1364-0321. doi: <https://doi.org/10.1016/j.rser.2014.07.093>. URL <http://www.sciencedirect.com/science/article/pii/S1364032114005450>.
- [41] Toby Lockwood. A comparative review of next-generation carbon capture technologies for coal-fired power plant. *Energy Procedia*, 114:2658–2670, 2017. ISSN 1876-6102. doi: <https://doi.org/10.1016/j.egypro.2017.03.1850>. URL <http://www.sciencedirect.com/science/article/pii/S1876610217320520>.
- [42] Bruce G. Miller. *13 - Carbon Dioxide Emissions Reduction and Storage*, pages 609–668. Butterworth-Heinemann, 2017. ISBN 978-0-12-811365-3. doi: <https://doi.org/10.1016/B978-0-12-811365-3.00013-2>. URL <http://www.sciencedirect.com/science/article/pii/B9780128113653000132>.
- [43] Cheng-Hsiu Yu, Chih-Hung Huang, and Chung-Sung Tan. A review of co 2 capture by absorption and adsorption. *Aerosol and Air Quality Research*, 12, 2012. doi: 10.4209/aaqr.2012.05.0132.
- [44] W. G. Whitman. The film theory of absorption. *Chemical and Metallurgical Engineering*, 29: 146–148, 1923.
- [45] P. V. Danckwerts. The absorption of gases in liquids. *Pure and applied chemistry*, 10(4):625–642, 1965.

- [46] W. Nernst. Theorie der reaktionsgeschwindigkeit in heterogenen systemen. *Z. Phys. Chem.*, 47: 52–55, 1904. URL <https://ci.nii.ac.jp/naid/10008278281/en/>.
- [47] P. V. Danckwerts. Significance of liquid-film coefficients in gas absorption. *Industrial & Engineering Chemistry*, 43(6):1460–1467, 1951. ISSN 0019-7866. doi: 10.1021/ie50498a055. URL <https://doi.org/10.1021/ie50498a055>.
- [48] H. L. Toor and J. M. Marchello. Film-penetration model for mass and heat transfer. *AIChE Journal*, 4(1):97–101, 1958. ISSN 0001-1541. doi: 10.1002/aic.690040118. URL <https://doi.org/10.1002/aic.690040118>.
- [49] Joseph McCabe and William Wesley Eckenfelder. *Biological treatment of sewage and industrial wastes. 2: Anaerobic digestion and solids-liquid separation*. New York (N.Y.): Reinhold, 1958. URL <http://lib.ugent.be/catalog/rug01:000945020>.
- [50] R. Higbie. The rate of absorption of a pure gas into a still liquid during short periods of exposure. *Trans. AIChE*, 31:365–389, 1935. URL <https://ci.nii.ac.jp/naid/10003391803/en/>.
- [51] Abass A. Olajire. Co2 capture and separation technologies for end-of-pipe applications – a review. *Energy*, 35(6):2610–2628, 2010. ISSN 0360-5442. doi: <https://doi.org/10.1016/j.energy.2010.02.030>. URL <http://www.sciencedirect.com/science/article/pii/S0360544210000848>.
- [52] Rens Veneman. *Adsorptive systems for post-combustion CO2 capture: design, experimental validation and evaluation of a supported amine based process*. Thesis, 2015.
- [53] Eizo Sada, Hidehiro Kumazawa, and M. A. Butt. Gas absorption with consecutive chemical reaction: Absorption of carbon dioxide into aqueous amine solutions. *The Canadian Journal of Chemical Engineering*, 54(5):421–424, 1976. ISSN 0008-4034. doi: 10.1002/cjce.5450540507. URL <https://doi.org/10.1002/cjce.5450540507>.
- [54] Haruo Hikita, Satoru Asai, Yoshio Katsu, and Seiichi Ikuno. Absorption of carbon dioxide into aqueous monoethanolamine solutions. *AIChE Journal*, 25(5):793–800, 1979. ISSN 0001-1541. doi: 10.1002/aic.690250507. URL <https://doi.org/10.1002/aic.690250507>.
- [55] G. Puxty, M. Maeder, and Paul H. M. Feron. 2 - *The fundamentals of post-combustion capture*, pages 13–33. Woodhead Publishing, 2016. ISBN 978-0-08-100514-9. doi: <https://doi.org/10.1016/B978-0-08-100514-9.00002-0>. URL <http://www.sciencedirect.com/science/article/pii/B9780081005149000020>.
- [56] Michael Caplow. Kinetics of carbamate formation and breakdown. *Journal of the American Chemical Society*, 90(24):6795–6803, 1968. ISSN 0002-7863. doi: 10.1021/ja01026a041. URL <https://doi.org/10.1021/ja01026a041>.
- [57] P. V. Danckwerts. The reaction of co2 with ethanolamines. *Chemical Engineering Science*, 34(4): 443–446, 1979. ISSN 0009-2509. doi: [https://doi.org/10.1016/0009-2509\(79\)85087-3](https://doi.org/10.1016/0009-2509(79)85087-3). URL <http://www.sciencedirect.com/science/article/pii/0009250979850873>.
- [58] Mahsa Aghaie, Nima Rezaei, and Sohrab Zendehboudi. A systematic review on co2 capture with ionic liquids: Current status and future prospects. *Renewable and Sustainable Energy Reviews*, 96:502–525, 2018. ISSN 1364-0321. doi: <https://doi.org/10.1016/j.rser.2018.07.004>. URL <http://www.sciencedirect.com/science/article/pii/S1364032118305100>.
- [59] Zhigang Lei, Chengna Dai, and Biaohua Chen. Gas solubility in ionic liquids. *Chemical Reviews*, 114(2):1289–1326, 2014. ISSN 0009-2665. doi: 10.1021/cr300497a. URL <https://doi.org/10.1021/cr300497a>.
- [60] Eleanor D. Bates, Rebecca D. Mayton, Ioanna Ntai, and James H. Davis. Co2 capture by a task-specific ionic liquid. *Journal of the American Chemical Society*, 124(6):926–927, 2002. ISSN 0002-7863. doi: 10.1021/ja017593d. URL <https://doi.org/10.1021/ja017593d>.

- [61] Rajesh A. Khatri, Steven S. C. Chuang, Yee Soong, and McMahan Gray. Carbon dioxide capture by diamine-grafted sba-15: a combined fourier transform infrared and mass spectrometry study. *Industrial & Engineering Chemistry Research*, 44(10):3702–3708, 2005. ISSN 0888-5885. doi: 10.1021/ie048997s. URL <https://doi.org/10.1021/ie048997s>.
- [62] Abdelhamid Sayari, Youssef Belmabkhout, and Rodrigo Serna-Guerrero. Flue gas treatment via co2 adsorption. *Chemical Engineering Journal*, 171(3):760–774, 2011. ISSN 1385-8947. doi: <https://doi.org/10.1016/j.cej.2011.02.007>. URL <http://www.sciencedirect.com/science/article/pii/S1385894711001756>.
- [63] Rodrigo Serna-Guerrero and Abdelhamid Sayari. Modeling adsorption of co2 on amine-functionalized mesoporous silica. 2: Kinetics and breakthrough curves. *Chemical Engineering Journal*, 161(1):182–190, 2010. ISSN 1385-8947. doi: <https://doi.org/10.1016/j.cej.2010.04.042>. URL <http://www.sciencedirect.com/science/article/pii/S1385894710003840>.
- [64] Alain Goeppert, Miklos Czaun, G. K. Surya Prakash, and George A. Olah. Air as the renewable carbon source of the future: an overview of co2 capture from the atmosphere. *Energy & Environmental Science*, 5(7):7833–7853, 2012. ISSN 1754-5692. doi: 10.1039/C2EE21586A. URL <http://dx.doi.org/10.1039/C2EE21586A>.
- [65] David W. Keith, Minh Ha-Duong, and Joshua K. Stolaroff. Climate strategy with co2 capture from the air. *Climatic Change*, 74(1):17–45, 2006. ISSN 1573-1480. doi: 10.1007/s10584-005-9026-x. URL <https://doi.org/10.1007/s10584-005-9026-x>.
- [66] Klaus Lackner, Sarah Brennan, Juerg Matter, Ah-Hyung Park, Allen Wright, and Bob Zwaan. The urgency of development of co2 capture from ambient air. *Proceedings of the National Academy of Sciences of the United States of America*, 109:13156–62, 2012. doi: 10.1073/pnas.1108765109.
- [67] Micah Broehm, Jessica Strefer, and Nico Bauer. Techno-economic review of direct air capture systems for large scale mitigation of atmospheric co2. *SSRN Electronic Journal*, 2015. doi: 10.2139/ssrn.2665702.
- [68] 2020. URL <https://www.climeworks.com/page/co2-removal>.
- [69] 2020. URL <https://globalthermostat.com/>.
- [70] 2014. URL <http://globalthermostat.com/wp-content/uploads/2014/10/MIT-Technology-Review-Global-Thermostat.pdf>.
- [71] Nicholas R. Stuckert and Ralph T. Yang. Co2 capture from the atmosphere and simultaneous concentration using zeolites and amine-grafted sba-15. *Environmental Science & Technology*, 45(23):10257–10264, 2011. ISSN 0013-936X. doi: 10.1021/es202647a. URL <https://doi.org/10.1021/es202647a>.
- [72] V. Nikulshina, N. Ayesa, M. E. Gálvez, and A. Steinfeld. Feasibility of na-based thermochemical cycles for the capture of co2 from air—thermodynamic and thermogravimetric analyses. *Chemical Engineering Journal*, 140(1):62–70, 2008. ISSN 1385-8947. doi: <https://doi.org/10.1016/j.cej.2007.09.007>. URL <http://www.sciencedirect.com/science/article/pii/S1385894707006134>.
- [73] V. Nikulshina and A. Steinfeld. Co2 capture from air via cao-carbonation using a solar-driven fluidized bed reactor—effect of temperature and water vapor concentration. *Chemical Engineering Journal*, 155(3):867–873, 2009. ISSN 1385-8947. doi: <https://doi.org/10.1016/j.cej.2009.10.004>. URL <http://www.sciencedirect.com/science/article/pii/S1385894709006962>.
- [74] S. Wagenaar S. Giannoulidis. Experimental testing and design of a direct air capture unit for methanol production. Report, TU Delft, 2018.

- [75] Daniel van Laake. Characterization of a sorbent for a small scale direct air capture system. Report, TU Delft, 2018.
- [76] Udara Arachchige, N. Aryal, Dag Eimer, and M. C. Melaaen. Viscosities of pure and aqueous solutions of monoethanolamine (mea), diethanolamine (dea) and n-methyldiethanolamine (mdea). *Annu. Trans.-Nord. Rheol. Soc.*, 21:299–306, 2013.
- [77] J. Fernandes, B. A Figueiredo. Modeling viscosity of liquid ammonia-water mixture.
- [78] Inna Kim and Hallvard F. Svendsen. Heat of absorption of carbon dioxide (co₂) in monoethanolamine (mea) and 2-(aminoethyl)ethanolamine (aeea) solutions. *Industrial & Engineering Chemistry Research*, 46(17):5803–5809, 2007. ISSN 0888-5885. doi: 10.1021/ie0616489. URL <https://doi.org/10.1021/ie0616489>.
- [79] Rocío Maceiras, Estrella Álvarez, and M. Ángeles Cancela. Effect of temperature on carbon dioxide absorption in monoethanolamine solutions. *Chemical Engineering Journal*, 138(1):295–300, 2008. ISSN 1385-8947. doi: <https://doi.org/10.1016/j.cej.2007.05.049>. URL <http://www.sciencedirect.com/science/article/pii/S1385894707003920>.
- [80] Jason J. Lee, Chia-Hsin Chen, Daphna Shimon, Sophia E. Hayes, Carsten Sievers, and Christopher W. Jones. Effect of humidity on the co₂ adsorption of tertiary amine grafted sba-15. *The Journal of Physical Chemistry C*, 121(42):23480–23487, 2017. ISSN 1932-7447. doi: 10.1021/acs.jpcc.7b07930. URL <https://doi.org/10.1021/acs.jpcc.7b07930>.
- [81] Kuijun Li, Joel D. Kress, and David S. Mebane. The mechanism of co₂ adsorption under dry and humid conditions in mesoporous silica-supported amine sorbents. *The Journal of Physical Chemistry C*, 120(41):23683–23691, 2016. ISSN 1932-7447. doi: 10.1021/acs.jpcc.6b08808. URL <https://doi.org/10.1021/acs.jpcc.6b08808>.
- [82] Yanxia Wang, Tuo Guo, Xiude Hu, Jian Hao, and Qingjie Guo. Mechanism and kinetics of co₂ adsorption for tpea- impregnated hierarchical mesoporous carbon in the presence of water vapor. *Powder Technology*, 368:227–236, 2020. ISSN 0032-5910. doi: <https://doi.org/10.1016/j.powtec.2020.04.062>. URL <http://www.sciencedirect.com/science/article/pii/S003259102030348X>.
- [83] Xia Wang, Dongying Wang, Mingjun Song, Chunling Xin, and Wulan Zeng. Tetraethylenepentamine-modified activated semicoke for co₂ capture from flue gas. *Energy & Fuels*, 31(3):3055–3061, 2017. ISSN 0887-0624. doi: 10.1021/acs.energyfuels.6b03177. URL <https://doi.org/10.1021/acs.energyfuels.6b03177>.
- [84] S. Childress. *An Introduction to Theoretical Fluid Mechanics*. Courant lecture notes in mathematics. Courant Institute of Mathematical Sciences, 2009. ISBN 9780821848883. URL <https://books.google.nl/books?id=tH4WBAAQBAJ>.
- [85] Hassan Aref, John R. Blake, Marko Budišić, Silvana S. S Cardoso, Julyan H. E Cartwright, Herman J. H Clercx, Kamal El Omari, Ulrike Feudel, Ramin Golestanian, Emmanuelle Guillard, GertJan F. van Heijst, Tatyana S. Krasnopolskaya, Yves Le Guer, Robert S. MacKay, Vyacheslav V. Meleshko, Guy Metcalfe, Igor Mezić, Alessandro P. S de Moura, Oreste Piro, Michel F. M Speetjens, Rob Sturman, Jean-Luc Thiffeault, and Idan Tuval. Frontiers of chaotic advection. *Reviews of Modern Physics*, 89(2):025007, 2017. doi: 10.1103/RevModPhys.89.025007. URL <https://link.aps.org/doi/10.1103/RevModPhys.89.025007>.
- [86] Hassan Aref. Stirring by chaotic advection. *Journal of Fluid Mechanics*, 143:1–21, 1984. ISSN 0022-1120. doi: DOI:10.1017/S0022112084001233. URL <https://www.cambridge.org/core/article/stirring-by-chaotic-advection/7B32CACE61D5AD79077846D7ACF4A31E>.
- [87] Andrei Nikolaevich Kolmogorov, V. Levin, Julian Charles Roland Hunt, Owen Martin Phillips, and David Williams. The local structure of turbulence in incompressible viscous fluid for very large reynolds numbers. *Proceedings of the Royal Society of London. Series A: Mathematical and Physical Sciences*, 434(1890):9–13, 1991. doi: 10.1098/rspa.1991.0075. URL <https://doi.org/10.1098/rspa.1991.0075>.

- [88] J. Ortega-Casanova. Enhancing mixing at a very low reynolds number by a heaving square cylinder. *Journal of Fluids and Structures*, 65:1–20, 2016. ISSN 0889-9746. doi: <https://doi.org/10.1016/j.jfluidstructs.2016.05.002>. URL <http://www.sciencedirect.com/science/article/pii/S0889974615300402>.
- [89] Chih-Chang Chang and Ruey-Jen Yang. Electrokinetic mixing in microfluidic systems. *Microfluidics and Nanofluidics*, 3(5):501–525, 2007. ISSN 1613-4990. doi: 10.1007/s10404-007-0178-z. URL <https://doi.org/10.1007/s10404-007-0178-z>.
- [90] Haim Bau, Jihua Zhong, and Mingqiang Yi. A minute magneto hydrodynamic (mhd) mixer. *sensors Actuators B*, 79:207–215, 2001.
- [91] D. M. Hobbs, P. D. Swanson, and F. J. Muzzio. Numerical characterization of low reynolds number flow in the kenics static mixer. *Chemical Engineering Science*, 53(8):1565–1584, 1998. ISSN 0009-2509. doi: [https://doi.org/10.1016/S0009-2509\(97\)00132-2](https://doi.org/10.1016/S0009-2509(97)00132-2). URL <http://www.sciencedirect.com/science/article/pii/S0009250997001322>.
- [92] 2008. URL <https://www.mouser.es/datasheet/2/6/AD12038GP-472052.pdf>.
- [93] 2016. URL <https://www.kdscientific.com/kds-100-legacy-syringe-pump.html>.
- [94] Gurumurthy Ramaiah, Ramesh.K.P, and Dinesh Bhatia. Structural analysis of merino wool, pashmina and angora fibers using analytical instruments like scanning electron microscope and infra-red spectroscopy. *International Journal of Engineering Technology Science and Research* 2394-3386, 4:112–125, 2017.
- [95] 2020. URL <https://o-ring.info/en/technical-info/technical-o-ring-handbook/>.
- [96] Anand Vijayaraghavan. Direct air capture – methods and analysis. Report, TU Delft, 2020.
- [97] 2020. URL <https://www.surflopump.com/sale-8181677-surflo-flowdrift-dc-electric-mini-gear-pump-kgp-001-series.html>.
- [98] 2017. URL <http://www.dlabsci.com/english/cplb/HotPlate/Magnetic/2018/0120/220.html>.
- [99] Andrea De Matteis, Filippo Faldella, and Daniele Tarantini. Simulation of unsteady, laminar flow over a backward-facing step using a uniform staggered grid. Report, TU Delft, 2018.
- [100] Abraham Stroock and Gregory McGraw. Investigation of the staggered herringbone mixer with a simple analytical model. *Philosophical transactions. Series A, Mathematical, physical, and engineering sciences*, 362:971–86, 2004. doi: 10.1098/rsta.2003.1357.
- [101] 2017. URL <https://pages.mtu.edu/~fmorriso/cm310/new04fluids.pdf>.
- [102] 2015. URL <https://www.pcmag.com/reviews/ultimaker-2-extended#:~:text=By%20default%2C%20the%20Ultimaker%20,print%20quality%20and%20printing%20time>.
- [103] 2020. URL <http://www.cmp.caltech.edu/~mcc/Ph127/b/Lecture15.pdf>.
- [104] Walter Christopher Wilfong, Chakravartula S. Srikanth, and Steven S. C. Chuang. In situ atr and drifts studies of the nature of adsorbed co2 on tetraethylenepentamine films. *ACS Applied Materials & Interfaces*, 6(16):13617–13626, 2014. ISSN 1944-8244. doi: 10.1021/am5031006. URL <https://doi.org/10.1021/am5031006>.
- [105] Glenn Brown. The history of the darcy-weisbach equation for pipe flow resistance. *Proc. Environ. Water Resour. Hist.*, 38, 2002. doi: 10.1061/40650(2003)4.
- [106] Saeed Moaveni and Sharma Ishan. *Engineering fundamentals: an introduction to engineering*. CT: Cengage Learning, Stamford, 15 edition, 2011.
- [107] JRC-EU. Direct air capture (dac) the debate. Report, 2019. URL https://ec.europa.eu/jrc/sites/jrcsh/files/factsheet_direct_air_capture_04.pdf.